



UNIVERSITÀ DEGLI STUDI DI NAPOLI
FEDERICO II

Scuola Politecnica e
delle Scienze di Base



Università degli Studi di Napoli Federico II

Dottorato di Ricerca in
Ingegneria Strutturale, Geotecnica e Rischio Sismico

THESIS FOR THE DEGREE OF DOCTOR OF PHILOSOPHY

Artificial Intelligence in Structural Engineering: Use Cases for Safety Management

by

GIULIO MARINIELLO

Advisor: Prof. Domenico Asprone



SCUOLA POLITECNICA E DELLE SCIENZE DI BASE
DIPARTIMENTO D STRUTTURE PER L'INGEGNERIA E L'ARCHITETTURA

ARTIFICIAL INTELLIGENCE IN STRUCTURAL ENGINEERING: USE CASES FOR SAFETY MANAGEMENT

Ph.D. Thesis presented
for the fulfillment of the Degree of Doctor of Philosophy
in Ingegneria Strutturale, Geotecnica e Rischio Sismico
by

GIULIO MARINIELLO

March 2023



Approved as to style and content by

Prof. Domenico Asprone, Advisor

Università degli Studi di Napoli Federico II

Ph.D. Program in Ingegneria Strutturale, Geotecnica e Rischio Sismico

XXXV cycle - Chairman: Prof. Iunio Iervolino



www.dist.unina.it/dottorati-di-ricerca/dottorati

Candidate's declaration

I hereby declare that this thesis submitted to obtain the academic degree of Philosophiæ Doctor (Ph.D.) in Ingegneria Strutturale, Geotecnica e Rischio Sismico is my own unaided work, that I have not used other than the sources indicated, and that all direct and indirect sources are acknowledged as references.

Parts of this dissertation have been published in international journals and/or conference articles (see list of the author's publications at the end of the thesis).

Naples, 07.03.2023

Giulio Mariniello

Abstract

Artificial intelligence (AI) is the most disruptive technology of recent decades. Notably, its implementation in many engineering fields has already begun to show the ability to improve design and construction methods, data management, and safety. Structural engineering plays a crucial role in managing the safety of structures and infrastructures. Whether at the design stage of a new building or during inspections of an existing viaduct, engineers' skills and knowledge must provide realistic judgments that are capable of ensuring the required safety but, at the same time, are economically, socially, and environmentally sustainable. In this process, artificial intelligence makes it possible to assist structural engineers in performing repetitive tasks or duties that require analyzing large amounts of data.

This thesis reports several use cases of AI in performing structural safety management operations throughout the structure's life cycle.

The first use case is the design of irregular structures. It is complex to obtain structural solutions with high structural performance for such structures using traditional methodologies. Therefore, this thesis propose a metaheuristic strategy for design optimization, the performance of which are compared by the solutions provided by engineering students.

The second use case is the management of structural data flows during construction. Proper and transparent management of material acceptance reports, inspections, and load tests is a guarantee of materials and construction processes. An AI and blockchain-based tool for automatic and transparent data management increments safety and provide more confidence in structures.

The third and fourth use cases are related to structure monitoring with dynamic and static data. The dynamic is related to the interpretation of accelerometer data for detecting, localizing, and quantifying structural

damage understood as reduced stiffness and plastic hinge formation. The static, instead, relates to the evaluation of prestress loss in prestressed concrete lattice bridges from measurements of innovative pressure sensors. The fifth use case is for supporting field engineers in post-earthquake inspections. Deep learning systems can process photos by identifying damage and validating and supporting engineers' opinions. Finally, the sixth use case is for the use of metaheuristics approaches for scheduling maintenance activities for a portfolio of bridges to minimize the portfolio's carbon footprint while meeting the constraints of safety, cost, and available workforce. A methodology based on implementing the Artificial Intelligence methodology was developed for each use case. The methodology were validated using real-world data, where available or already in the literature, and simulated data using computationally robust techniques.

Keywords: Structural Safety, Machine Learning, Blockchain, Artificial Intelligence, Optimization

Sintesi in lingua italiana

L'intelligenza artificiale è la tecnologia più dirompente degli ultimi decenni. La sua implementazione nel settore delle Costruzioni ha già iniziato a mostrare la capacità di migliorare le modalità costruttive, la gestione dei dati e la sicurezza. L'ingegneria strutturale ricopre un ruolo cruciale nella gestione della sicurezza delle strutture e infrastrutture. Sia in fase di progetto di un nuovo edificio che durante le verifiche di un viadotto esistente è necessario che le competenze e le conoscenze degli ingegneri forniscano dei giudizi realistici che siano in grado di garantire la sicurezza richiesta ma allo stesso tempo siano sostenibili dal punto di vista economico, sociale e ambientale. In questo processo l'intelligenza artificiale consente di assistere gli ingegneri strutturisti nell'esecuzione di operazioni ripetitive o che richiedono l'analisi di grandi quantità di dati. In questo lavoro di tesi sono riportate diverse metodologie per l'implementazione dell'approccio dell'Intelligenza artificiale nell'esecuzione di alcune delle operazioni per la gestione della sicurezza strutturale durante tutto il ciclo di vita della struttura.

Il primo caso d'uso è la progettazione di strutture irregolari in pianta. Per tali strutture è complesso ottenere soluzioni strutturali con elevate performance strutturali con le tradizionali metodologie. Si analizzano e si propone quindi una strategia metaeuristica per la progettazione ottimizzata e si testano le performance confrontandole con le soluzioni progettuali di studenti di Ingegneria Strutturale.

Il secondo caso d'uso è la gestione dei flussi di dati strutturali in fase di costruzione. La gestione corretta e trasparente dei report di accettazione dei materiali, ispezioni e prove di carico è una garanzia sui materiali e sui processi costruttivi. In definitiva, uno strumento basato su AI e blockchain per la gestione automatica e trasparente dei dati consente di aumentare la sicurezza e la fiducia nelle strutture.

Il terzo e il quarto caso d'uso sono relativi al monitoraggio delle strutture. Il terzo è relativo all'interpretazione dei dati accelerometrici per la rilevazione, localizzazione e quantificazione del danneggiamento strutturale inteso come riduzione di rigidità e formazione di cerniere plastiche. Il quarto, invece, è relativo alla valutazione della perdita di precompressione in ponti a graticcio in c.a.p. a partire dalle misure di innovativi sensori di pressione.

Il quinto caso d'uso è per il supporto agli ingegneri di campo nelle ispezioni post-sisma. Infatti, sistemi di deep learning possono processare le foto individuando i danni validando e supportando i pareri dei tecnici.

Infine, il sesto caso è relativo all'utilizzo di metaeuristiche per lo scheduling delle attività di manutenzione di un portfolio di ponti con l'obiettivo di minimizzare la carbon footprint del portfolio rispettando i vincoli di sicurezza, costo e manodopera disponibile.

Per ciascuno dei casi d'uso è stata sviluppata una metodologia basata sull'implementazione dell'approccio dell'Intelligenza artificiale. Gli approcci sono stati validati utilizzando sia dati reali, qualora disponibili o già presenti in letteratura, sia dati simulati utilizzando tecniche robuste e sostenibili dal punto di vista computazionale.

Parole chiave: Sicurezza Strutturale, Intelligenza Artificiale, Machine Learning, Blockchain, Ottimizzazione.

Contents

Abstract	ii
Sintesi in lingua italiana	iv
Acknowledgements	x
List of Figures	xiv
List of Tables	xvii
1 AI in Design: Optimized structural design of irregular buildings	9
1.1 Introduction	9
1.2 Mathematical Formulation	13
1.3 Hybrid Learn-heuristic approach	19
1.3.1 Genetic Algorithm	19
1.3.2 Local search	22
1.3.3 k-Means Clustering: controlling cross-section diversity	22
1.4 Validation	24
1.4.1 Preliminary Analysis	25
1.4.2 Structural Pre-dimensioning Contest	28
1.4.3 Testing the cross-section diversity control	33
1.5 Potential Additional Objectives: Costs and IDR Distribution	36
1.6 Final Computational Remarks	38

2	AI in Construction: Blockchain in structural information flows	41
2.1	Introduction	41
2.1.1	Problem statement	41
2.1.2	Blockchain technology in the construction sector	43
2.2	Integrating smart contracts into BIM collaborative processes	48
2.2.1	Levels of implementation of smart contracts	51
2.3	The first implementation of a basic level smart contract	54
2.3.1	An application to the construction process of structural systems	56
2.4	Discussion	59
3	AI in Vibration-based SHM: the D²-DTE approach	63
3.1	Introduction	63
3.2	D ² -DTE methodology	67
3.2.1	Structural modeling and Damage simulation	69
3.2.2	Training data generation	72
3.2.3	DTE Training	76
3.2.4	DTE performance estimation metrics	77
3.3	Numerical Validation	78
3.3.1	R.C. frames and 3D steel truss system	79
3.3.2	IASC-ASCE benchmark	87
3.3.3	QUGS	95
3.4	Discussion	97
4	AI in Stress-based SHM: the LA-ELM approach	99
4.1	Introduction	99
4.2	Methods	103
4.2.1	Structural FE Modelling	106
4.2.2	Damage simulation	109
4.2.3	Data extraction	110

4.2.4	Extreme Learning Machine	112
4.2.5	Layout-aware random weight distribution	114
4.2.6	Evaluation Metrics	115
4.3	Computational Results	117
4.3.1	Input comparison: stress and vibration	118
4.3.2	Testing layout-aware random weights	120
4.3.3	Comparing learning models	123
4.3.4	Parametric Analysis	126
4.4	Limitations	128
5	AI in Inspections: Fast Post-seismic assessment of masonry buildings	131
5.1	Introduction	131
5.2	Materials and Methods	133
5.2.1	The Proposed Approach	133
5.2.2	Data preparation	134
5.2.3	Crack detection with Convolutional Neural Networks	136
5.2.4	Building zones labeling	137
5.3	Experimental Results	139
6	AI in Maintenance: Minimizing the Carbon Footprint of Bridges	143
6.1	Introduction	143
6.2	Formal description of the problem	145
6.3	Proposed solution methodology	146
6.3.1	Adaptive Large Neighborhood Search	147
6.3.2	Monte Carlo simulations	149
6.4	Computational Analysis	150
6.4.1	Benchmark Dataset	151
6.4.2	Numerical Results	152

Bibliography	185
Author's publications	187

Acknowledgements

I would like to express my sincerest gratitude to my advisor Prof. Domenico Asprone for giving me the opportunity to work in a stimulating and challenging environment that has allowed me to grow tremendously both personally and professionally. Their expertise, guidance, and support have been invaluable throughout my doctoral studies.

A special mention is due to Tommaso Pastore, whose unwavering support throughout this project has been truly invaluable. His commitment to excellence and his tireless efforts to provide guidance and advice have been a constant source of inspiration and motivation. I am deeply grateful for his friendship, support, and encouragement.

I am also grateful to Prof. Costantino Menna, Prof. Fulvio Parisi, and Prof. Antonio Bilotta for their insightful comments and feedback. Their expertise and input have been instrumental in shaping the direction of this research.

In particular, I would like to extend my thanks to Prof. Carlo Sansone, Stefano Marrone, and Giovanni Giacco from DIETI for their support and collaboration throughout a part of this project. Their contributions, including their insights, feedback, and resources, have been vital to the success of this research.

Furthermore, I would like to express my gratitude to all the Department of Structures at the University of Naples for their support and resources that have been instrumental in the development of this research.

Special thanks go to LACOD, my research group, for their collaboration and support during this project. In particular, I would like to thank Vittoria and Christian for their contributions to this research and for the valuable insights and feedback they provided.

I would also like to thank Alessandro, Angelo, Jacopo, and Pierluca, my office mates, for their support and friendship.

I am especially grateful to my girlfriend Martina for her unwavering support, and love throughout this journey. Her understanding, patience, and encouragement have been a constant source of strength, and I am deeply grateful for her presence in my life. She has been my rock, and I could not have accomplished this without her.

Finally, I would like to express my gratitude to my Family for their constant encouragement and support throughout my academic journey. Their love and support have been the foundation upon which I have built my academic achievements.

Thank you all for your invaluable contributions to my research, and for making this thesis possible.

Naples, 07.03.2023

Giulio Mariniello

List of Figures

1	Thesis structure	2
1.1	(a) L-shaped irregular plan, and (b) an example dimensioning that orientates the columns to regularize the structural behavior.	15
1.2	Irregular plans considered in the first set of numerical experiments: (a) Rectangular plan, (b) L-shape, (c) T-shape (d) O-shape.	26
1.3	(a) View in plant of contest structure (b) 3D View of contest structure	29
1.4	Response spectrum for Avellino, Italy, built according to NTC 2018 considering elastic behaviour ($q=1$), $T_r=50y$ and $P_{V_R}=0.63$ for $V_r=50y$	30
1.5	Cross-sections usage in the solutions provided in the Pre-dimensioning Contest (PhD1-PhD4).	34
1.6	Cross-sections usage in the solutions provided in the Pre-dimensioning Contest (PhD5-Optimized).	34
1.7	Comparison of objective function values achieved for different K_{diff} choices.	35
1.8	Comparison of the employed concrete volumes of the optimized solution and Ph.D. 1-6.	37

1.9	IDRs in directions x and y for Ph.D 1, Ph.D. 3, Opt, and $K_{diff} = 6$	37
2.1	Blockchain technology research in the construction industry: publications by year (Scopus).	43
2.2	Possible configuration of CDEs in the construction stage.	50
2.3	Notarization on the blockchain of information flows among CDEs.	51
2.4	Recalling information from the blockchain.	52
2.5	Basic level smart contract.	53
2.6	Intermediate level smart contract.	54
2.7	Advanced level smart contract.	55
2.8	Overview of the tool's user interface.	57
2.9	Sending information containers.	58
2.10	Receiving and verifying information containers.	59
3.1	Depiction of the D ² -DTE methodology.	68
3.2	Representation of the joint, modeled as four constrained connection nodes.	71
3.3	Representation of the story localization scales for the cracking phenomena and joint damage.	73
3.4	Representation of the column and floor-beam (a) and element (b) localization scales for the cracking phenomena.	74
3.5	Representation of the node (a) and hinge (b) localization scales for the joint damage.	76
3.6	Depiction of the decision tree ensemble obtained with the bagging meta-algorithm.	77
3.7	Depiction of the error estimation in relation to the damage localization.	79
3.8	2D r.c. frame considered in the numerical validation.	80
3.9	3D r.c. frame considered in the numerical validation.	81

3.10	Depiction of the 3D truss structure.	81
3.11	Damage patterns considered in the IASC-ASCE benchmark.	91
3.12	Confusion matrices for cases 1-7.	93
3.13	Confusion matrices for case 8.	94
3.14	Confusion matrix QUGS dataset.	96
4.1	Graphical depiction of the proposed methodology.	106
4.2	Numerical Model of a PSC bridge modelled using PEB approach.	107
4.3	Graphical depiction of the damage generation process.	109
4.4	Graphical depiction of the positioning of stress sensors. (a) cross-section view at mid-span; (b) deck as seen from above.	111
4.5	Schematic representation of ELM – feedforward neural network.	113
4.6	Scaling procedure	115
4.7	Visualization of average and worst case performances recorded for the ELM, in the cases of: $L = 30$ m, Noise = 1% and using stress data.	119
4.8	Comparison between regression quality achieved using Vibration data (left) and Stress data (right) as inputs, noise level 3%.	121
4.9	Comparison of the RMSE of LA-ELM with respect to other well established supervised learning algorithms.	124
4.10	Comparison of the computational times required by the compared methodologies, normalized with respect to the average time required by LA-ELM.	125
4.11	Analysis of RMSE scores with respect to different values for: length a), Gaussian noise b), and Beam number c).	127

5.1	The workflow of the proposed approach. On the right there is an example of the building zones subdivision: P_i represents a pier, S_i represents a spandrel, R_i a rigid zone. On the right there is an example of the matrix of damages. . . .	133
5.2	Results for the patch classification task. (a) Metrics of the networks;(b) Confusion Matrix for ResNet34 model	139
5.3	(a) FP example; (b) Wrong FP: patch labeled in the dataset as "no-crack", but it contains a crack that the model detects; (c)(d) FN examples	141
5.4	Final result example of the overall proposed approach. . . .	142
6.1	Evolution of the reliability index of a bridge.	146
6.2	Pseudocode of a generic ALNS algorithm.	148
6.3	Evolution of the costs implied by the three maintenance strategies in time.	154
6.4	Evolution of the emissions caused by the three maintenance strategies in time.	155
6.5	Evolution in time of the reliability indices of the three bridges characterized by the lowest values at $t = 0$	155
6.6	Chapters and Technologies.	157

List of Tables

1.1	Participating mass ratios of the dimensioning of Figure 1.1b.	16
1.2	Participating mass ratios of the dimensioning using only 40cm x 30cm sections.	16
1.3	Symbols and Definitions.	18
1.4	Summary of floor plan characteristics considered in cases (a) - (d).	27
1.5	Summary of available sections for columns – S^c – and beams – S^b – considered in cases (a) - (d).	27
1.6	Summary of results achieved for cases (a) - (d). According to the parameters of Table 1.4, the value of \mathcal{T} computed is equal to 0,38971 s.	28
1.7	Seismic hazard parameters for Avellino, Italy, according to NTC2018.	31
1.8	Summary of available column sections in the pre-dimensioning challenge.	31
1.9	Summary of objective function and gap values achieved in the Structural Pre-dimensioning Contest.	31
1.10	Summary of structural checks.	33
2.1	Recap of pointed-out criticalities and benefits implicated by our proposal	60

3.1	Summary of Element stiffness reductions for damage simulation in r.c. and steel structures.	71
3.2	Relationship between the input features and accuracy: 2D r.c. frame, single crack, 6% noise.	83
3.3	Summary of performances on 2D r.c. frame, cracking damage.	86
3.4	Summary of performances: 2D frame, joint damages.	87
3.5	Summary of performances: 3D frame, single cracked element	88
3.6	Summary of performances : 3D Frame, single joint damage	89
3.7	Summary of performances: 3D truss, single section reduction damage.	89
3.8	Cases analyzed in the IASC-ASCE benchmark.	90
3.9	Comparison of the performances achieved by D ² -DTE , and the two methods described in Azimi and Pekcan [10].	94
4.1	Characteristic features of PSC bridges considered.	108
4.2	Summary of results obtained comparing ELM-vibration and ELM-stress.	118
4.3	Summary of the comparison between Layout-aware ELM (LA-ELM) and ELM with completely random weights.	122
4.4	Domains of the independent parameters characterizing the dataset.	126
5.1	Metrics of the networks used for building openings segmentation	140
6.1	Summary of the bridges considered in the numerical experiments.	151
6.2	Summary of the possible maintenance operations considered in the analyses.	152

6.3	Comparison of the optimized solution (ALNS) whit the maintenance schedule of the Condition-based and Time-based approaches	153
-----	--	-----

Introduction

A country's economic growth is strongly correlated to its infrastructure endowment. Buildings, roads, bridges, airports, railways, and ports are critical assets for the long-term development of countries that increasingly need more facilities and routes.

Therefore, the health of the Architecture, Engineering, and Construction (AEC) sector is a critical aspect of a country's well-being.

In addition, only the construction sector accounts for between 13% and 15% of the world's Gross Domestic Product, thus highlighting a direct significant on the economy in the short term [17].

Despite being one of the most impactful sectors, the construction field shows a high degree of resistance to changes due to numerous factors, such as lack of digitalization, low-skilled labor, and others. These issues results in limited growth of the sector. In fact, differently from all other industry, the AEC has only increased by 1% annually over the past two decades showing all its limitations [161].

Challenges in the AEC sector are related to more than just inefficiency. Over the past two decades, the sector has faced material and labor shortages, managing aging facilities and infrastructure, and limited economic resources. In addition, the need to comply with regulations that take into account environmental concerns has made projects even more difficult to implement.

On the other hand, with the widespread diffusion of digital systems and the revolution of Industry 4.0, new opportunities opened in the 2010s for the construction sector.

Industry 4.0, also known as the Fourth Industrial Revolution, is a term

used to describe the current trend of automation and data exchange in manufacturing technologies, including developments in artificial intelligence, the Internet of Things, and cyber-physical systems. This trend is expected to profoundly impact how companies do business and could lead to increased productivity, efficiency, and profits [106, 13].

Structural engineering is one of the main areas where research and development have focused on implementing Industry 4.0 technologies, especially Artificial Intelligence (AI). AI is the ability of computer systems to perform tasks that usually require human intelligence, such as learning, problem-solving, and decision-making. It is disruptive in different areas of industry, and it is the most promising technology to implement in the AEC sector. AI has the potential to revolutionize the field of structural engineering by automating specific tasks, improving accuracy, and reducing the need for human labor. For example, AI algorithms can quickly analyze and compare multiple design options, helping structural engineers find the most efficient and effective solution. It can also be used to optimize the use of materials in construction, reducing waste and increasing sustainability.

This thesis analyzed solutions based on AI for the improvement of structural safety implementing smart designing, transparent constructing data flow, smart monitoring and inspections, and low emission in maintaining. Specifically, the potential of AI methods was analyzed for each stage of the facilities' life cycle and then used by developing a method to support designers and engineers, increase the safety level of facilities, and reduce emissions. The main idea is to define procedures and methodologies based on AI that will permit the existing structures to become smarter.

Figure 1 a diagram highlighting the structure of the thesis by identifying the structural stages and different chapters.

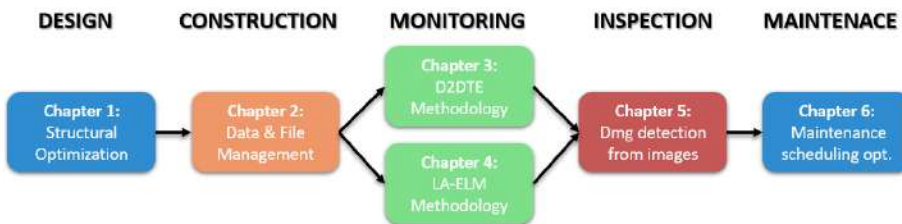


Figure 1. Thesis structure

For each stage, traditional procedures were analyzed, and a logical-mathematical representation was reconstructed to highlight current limitations and possibilities for applications of innovative techniques.

In this context, mathematical models and numerical simulations were used to represent the behavior of structures to investigate the applicability of the proposed methodologies.

The objective of Chapter 1 is to propose a hybrid technique that can support the designer in identifying the dimensioning of highly irregular structures. In this way, a structure can make the best use of its structural capabilities by avoiding stress localization, i.e., not using all its ductile reserves. The capacity-based approach introduced the issue of evaluating the regularity in the dynamic behavior of structures. In particular, while earlier regulatory codes treated reinforced concrete (r.c.) structures independently from their regularity in plan and elevations, modern design rules consider regularity by penalizing irregular structures by tuning the *behavior factor*. Since controlling the structure's dynamic behavior is particularly challenging when dealing with irregular plans, common sense rules and classical preliminary dimensioning (pre-dimensioning) methods often require several trial-and-error attempts to achieve a satisfactory dimensioning. Consequently, this intrinsic complexity fosters the development of practical and automated algorithmic procedures that can provide reliable dimensioning solutions for many structural typologies.

To achieve a high structural performance system, there is a need not only for sophisticated design methodologies but is necessary to guarantee the quality of materials and construction methodologies. Therefore, following the flow shown in the Figure 1, the focus of the thesis shifts to the construction phase.

From the material acceptance test to the last structural test during the closeout phases, lots of documents are produced for each phase related to a specific aspect of structural safety. For instance, when materials arrive on the construction site, their datasheets are stored, and according to the national code, many tests are made to establish material conformity. The interaction between Blockchain technology and artificial intelligence permits the building of a framework to certify exchanged data and check structural information's formal and substantial validity.

Chapter 2 proposes a proof-of-concept of integrating blockchain tech-

nology and smart contract into information flows that deploy among different Common Data Environments (CDEs). The ultimate purpose is to improve transparency and coordination of information flow related to structural safety during construction and closeout phases. To this end, this work will refer exclusively to the construction process of structural systems.

In detail, structural and civil engineers with the role of Project Managers and inspection engineers oversee construction works and ensure the structural safety of works by:

1. Checking structural materials when they arrive on construction sites;
2. Interpreting and analyzing results of tests on structural materials;
3. Inspecting structural systems to ensure compliance with safety standards and project specifications;
4. Overseeing closeout tests.

These are primarily manual human-dependent tasks that return reports in PDF format or scanned paper documentation as outputs that often require collecting multiple signatures. Nonetheless, this documentation is fundamental to demonstrating the safety and integrity of as-built structural systems; therefore, it represents an essential asset information model (AIM) component. Additionally, this documentation is exchanged mainly by email (or certified email) to collect signatures. Sometimes, this process is manually executed when digital approaches still need improvement. Consequently, efficiency, consistency, and coordination of structural-safety outputs suffer from these traditional approaches, which entail delays, redundancy, loss of documentation, and errors caused by human-dependent document management.

Despite the significant developments in design and construction, the most challenging objective for structural engineering is to ensure adequate safety levels for existing structures and infrastructures (Fig.1).

Chapters 3 and 4 discuss two different methodologies for structural damage detection, localization and evaluation.

Structural health monitoring (SHM) involves the implementation of detection and data-collection schemes to measure physical responses and

assess the current state of a system's health and operations. The physical response of the system can be measured according to a wide variety of parameters that depend both on the structure of interest and case-specific requirements. For example, health monitoring can be based on measures of local accelerations, displacements, rotations, temperature, corrosion- in metal components -local stresses and strains, and so forth. A constant challenge of SHM is to correctly identify when the measurements obtained are due to damage caused by, for example, structural deterioration or earthquakes rather than the natural or stable movement of the structure in its environment. Based on the structural response, the goal of SHM is to correctly detect damages, assessing - with an increasing level of detail - (i) damages' presence; (ii) geometric locations of damages; (iii) damage severity; and an (iv) estimation of the remaining service life of the structure, e.g., see [165, 58, 35, 65]. Properly implementing a monitoring system can help detect deterioration in structures early, increase safety levels, and bring efficiency and effectiveness to maintenance operations.

Chapter 3 reports $D^2 - DTE$ framework for structural damage detection based on the classification of dynamic properties of the structure. The presented methodology consents to identify, localize and quantify structural damage using a Decision Tree Ensemble Algorithm to assess the health condition of the monitored structure.

Despite the excellent performance in stiffness reduction identification, vibration data show low sensitivity to the damage of prestressed concrete (PSC).

In the '60s and '70s, the unprecedented wide use of PSC allowed the construction of large-span bridges in short times [18]. However, over the years, some shortcomings of this structural paradigm became apparent, with the main issues related to tendon durability and proneness to corrosion phenomena [107]. Nowadays, the status of these aging structures presents a widespread threat to reliability and safety.

These issues give rise to a growing need to monitor and maintain PSC bridges to prevent failures that could severely harm the health of their users. Indeed, several durability-related events were recorded in the past few years, such as the one affecting the Hammersmith Flyovver [42], and the collapse of the Polcevera bridge in Genoa, in which a sudden shearing of the prestressing cables caused the death of 43 people [29].

Therefore, Chapter 4 presents a new computational methodology based on Extreme Learning Machine (ELM) to estimate the remaining prestress levels in longitudinal beams of girder bridges.

Although structural health monitoring offers high opportunities for damage detection and residual lifetime evaluation, accurate inspections must be considered in critical situations such as after an earthquake. Indeed, human intervention is needed under certain conditions to quickly assess the state of structures in a wide area, while only a little part of it is provided with sensors. Moreover, on some occasions, the event may be of such magnitude that the monitoring system may be compromised. Then, concerning Fig. 1, we move on to the structure inspection stage.

After a seismic event occurs, public protection authorities initiate rescue procedures in seismic areas. The organization of rescues requires an expeditious assessment of the areas most subjected to damage and the identification of the safest access routes. Numerous studies about seismic damage simulation in inhabited areas are based on building characteristics. Despite the high simulation reliability, detecting actual damage conditions is essential to characterize the scenario better. In this context, systems for rapid damage assessment using Unmanned Aerial Vehicles (UAVs) could better characterize maps and define the details of rescue missions. When the rescue operations are over, rapid assessments of damaged structures are mandatory before allowing access to residents. The structures are evaluated by groups of volunteer engineers, who compile synthetic reports on the state and define the practicability of the building. Technicians quickly evaluate hundreds of buildings in complex contexts; this determines a high risk of error in verifying and compiling reports. With this in mind, Chapter 5 proposes a methodology to support engineers in inspection, using a Convolutional neural network to identify damages in the photo of inspected structures.

In the last part of the thesis, the attention is focused on scheduling structural maintenance activities (Chapter 6), specifically for large portfolios of bridges. In fact, due to the widespread diffusion of aging infrastructures, timely maintenance is a fundamental element to ensure serviceability and adequate safety levels. One of the first conventional approaches to planning interventions is time-based maintenance. According to this strategy, components are replaced or maintained at fixed time intervals without

analyzing their actual conditions. Therefore, this proactive and conservative strategy yields regular and possibly unnecessary interventions. This paradigm processes the information of inspections and monitoring systems and plans maintenance interventions as soon as either damage or dangerous degradation is detected. Apart from these two classical paradigms, many research efforts studied the planning of maintenance operations to address the challenges of having efficient structures with reduced costs. In this context, the Chapter proposes a maintenance operations scheduling algorithm to reduce the emissions that allows emissions to be reduced while ensuring the appropriate performance required and meeting budget and workforce constraints.

Thesis Outline

The thesis is composed of six chapters:

- Chapter 1 presents an algorithmic procedure for structural performance optimization in the structural design phase;
 - Chapter 2 provides a Proof of Concept of blockchain and artificial intelligence for managing and verifying documents of structural relevance;
 - Chapter 3 and Chapter 4 discuss two different SHM data interpretation methodologies, the first based on dynamic data from accelerometers, while the second from innovative stress sensors;
 - Chapter 5 proposes a Deep Learning-based method for image analysis of earthquake-damaged structures;
 - Chapter 6 reports on an optimized scheduling strategy of bridge maintenance activities for reducing environmental impact.
-

AI in Design: Optimized structural design of irregular buildings

1.1 Introduction

The use of optimization algorithms in structural design and construction has recently seen significant growth, given the advancements in the study of optimization techniques and the diffusion of powerful computational hardware. Therefore, in recent years, research works on structural optimization increased drastically. However, most of the papers in the literature focus on cost-minimization problems. In this approach, structural performance is often considered a constraint to ensure. For example, Mirzaei and Nasseradi [135] describe a Genetic Algorithm to minimize life-cycle cost of structures designed for a probable earthquake, and overcome the computational challenges of life-cycle cost estimations making use of an efficient methodology based on fragility functions.

Rezaeian and Der Kiureghian [162] propose an Evolution Strategy technique to optimize the cost of the structure, expressed as a function of its weight, and analyze the structural performances by means of a nonlinear response history analysis. The approach is validated in the optimization of two 2D r.c. frames, respectively characterized by 2-storeys and 1 bay, and 6-storeys and 2-bays.

By means of two cosmology-based meta-heuristics, Gholizadeh et al. [72] optimized the cost of planar structures, under performance constraints, such as element stress and nodal displacement in the case of steel frames. In particular, the cost function is expressed either using weight as a proxy – in the optimization of steel structures – or as a direct estimation – when dealing with r.c. frames. The proposed approach is validated on a set of 2D test cases composed of truss structures, and steel and r.c. frames.

Addressing cost minimization, Camp and Huq [30] adopted a hybrid Big Bang-Big Crunch algorithm to design optimized r.c. frames, including also a study on the optimization of a CO₂ emission function. From their analysis, the authors evidenced how the structure obtained considering CO₂ emissions in the objective function is characterized by a relatively small increase in the cost with respect to the structure achieved by means of classical cost minimization, thus evidencing that it is possible to design more sustainable r.c. frames at a reasonable cost.

Differently from cost optimization algorithms, recent developments consider the use of heuristics approaches to optimize structural performances. These scientific contributions can be mainly classified according to the decision variables of the problem, i.e. the structural parameters modified in the optimization process.

Extending the works presented by Miles et al. [133], Shaw et al. [174] optimized column overall height and grid uniformity in orthogonal framed building, by means of an algorithmic frameworks named OBGRID, that explored optimized configurations of column spacings through genetic operators.

In the context of beam-slab layout design, starting from the genetic algorithm described in Nimitawat and Nanakorn [142], the same authors [143] discussed the problem of column utilization efficiency in rectilinear structures. In particular, the genetic algorithm adopted evaluates how efficiently the columns sustain slabs, while enforcing constraints related to the layout of walls, the maximum slab dimensions, and the total floor area.

Sharafi et al. [173] formulated the problem of achieving an optimized conceptual designs as a variation of the classical knapsack problem [182]. The authors described a mathematical formulation in which the shape of the building plan, the number of bays and the size of unsupported spans are variables, and the objective function takes into account both the cost

and the eccentricity of the structure. The proposed solution framework relies on a bi-objective ant colony algorithm that is validated on an eight-storey r.c. building under wind loading conditions.

Performance-based seismic design of reinforced concrete frames is discussed by Mergos [131], that tackled the problem by means of an iterative methodology that designs steel reinforcements in r.c. frames to meet reference performance objectives, once the cross-sectional dimensions of structural elements has been set. This approach evaluated the performances of the solutions exploiting non-linear analyses and is validated on two regular 2D r.c. frames, evidencing that this methodology is able to achieve robust designs.

Notably, a related research stream addressed the optimization of seismic performances investigating the optimization of viscous damping systems; see [44] for a thorough survey of this field. Prevalingly, given the inherent complexity of the problem, most of these works rely on heuristic techniques to find optimized configurations. For example, Hejazi et al. [84] implement a genetic algorithm to minimize three-dimensional displacements at different storey levels and the occurrences of plastic hinges.

To optimize the achievements of seismic retrofit, Pollini [155] mathematically formalized the cost-optimization problem of fail-safe fluid viscous dampers. In his work, the author considered a proxy for costs as the objective function and structural constraints related to a diverse set of failure scenarios. Leveraging the differentiability of the mathematical formulation, the problem was solved through a gradient-based algorithm. Notably, the proposed solution approach makes use of a working-set strategy that significantly reduces the computational burden.

Describing a novel evolutionary computational framework, Apostolakis [7] optimized the seismic design of both regular and irregular three-dimensional frame structures. Within his solution framework, the author employed a mega-brace architecture that allowed for a successful reduction of the combinatorial solution space, while preserving the quality of optimized global level topology architectures and patterns that can be achieved.

The first thing that can be observed by reviewing the literature is that the vast majority of the optimization algorithms employed belongs to the class of meta-heuristic methods. The main advantages that characterize

techniques of this class are related to their suitability in the solution of complex problems, that often are characterized by integer or mixed-integer decision variables and a high number of feasibility constraints. Among these techniques, given the simplicity in their implementations, many optimization problems arising in engineering applications are solved by means of Particle Swarm Optimization and Genetic Algorithms.

Additionally, the research efforts that study the optimization at the pre-dimensioning phase mainly refer to the optimization of regular structures, and their validation process is often based on the analysis of simple 2D frames. Nevertheless, if the aim is to affect the dynamic behavior of a structure, the significant geometric differences that characterize 3D irregular structures have to be accurately modeled, to properly represent the complexity of the structural system. On the other hand, the research stream studying the optimization of damping systems involved both numerically accurate simulation scenarios and complex structures, yet the application field of these techniques and the structural specimens therein considered mostly refer to retrofit operations.

With in mind a context in which practitioners are called upon to design reliable dimensioning solutions for possibly complex structures in a short time, the aim of the present work is to mathematically formalize the pre-dimensioning problem, and describe a learn-heuristic method that combines a genetic algorithm and a k-means procedure. The hybridization of these algorithmic procedure aims to the size-optimization of structural elements belonging to 3D irregular structures in plan and elevation at a design stage, possibly including additional constraints to limit cross-section diversity.

In particular, given an irregular floor-plan and structural elements with preset positions, the problem here described optimizes elements' sections and orientations in order to achieve a set of target structural performances. In accordance with standard seismic performance requirements, the present work evaluates inter-storey drifts and torsional effects as target estimators.

Additionally, given the importance of a validation in a realistic geometric scenario, the algorithmic procedure employed in the solution of the proposed pre-dimensioning problem is tested on a set of 3D models of real-world structures.

The main contribution of this paper are:

1. Mathematical formulation of the behavior-regularization problem for 3D irregular structures;
2. Implementation of a learn-heuristic method to tackle the problem;
3. Use of a k-means clustering approach to address construction feasibility constraints that limit cross-section diversity.
4. Structural pre-dimensioning challenge to test the proposed approach in an operational scenario.

The present chapter is organized as follows: Section 1.2 introduces the formal description of the problem, while Section 1.3 reports the main principles characterizing the learn-heuristic employed in the solution process. A two thorough computational validation is described in Section 1.4, that includes different test-cases: a numerical tests that includes several 3D r.c. structures, and a structural design challenge in which the algorithmic performances achieved in the dimensioning of a 6-storey irregular r.c. building are compared to those accomplished by a group of Ph.D. candidates. The results are discussed in detail in Section 1.5, while concluding remarks are given in Section 1.6.

1.2 Mathematical Formulation

The problem described in the present chapter consists in achieving a cross-section sizing and orientation of r.c. structural elements – beams and columns – that regularizes the structural behavior of a system possibly characterized by geometric irregularities in plan and elevation. In this context, the positioning of structural elements is considered preset, as often happens in practice, where the architectural designers define elements' placing beforehand.

To formally model the problem, let n and m be the total number of columns and beams of the structure at the ground floor. Let $\mathbf{s} = (s_1, s_2, \dots, s_{n+m}, \tau)$ be a vector of decision variables indicating the rectangular cross-sections of each one of the $n + m$ structural elements, and let τ be the variable indicating the tapering strategy adopted to design upper floors.

In particular, each section s_i is defined through its two dimensions b_i and h_i , and its therefore characterized by an area $a_i = b_i \cdot h_i$. Starting from the values of the sections at the ground s_i , $i = 1, \dots, n+m$, the value of τ is selected within a discrete set of pre-determined tapering strategies, and determines the cross-sections characterizing upper floors. In particular, the tapering strategies define how frequently, and by which amount – if any – the dimensions of the structural elements of the upper storeys are reduced with respect to those present at ground floor. Additionally, having a discrete set of pre-defined tapering schemes automatically ensures that columns in lower storeys are not smaller than those present in upper storeys.

As objective function, the mathematical framework adopted in the present work evaluates the regularity of the seismic response minimizing the sum of two different terms, \mathcal{D} and \mathcal{M} , respectively related to the maximum inter-storey drift values and participating mass ratios.

Inter-storey drift ratios (IDRs) are classically used as *damage limitation requirement* – see [41] sec. 4.4.3.2 – and are restricted in the regulatory codes of many countries [4, 198, 46]. Additionally, their study in the context of automatic pre-dimensioning is particularly suitable since IDRs mainly depend on the sections and their orientations rather than on elements of later design phases, such as reinforcements.

Given a specified *limit state* of interest [156] and a specific section distribution \mathbf{s} , D_x and D_y can be defined as the maximum inter-storey drift ratios along the x and y directions, respectively; then the proposed form for the evaluation of inter-storey drift ratios, $\mathcal{D}(\mathbf{s})$, is obtained as:

$$\mathcal{D}(\mathbf{s}) = \frac{|D_x - D_y|}{\max(D_x, D_y)}. \quad (1.1)$$

In particular, $\mathcal{D}(\cdot)$ penalizes the relative differences encountered in IDRs with respect to the x and y directions, emphasizing that a regular behavior requires comparable inter-storey displacements both in x and in y .

Additionally, to reduce torsional effects, the second term characterizing the objective function attempts the minimization of the modal participating rotational mass ratios of the first two modes. In particular, this property is indirectly enforced acting upon the participating ratios of first

two translational modes.

Given an arbitrary section distribution \mathbf{s} , let U_X^I, U_X^{II} , and U_Y^I, U_Y^{II} be the participating mass ratios – along x and y directions – of the first two modes, then the second term characterizing the objective function $\mathcal{M}(\mathbf{s})$ is written as:

$$\mathcal{M}(\mathbf{s}) = \max(1 - \max(U_X^I, U_X^{II}), 1 - \max(U_Y^I, U_Y^{II}), \min(U_X^I, U_X^{II}), \min(U_Y^I, U_Y^{II})), \quad (1.2)$$

where

$$U_X^I, U_X^{II}, U_Y^I, U_Y^{II} \in [0, 1].$$

The participating mass ratios are computed as a result of a classical modal analysis [38]. In the experiments presented in Section 1.4 the modal analysis is carried out on a linear elastic model implemented in OpenSees [130].

To better evidence the use of equation (1.2) in the dimensioning of concrete frame structures, consider the three-storey structure whose L-shaped plan is reported in Figure 1.1a. In the preliminary dimensioning phase, correct orientation of the columns (as in Figure 1.1b) favors the achievement of regular behavior, obtained as purely translational first two modes. Evidence of this feature is observed in Table 1.1.

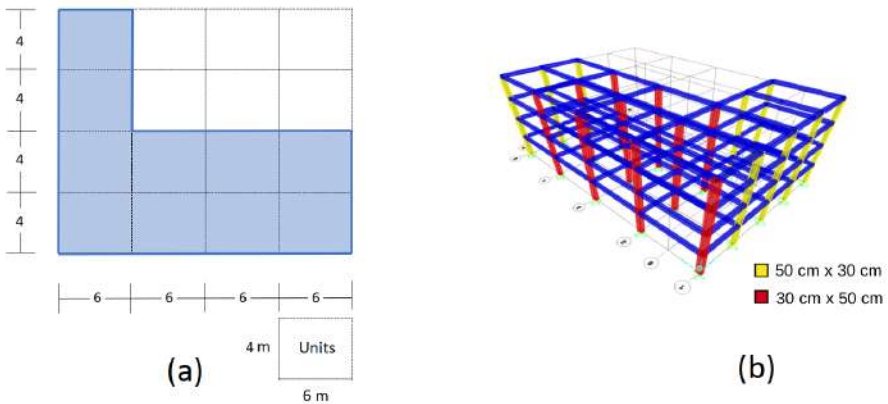


Figure 1.1. (a) L-shaped irregular plan, and (b) an example dimensioning that orientates the columns to regularize the structural behavior.

Mode	U_X	U_Y
I	0.009	0.810
II	0.695	0.015

Table 1.1. Participating mass ratios of the dimensioning of Figure 1.1b.

As a result, applying equation (1.2), the \mathcal{M} value associated with the dimensioning of Figure 1.1b) is $\approx 0,305$.

Comparatively, a dimensioning that disregards a correct orientation of the columns – e.g. one that equally applies sections of 40cm x 30cm – presents a less regular behavior. As shown in the mass ratios of Table 1.2, the second vibration mode presents participating masses in both directions, thus indicating the presence of torsional behavior.

Mode	U_X	U_Y
I	0.162	0.598
II	0.649	0.221

Table 1.2. Participating mass ratios of the dimensioning using only 40cm x 30cm sections.

This difference in terms of regularity is detected by equation (1.2), that for the second dimensioning computes scores a total of 0,402. Therefore, the minimization of \mathcal{M} favors structures that exhibit more regular behaviors.

The terms evaluating the IDRs and the modal participating masses are combined in a single objective function f to be minimized, through a convex combination:

$$f(\mathbf{s}) = \lambda \mathcal{D}(\mathbf{s}) + (1 - \lambda) \mathcal{M}(\mathbf{s}) \quad \lambda \in [0, 1]. \quad (1.3)$$

Ultimately, a mathematical description of the pre-dimensioning optimization problem can be formulated as follows

$$\min_{\mathbf{s}} f(\mathbf{s}) = \lambda \mathcal{D}(\mathbf{s}) + (1 - \lambda) \mathcal{M}(\mathbf{s}) \quad (1.4)$$

s.t.

$$D_x \leq \delta \quad (1.5)$$

$$D_y \leq \delta \quad (1.6)$$

$$\nu_i \leq \nu_{max} \quad \forall \text{ column } i \quad (1.7)$$

$$s_i \in S^c \quad \forall \text{ column } i \quad (1.8)$$

$$s_j \in S^b \quad \forall \text{ beam } j, \quad (1.9)$$

With constraints (1.5) and (1.6) that bound IDRs from above according to the maximum allowed IDR by Structural Code, δ ; with S^c and S^b representing the available cross sections for columns and beams; and, constraint (1.7) that restricts the value of the maximum axial load level, where – for a given column i of cross-section a_i – the corresponding axial load level is computed as

$$\nu_i = \frac{N_{ed}}{a_i f_{cd}}, \quad (1.10)$$

with N_{ed} and f_{cd} being, respectively, the column design axial load and the characteristic compressive strength of the material.

As stated previously, the main objective of the proposed optimization problem consists in the regularization of the dynamic behavior of irregular structures. At the same time, alongside the regularizing objective function, the aim of the introduced constraints is to let the optimized solution comply with regulatory codes. Accordingly, the the validation presented in Section 1.4 presents an analysis of the designed solutions with respect to a regulatory code of reference NTC 2018 [47].

Lastly, to address the feasibility of the designed pre-dimensioning from the standpoint of the construction process, an additional constraint limiting the number of different cross-section employed is addressed, as specified in Section 1.3.3.

All the symbols and definitions introduced in the present section are summarized in Table 1.3.

Symbol	Definition
a_i	Area of the cross-section of the i^{th} structural element
\mathcal{D}	Drift objective function, eq. (1.1)
D_x	Inter-storey drift ratio, x direction
D_y	Inter-storey drift ratio, y direction
f	Objective function, eq. (1.3)
f_{cd}	Characteristic material compressive strength
\mathcal{M}	Mass objective function, eq. (1.2)
m	Beams per floor
n	Columns per floor
N_{ed}	Column design axial load
\mathbf{s}	Vector of cross-sections
S^b	Set of available beam sections
S^c	Set of available column sections
U_X^I	Modal participating mass ratio, x direction, 1° vibration mode
U_X^{II}	Modal participating mass ratio, x direction, 2° vibration mode
U_Y^I	Modal participating mass ratio, y direction, 1° vibration mode
U_Y^{II}	Modal participating mass ratio, y direction, 2° vibration mode
δ	Maximum inter-storey drift ratio allowed
ν	Column axial load level
ν_{max}	Maximum column axial load level allowed

Table 1.3. Symbols and Definitions.

1.3 Hybrid Learn-heuristic approach

The present Section describes in detail the optimization algorithm implemented to solve the pre-dimensioning problem. In particular, the approach herein proposed is composed of three different components:

- Genetic Algorithm: to serve as a core heuristic method to yield a set of well-performing pre-dimensioning solutions;
- Local Search procedure: for intensification purposes, to improve the best solution found by the GA and achieve a high-quality output solution;
- k-Means algorithm: to address the additional constraint that limits the number of different cross-sections used in the dimensioning.

Sections 1.3.1 - 1.3.3 detail each of such characteristic components.

1.3.1 Genetic Algorithm

Genetic Algorithms (GA) represent one of the most employed methodologies in the landscape of heuristic optimization. These methods are iterative algorithms that operate on a set – *population* – of candidate solutions, that is improved through randomized recombination operators according to a given objective function – *fitness*. The simplicity in their implementation and their general optimization framework that does not rely upon derivative information makes them a standard for tackling many engineering problems [67, 189, 114], and encouraged their use in a wide variety of application scenarios, ranging from finance [132] to the prediction of the quality of life for lung transplant recipients [148].

Starting from a population of random solutions, P , where the cardinality $|P|$ is equal to an user defined parameter Π , the general structure of a genetic algorithm is mainly based on the iteration of three operators: *Selection*, *Crossover*, and *Mutation*, where

- *Selection*: selects two or more candidate solutions from P (elite individuals);
 - *Crossover*: recombines the selected solutions to generate new candidate solutions to be inserted in P ;
-

- *Mutation*: introduces random variations in the generated solutions to diversify the search process and avoid to get stuck in local optima.

The pseudo-code of the GA implemented for the pre-dimensioning problem is reported in Algorithm 1. A first initialization phase randomly generates the solution populations P and sorts its element according to their objective function values $f(\cdot)$. After the initialization phase, the main loop starts and is carried over until the maximum number of iterations has been reached.

The goal of the generic iteration consists in the generation of new candidate solutions to be inserted in the population P , with the aim of increasing the quality of explored pre-dimensioning solutions. The generations of new solutions – *offsprings* – starts with the random selection of two parents from P , \mathbf{s}^1 and \mathbf{s}^2 . The random selection is biased by the values of $f(\cdot)$: the better the values, the higher the probability of selecting the corresponding solutions. This guiding principle is founded on the natural observation that, during an evolution process, the better genes are those more likely to be passed to the next generations.

Algorithm: Genetic Algorithm(Π , MaxIt , μ , $f(\cdot)$)

```

Initialize  $P$  ;
Evaluate  $f(\mathbf{s})$ ,  $\forall \mathbf{s} \in P$ ;
Sort  $P$  according to  $f(\cdot)$ ;
 $It = 0$ ;
while  $It \leq \text{MaxIt}$  do
    for to be generated do
         $[\mathbf{s}^1, \mathbf{s}^2] = \text{SelectFrom}(P)$ ;
         $[\mathbf{s}', \mathbf{s}'] = \text{Crossover}(\mathbf{s}^1, \mathbf{s}^2)$ ;
         $\text{Mutate}(\mathbf{s}', \mathbf{s}'')$ ;
        insert in  $P$ ;
    end
    remove from  $P$  the worst solutions;
     $It = It + 1$ ;
end
return best solution found  $\mathbf{s}^*$ ;

```

Algorithm 1: Pseudo-code for a genetic algorithm.

In particular, for each $\mathbf{s}^i \in P$ the corresponding selection probability

$\mathcal{P}(\mathbf{s}^i)$ is obtained as :

$$\mathcal{P}(\mathbf{s}^i) = \frac{\frac{1}{1+f(\mathbf{s}^i)}}{\sum_{j=1}^{|P|} \frac{1}{1+f(\mathbf{s}^j)}}, \quad (1.11)$$

with $|P|$ being the cardinality of P , so that solutions with better objective function values are more likely to be selected as parents.

In optimization literature, the idea of introducing biased probabilities as in eq. (1.11) proved to be effective in different steps of the optimization process, including the construction phase [62] and the diversification phase [149].

To better grasp the functioning of \mathcal{P} , considering three different solutions, with respective objective function values of 0.1, 0.5, and 0.9. Applying equation (1.11), the corresponding selection probabilities are, approximately, 43%, 32%, and 25%, thus favoring the solution with minimum objective function value.

Starting from two parent solutions \mathbf{s}^1 and \mathbf{s}^2 selected according to \mathcal{P} , two offsprings \mathbf{s}' and \mathbf{s}'' are then generated. The generation is carried out by means of a 1-point crossover operator [154]: starting from a vectorial representation of the parent solutions, a cut-off point κ is selected uniformly at random and the offsprings are obtained cross-combining the components of \mathbf{s}^1 and \mathbf{s}^2 around κ .

The next step consists in the mutation of \mathbf{s}' and \mathbf{s}'' . For each offspring, and for each component of its vector representation, a number $r \in [0, 1]$ is drawn uniformly at random, and if r is lower than a user-defined mutation probability, μ , then the component is randomly modified.

Subsequently, the objective function values of the mutated offsprings are evaluated, and the solutions inserted in the population P . At the end of the iteration, only the Π best solutions are kept in the population.

This iterative scheme is continued until a specific termination criterion is not fulfilled. Classical strategies bound the maximum number of iterations or evaluate the convergence of the population i.e. estimating whether the average value of $f(\cdot)$ over the population is close to the best value f^* found. At the end of its execution the algorithm returns as output the best solution found in the search process \mathbf{s}^* . In the numerical validation presented in the next section, the optimization algorithm is terminated if

and only if both the two following occurrences take place: (i) a minimum number of iterations has been performed, (ii) convergence is observed in the population. Moreover, in the computational experiments considered, to avoid premature convergence the minimum number of iterations to be executed is set to 150. Additionally, the mutation probability is 0.1, while, as a reference case, the population size and the number of new solutions generated at each iteration are set to, respectively, 100 and 30. A set of preliminary analyses tested the effect of the changes of population size on solution quality. Four different population sizes were tested (50,100,150, and 200) – keeping constant the ratio between total population and new individuals to 10 : 3 – yet the numerical experiments evidenced that the objective function values yielded by the algorithm were equal to the third decimal digit.

1.3.2 Local search

In the local search phase, the algorithm performs an intensification phase, exploring the neighborhood of the solution obtained as output of the GA, to improve the quality of the pre-dimensioning. To this extent, the implemented procedure uses a 1-exchange (flip) neighborhood function, according to which two solutions are neighbors if and only if they differ in at most one component. Therefore, if there exists a better solution \bar{s} that differs only for one vector component from the current solution s , the current solution s is set to \bar{s} and the procedure restarts. If such a solution does not exist, the procedure ends and returns the current solution s .

This local search operator has been implemented considering the first improvement strategy. According to this paradigm, the current solution is replaced by the first improving solution found in its neighborhood, and such improving solution is then used as a starting point for the next local exploration.

1.3.3 k-Means Clustering: controlling cross-section diversity

Frequently, while pre-dimensioning a structure, the use of a limited number of different cross-section sizes is a desirable property. Indeed, this requirement could facilitate the construction process in situ. Limiting the

number of distinct cross-section sizes in a structure directly implies that many elements would be characterized by the same cross-section dimensions, meaning that in an algorithmic framework a small set of optimized choices are shared between few groups of columns/beams.

In a scenario in which the number of different cross-sections has to be lower than a critical parameter K_{diff} , three straightforward approaches could be followed, each of which is characterized by its shortcomings.

(i) Randomly generating pre-dimensioning and discarding those that present a total of different cross-sections that is higher than K_{diff} would be extremely inefficient, especially when K_{diff} is significantly lower than the number of available cross-section sizes.

(ii) Reducing the section database so that the number of available cross-section sizes is equal to K_{diff} would imply an a priori choice on the specific cross-sections to be evaluated. This choice would substantially reduce the flexibility of the optimization procedure and the benefits of its application.

(iii) Or else, it is possible to introduce a penalization term in the objective function that assigns worst objective function values at the solutions whose number of different cross-sections exceeds K_{diff} , yet this approach would aggregate the structural information of eq. (1.4) with the penalization term, possibly favoring solutions that yield poor structural performances.

To include a restriction on the different number of cross-section sizes employed, this work implements a k-means clustering procedure within the Genetic Algorithm to partition the structural elements in K_{diff} distinct groups. Then, each element of a group is characterized by a single decision variable, implying that all elements of the group will be characterized by the same cross-section dimensions. The use of a k-means clustering algorithms bypasses the defects of (i)-(iii) since it does not need to discard pre-dimensioning solutions as (i) does; does not reduce a priori the types of cross-sections that can be used as (ii) does; and does not need a penalization term in the objective function, as implied by (iii).

Since the k-means algorithm partitions a set of points of an Euclidean spaces, each structural element needs to be characterized as a vector (or point) of an Euclidean space, meaning that each element is identified by a vector of significant numerical properties.

The k-means algorithm is an iterative procedure: initially it creates k partitions and randomly assigns the structural elements to each partition; then it computes the centroid of each group in the Euclidean space; it constructs a new partition by associating each entry point with the group whose centroid is closest to it; finally the centroids for the new groups are recomputed, and so on, until the algorithm converges.

To run the clustering algorithm, the columns of the building are represented as points of an Euclidean space according to the following characterization. Let C be a column of the structure, then C is represented as a vector $\mathbf{v}(C) = (v_1, v_2, v_3) \in \mathbb{R}^3$. The first component of this vectorial representation, v_1 , is associated to the area of influence of C , so that, in the clustering process, columns bearing similar loads are closer in \mathbb{R}^3 . The next two components, v_2 and v_3 , are obtained as follows. Let s_{min} the pre-dimensioning solution that for each column considers the minimum cross-sections that respects constraint 1.7, and let $f(s_{min})$ the objective function value associated to s_{min} . Let Sec_x and Sec_y be the two cross-sections of the column database characterized by the largest moment of inertia respect to x and y direction, respectively. Let s'_{min} (resp. s''_{min}) be the pre-dimensioning obtained from s_{min} by imposing in C the use of the section Sec_x (resp. Sec_y). Then, v_2 (resp. v_3) is obtained as percentage variation of the objective function $f(s'_{min})$ (resp. $f(s''_{min})$) respect to $f(s_{min})$. The last step of this process consists in the normalization of v_i , $i = 1, 2, 3$, for all the columns C . Section 1.4.3 investigates the results when imposing different K_{diff} values.

1.4 Validation

The performances achieved by the Learn-heuristic algorithm here presented are assessed by means of three different validation steps:

1. **Preliminary Analysis;**
2. **Pre-dimensioning Contest;**
3. **Cross-section diversity limitation test.**

The goal of the preliminary analysis – Section 1.4.1 – consists in the appraisal of the influence of the Genetic Algorithm on the dynamic of four

different r.c. structures – mostly irregular in plan. In particular, this analysis focuses on the optimization with respect to a simplified objective function, based on the difference of the first two modal periods, that can approximate the dynamic behaviour of the structure, without resorting to the complex interactions between $\mathcal{M}(\cdot)$ and $\mathcal{D}(\cdot)$ that characterize equation (1.3). The results achieved by the GA are compared with the structural performances of the dimensioning based on gravity loads, used as reference solutions. At this stage, only the core of the optimization procedure, i.e. the GA, is considered.

Differently, the second validation step is carried out under the form of a structural design challenge of a 6-storey irregular r.c. building – Section 1.4.2 –, in which the performances of the optimization method are compared against those achieved by a group of Ph.D. candidates. The goal of this experiment consists in the validation of the algorithm in an operational scenario. To this extent, the pre-dimensioning problem is solved considering an algorithmic setup based on GA + Local Search (Section 1.3.2). Since the aim of the challenge is to explore the design freedom enabled by the proposed optimization algorithm, the restrictions considered are those of equations (1.4)-(1.9), without any limitations on the number of different cross-section dimensions.

Lastly, the *Cross-section diversity limitation test* – Section 1.4.3 –, introduces a constraint limiting the number of different cross-sections that can be used in the structure, according to a diverse set of K_{diff} parameters, and studies the quality of corresponding solutions.

The optimization code is implemented in Matlab, and the computations are conducted on a computer with a Intel Core i9-9900X@3.5 GHz processor with 32 GB of RAM, and an Windows 10 operating system.

1.4.1 Preliminary Analysis

The first validation phase focuses on the evaluation of the effectiveness of the Genetic Algorithm in influencing the dynamic behaviour of the structure. In particular, in this first experimentation, the objective function $f(\cdot)$ of eq. (1.3) is replaced by a simple criterion that can summarize regularity requirements studying a single set of parameters, namely vibration periods. More specifically, the objective of this phase aims to reducing the difference ΔT between the first two modal periods – T_1 and

T_2 , respectively –,

$$\Delta T = |T_1 - T_2|. \quad (1.12)$$

This optimization is carried out on a set of four different structures, the characteristics of which are depicted in Figure 1.2 and reported in Table 1.4.

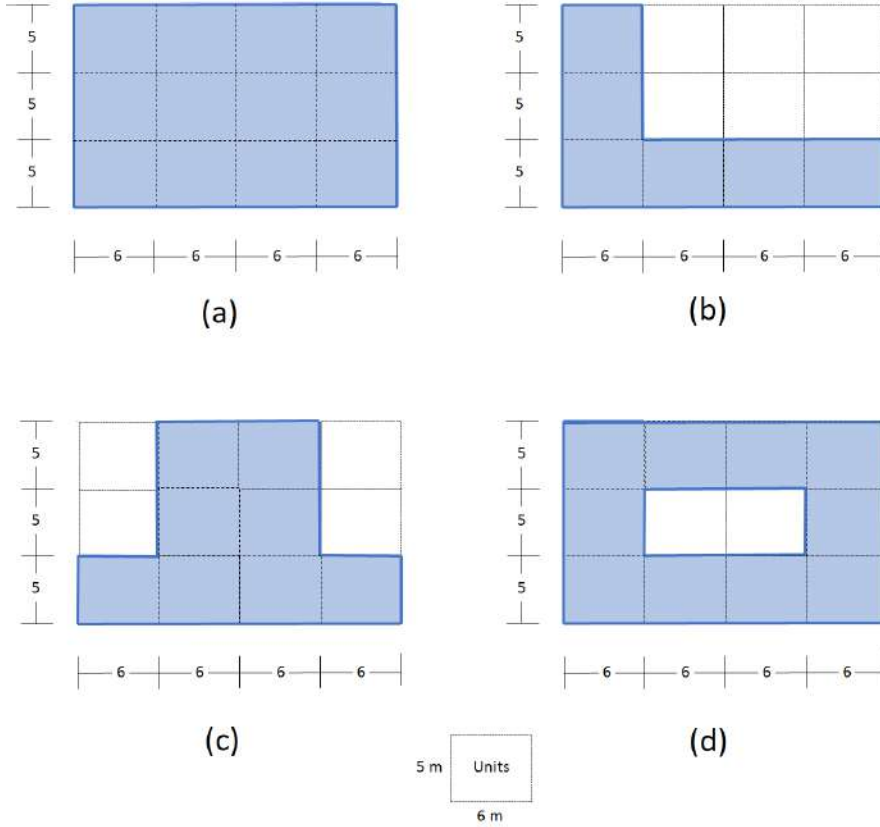


Figure 1.2. Irregular plans considered in the first set of numerical experiments: (a) Rectangular plan, (b) L-shape, (c) T-shape (d) O-shape.

In the solution of the pre-dimensioning problem of cases (a) - (d), the available sections for columns, S^c , are obtained starting from the the 30 cm \times 30 cm square section as base cross-section – the minimum

Plan	storeys	storey Height [m]	Columns	Beams
Rectangular	3	3	20	31
L - shape	3	3	14	19
T - shape	3	3	16	23
O - shape	3	3	20	30

Table 1.4. Summary of floor plan characteristics considered in cases (a) - (d).

squared section by Italian standards NTC 2018 [47] –, and increasing one of its dimensions by 10 cm, so as to obtain rectangular cross-sections. An analogous strategy is adopted for beam cross-sections, S^b , starting from 30 cm × 40 cm and increasing one dimension by 5 cm. The set of available cross-sections for columns and beams are summarized in Table 1.5.

S^c			
30x30	30x40	40x30	30x50
50x30			
S^b			
30x40	30x45	30x50	30x55
30x60			

Table 1.5. Summary of available sections for columns – S^c – and beams – S^b – considered in cases (a) - (d).

Table 1.6 lists the ΔT values obtained in the optimized solutions (“Opt”) and the pre-dimensioning obtained considering gravity loads (“GLoad”). Additionally, as discussed in [46] sec. 7.3.3.2, the modal period of an r.c. structure whose height is lower than 40 m can be estimated by \mathcal{T} , where

$$\mathcal{T} = 0.075 \cdot H^{\frac{3}{4}}, \quad (1.13)$$

with H being the height of the building from the foundation floor. The value of \mathcal{T} allows for an estimation of ΔT in terms of approximate percentage difference:

$$\% \Delta T = 100 \cdot \frac{\Delta T}{\mathcal{T}}. \quad (1.14)$$

Analyzing the results presented in Table 1.6 it is possible to observe that the optimized solution is characterized by vibration periods that on average exhibit a 3.59% difference, that never exceeds 6.16%. Additionally, it can be observed that the solution achieved by the Genetic Algorithm outperforms the gravity load solution in three out of four cases, with a tie recorded on the L-shaped structure, thus evidencing that the dynamic behavior of the structure can be effectively influenced by the optimization algorithm.

Plan	ΔT [s]		$\% \Delta T$	
	GLoad	Opt	GLoad	Opt
Rectangular	0.030	0.021	7.70	5.39
L - shape	0.024	0.024	6.16	6.16
T-shape	0.028	0.005	7.18	1.28
O - shape	0.030	0.006	7.70	1.54
average	0.028	0.014	7.18	3.59

Table 1.6. Summary of results achieved for cases (a) - (d). According to the parameters of Table 1.4, the value of \mathcal{T} computed is equal to 0,38971 s.

1.4.2 Structural Pre-dimensioning Contest

The second step of the validation process consists in the testing of the proposed optimization approach in an operational scenario in which the algorithm has to achieve a pre-dimensioning of an r.c. structure that is then compared to the solutions designed by a group of engineers. This validation phase – named *Structural Pre-dimensioning Contest* – was conducted at the Department of Structures for Engineering and Architecture of the University of Naples “Federico II”. The engineers involved were selected among the Ph.D. candidates with specific expertise in the design and retrofit of r.c structures.

The case-study considered in the challenge is a 6-storey 3D structure with an irregular C-shaped plant (see Figure 1.3). The building is char-

acterized by an inter-storey height of 3 metres, and the dimensions of the irregular plan are 44 and 37 m along the y and x directions, respectively. To simulate the presence of an architectural model, an irregular mesh has been placed onto the plan, and the nodes of the mesh are taken as preset positioning for the columns.

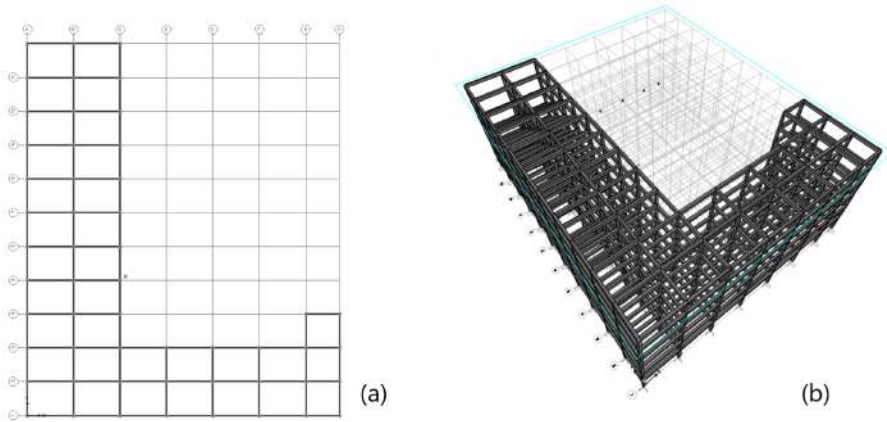


Figure 1.3. (a) View in plan of contest structure (b) 3D View of contest structure

Contest participants were given a total of 6 hours to size the elements of the structure according to the criteria of good design [41, 151], in particular by addressing the mathematical model in equations (1.4)-(1.9) in order to reduce the torsional effects in the first vibration modes of the structure and control inter-storey drift ratios at damage state limit. To ensure fairness in the evaluation of pre-dimensioning solutions, the Ph.D. candidates were provided with an automated script that, taking their solution as input, computes $\mathcal{D}(\cdot)$ and $\mathcal{M}(\cdot)$ in accordance to the objective function in eq. (1.4), as done for the proposed optimization algorithm.

The computation of IDRs is based on a linear static analysis with force distribution evaluated according to Italian NTC2018 for a structure located in Avellino, in the south of Italy. Table 1.7 reports the seismic hazard parameters for Avellino, and the elastic response spectrum for damage limit state is obtained in accordance to Italian NTC 2018 [47] (see Figure 1.4).

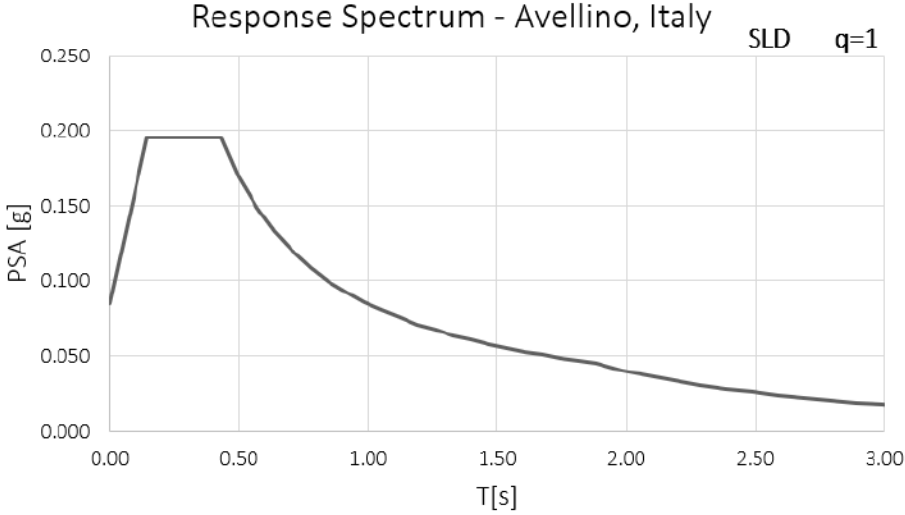


Figure 1.4. Response spectrum for Avellino, Italy, built according to NTC 2018 considering elastic behaviour ($q=1$), $T_r = 50y$ and $P_{V_R} = 0.63$ for $V_r = 50y$.

In these analyses, the value of ν_{max} is set to 0.5, to fulfill the basic requirements specified in Italian NTC 2018 [47], while the value selected for λ is 0.5 to equally balance $\mathcal{D}(\cdot)$ and $\mathcal{M}(\cdot)$.

The set of available column sections S^c – listed in Table 1.8 – is larger with respect to the one considered in the preliminary analysis, and includes cross-sections with wider area, in order to sustain the loads acting on a heavier structure. On the other hand, the challenge excluded the variability in the cross-sections of the beams that all have 30cm x 50cm dimensions.

The possible tapering schemes explored by the algorithm in the contest are: (i) no tapering, i.e. the cross-sections of the upper floors are those present at ground floor, (ii) tapering each two floors, and (iii) each three floors, namely by reducing columns cross-section by 10 cm along the direction characterized by the larger dimension.

Table 1.9 lists the performances achieved by the solutions competing in the Structural Pre-dimensioning Contest. In particular, for each solution are reported the objective function f – computed according to (1.3) – and the optimality gap (Gap %), that measures the percentage relative increase

Parameter	Value
a_g	0.021 g
F_0	2.317
T_c	0.311 s

Table 1.7. Seismic hazard parameters for Avellino, Italy, according to NTC2018.

Column Sections			
30x30	30x40	40x30	30x50
50x30	40x40	30x60	60x30
40x50	50x40	30x70	70x30
40x60	60x40	40x70	70x40

Table 1.8. Summary of available column sections in the pre-dimensioning challenge.

in terms of $f(\cdot)$ of a given solution with respect to the best (minimum) solution found, i.e. for a solution \mathbf{s} , the % Gap is computed as

$$\% \text{Gap} = 100 \cdot \frac{f(\mathbf{s}) - f(\mathbf{s}^*)}{f(\mathbf{s}^*)}, \quad (1.15)$$

where \mathbf{s}^* is the minimum solution found for the structure of interest.

Solution ID	f	% Gap
Ph.D. 1	0.275	882.1%
Ph.D. 2	0.263	839.3%
Ph.D. 3	0.238	750.0%
Ph.D. 4	0.248	785.7%
Ph.D. 5	0.243	767.9%
Ph.D. 6	0.243	767.9%
Optimized	0.028	0.0%

Table 1.9. Summary of objective function and gap values achieved in the Structural Pre-dimensioning Contest.

Analyzing the results reported in Table 1.9, it is possible to note how

the best values are those of the pre-dimensioning achieved by the proposed learn-heuristic framework, that reached a solution characterized by an objective function value $f = 0.028$. Differently, the solutions yielded by the Ph.D. candidates exhibit dynamic behaviors that worsen the optimized solution approximately by one order of magnitude. In fact, for such solutions, the measured relative worsening (% Gap value) falls between 750% and 882.1%, with a mean worsening of approximately 798.8%. Furthermore, it is reported that the optimization algorithm achieved a solution characterized by a τ that does not present the tapering of the columns.

Additionally, with the aim of better evaluating the pre-dimensioned structures, and to validate the mathematical formulation presented in Section 1.2 from the standpoint of a regulatory code, each one of the solutions designed in the pre-dimensioning challenge has been implemented in a geometric model of the Edilus software. In particular, Edilus is a commercial software of common use [179] that, starting from a geometric model, automatically defines section reinforcements and carries out structural analyses to check whether the designed solution complies with a reference regulatory code or not. More specifically Edilus includes all the structural checks specified in NTC 2018 [47], with these being related to both the structural elements' cross-sections and their reinforcement. Checks such as those involving bending moments mainly depends on reinforcements and are automatically complied by the software. Conversely, checks that involve shear forces, nodes and beam-column capacity design, are mostly related to the choice of the elements' cross-sections. Table 1.10 reports the outcome of this former group of structural checks, listing, for each one of those – named Shear Forces, Node, and Capacity Design (Beam-Column) – whether the designed solution passed or failed the check.

Observing the results related to the structural checks reported in Table 1.10 it can be noted how the optimized solution and the pre-dimensioned structures of Ph.D. 1 and Ph.D. 3 are compliant with NTC 2018 [47] and can be immediately used for a construction project. Instead, it is observed how the solutions proposed by Ph.D. 2 and Ph.D. 6 require limited intervention, while the solutions of Ph.D. 4 and Ph.D. 5 require extensive modifications to comply with regulatory codes.

Moreover, it is possible to relate the outcomes of the structural checks with the axial load levels targeted by the designers. In particular, the

Solution ID	Shear Forces	Node	Capacity Design (Beam-Column)
Ph.D. 1	✓	✓	✓
Ph.D. 2	✓	✓	✗
Ph.D. 3	✓	✓	✓
Ph.D. 4	✗	✗	✗
Ph.D. 5	✗	✗	✗
Ph.D. 6	✓	✗	✓
Opt	✓	✓	✓

Table 1.10. Summary of structural checks.

students that designed pre-dimensioning solutions that satisfy structural checks, either completely or almost completely, – Ph.D. 1,2,3,6 – targeted lower ν values (≈ 0.3), while Ph.D. 4 and 6, whose solution fail to comply with the three structural checks, aimed to have a higher axial loads acting upon the columns, targeting $\nu \approx 0.5$. Conversely, the proposed learn-heuristic algorithm allowed to consider the same higher target axial loads ($\nu \approx 0.5$) while optimizing the dynamic behavior of the structure so that all the structural checks are satisfied.

1.4.3 Testing the cross-section diversity control

Lastly, to appraise the effects of the cross-section diversity constraint, the present section reports the results of a set of numerical experiments that include such restriction on the columns in accordance to a diverse set of K_{diff} values. In particular, the optimization algorithm is independently executed considering $K_{diff} \in \{3, 4, 5, 6, 7, 8, 9, 10\}$, and the constraint is enforced using the k-means clustering approach described in Section 1.3.3.

The computational results are represented in Figure 1.7 that for each K_{diff} imposed reports the corresponding objective function value.

Interesting insights can be gathered observing the cross-sections employed in the solutions of the contest. For each solution, Figure 1.6 reports a histogram depicting the absolute frequencies of each available cross-sections.

Observing the results of Figures 1.5 and 1.6, it stands out that the

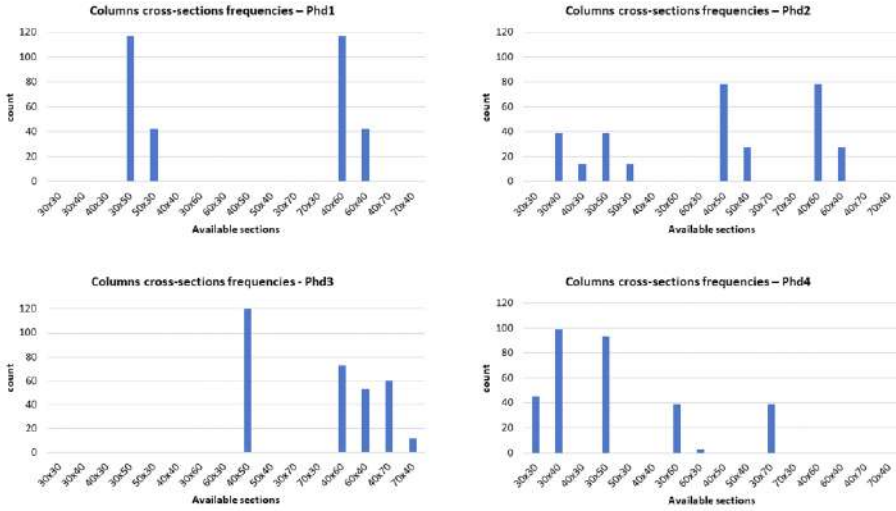


Figure 1.5. Cross-sections usage in the solutions provided in the Pre-dimensioning Contest (PhD1-PhD4).

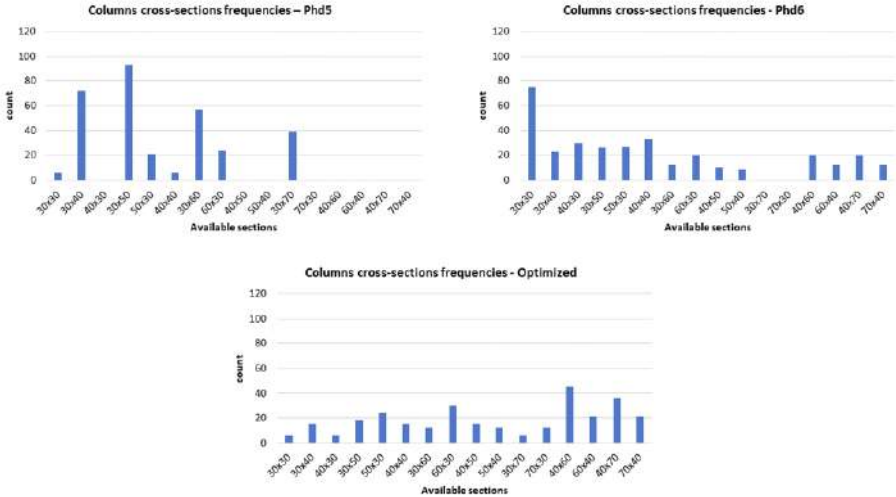


Figure 1.6. Cross-sections usage in the solutions provided in the Pre-dimensioning Contest (PhD5-Optimized).

number of different cross-sections considered by the Ph.D. students is generally reduced with respect to those employed by the optimization algorithm, that employs 15 out of the 16 available cross-sections at least once. The higher number of different cross-section found in the optimized solution is related to the randomized process guiding the genetic algorithm that allows for a strong diversification in the choice of decision variables. From the standpoint of the construction process of the structure, this diversity is not necessarily favorable, since it can be desirable to simplify a pre-dimensioning solution limiting the number of different cross-section employed.

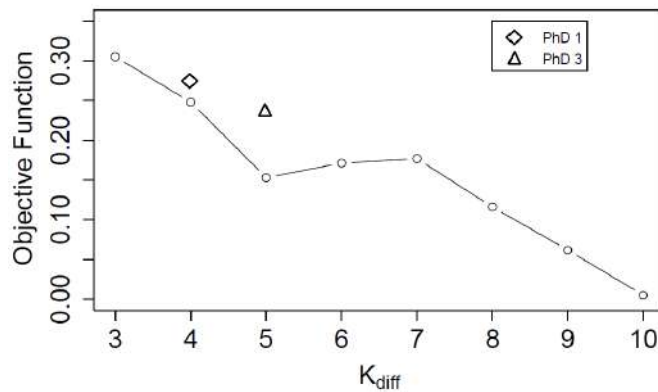


Figure 1.7. Comparison of objective function values achieved for different K_{diff} choices.

If the use of a reduced number of different cross-sections is considered as a key characteristic of the pre-dimensioning solution, it is possible to enforce this property by means of the clustering approach described in Section 1.3.3. Whenever the optimization includes limitations on the maximum number of different cross-sections (Figure 1.7), as expected, the overall tendency is that for higher values of K_{diff} the algorithm has more freedom to explore different solution configurations, and thus generally the objective function value achieved improves. Nevertheless, since the k-means clustering induces a heuristic grouping, monotonicity is not ensured

for successive K_{diff} values, and as can be observed from the comparison between $K_{diff} = 5$ and $K_{diff} = 6$ – (equivalently $K_{diff} = 6$ and $K_{diff} = 7$ – it can happen that a more restrictive K_{diff} leads to slightly better solutions.

Comparatively, it is possible to observe from Figures 1.5 and 1.6 that Ph.D. 1 and Ph.D. 3 made use of, respectively, 4 and 5 different cross-sections. When imposing the constraint limiting cross-section diversity with such K_{diff} values, it is possible to see that the proposed learn-heuristic achieved better performing solutions. Nevertheless, as expected, when the limitation on cross-section diversity is more restrictive ($K_{diff} = 4$) the improvement respect to the Ph.D. pre-dimensioning is marginal, while the optimized performance are significantly better for $k_{diff} = 5$. This behavior can be related to the observation that the optimization approach can attain its full potential when few constraints allow for an extensive exploration of the solution space.

1.5 Potential Additional Objectives: Costs and IDR Distribution

Questions may arise concerning the trade-off between classical objectives, such as volumes/costs or IDRs distribution, and the objective function of eq. (1.4). To investigate the material usage of the solutions featured in the Structural Pre-dimensioning contest, Figure 1.8 reports a comparison of the employed concrete volumes.

In particular, it is possible to observe how the volume employed by the optimized solution (193.68 m^3) is higher with respect to the average volume employed by the students ($\approx 172.7 \text{ m}^3$). Nevertheless, considering only the students' solutions that comply with the regulatory codes – as the optimized solution does – we can observe how Ph.D. 3 designed a solution that is more expensive than the optimized one (223.2 m^3), while the amount of concrete used by Ph.D. 1 is lower (186.03 m^3). Ultimately, this analysis evidences that the optimized solution achieves a good trade-off between material usage and regularization of dynamic behavior, in fact, the remarkable structural performance observed comes at the price of a 4.1% increase of material with respect to Ph.D. 1.

Lastly, Figure 1.9 shows for each of the storey level the IDR val-

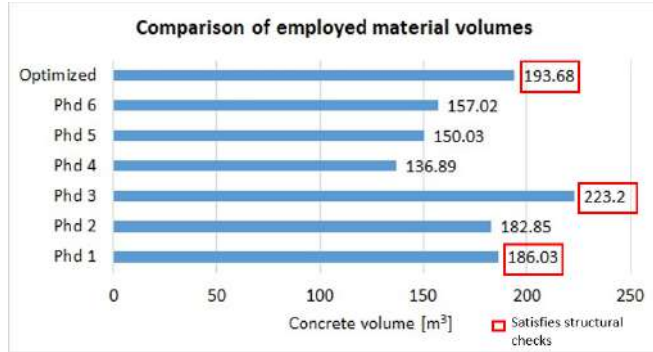


Figure 1.8. Comparison of the employed concrete volumes of the optimized solution and Ph.D. 1-6.

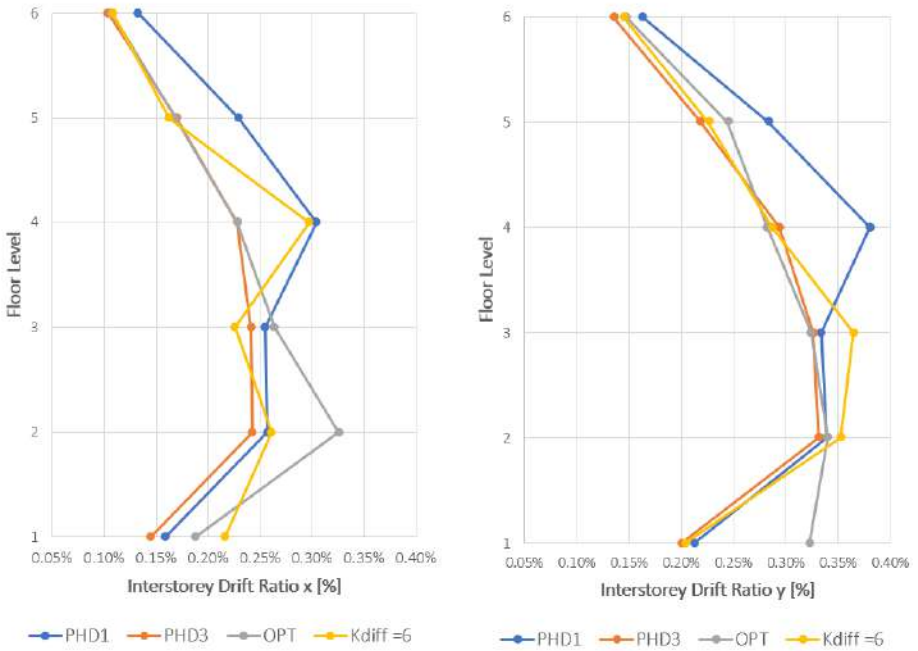


Figure 1.9. IDRs in directions x and y for Ph.D 1, Ph.D. 3, Opt, and $K_{diff} = 6$.

ues respect to directions x and y . This comparison considers both pre-dimensioning solutions of Ph.D. 1 and 3, and two solution of the proposed optimization method: the structure obtained in the pre-dimensioning contest, and the solution obtained for $K_{diff} = 6$. The first thing that can be observed is that all IDR values are below 0.5%, as required by equations (1.5) and (1.6). Moreover, in general it can be seen that the solutions obtained with the proposed learn-heuristic attain IDR distributions that are intermediate between those achieved by the pre-dimensioning designed by the Ph.D students. In particular, optimized solutions exhibit IDRs that are closer to those of Ph.D. 3, while the solution proposed by the Ph.D. 1 shows a greater drift on the upper levels. This property is probably related to the use of smaller sections, and thus less weight, as correctly reflected by Figure 1.8.

1.6 Final Computational Remarks

The numerical validation presented in Section 1.4.2 includes a diverse set of 3D structures, and as well a structural pre-dimensioning challenge, to evaluate the approach in an environment as close as possible to an operational scenario. In this context the structure pre-dimensioned with the proposed methodology was then compared with structures pre-dimensioned by practitioners who used their experience to limit the time of a trial and error pre-dimensioning approach. The comparison showed that the regularization function considered in the problem description was significantly better minimized by the proposed algorithm rather than by any one of the practitioners. Moreover, additional information were gathered studying the cross-sections employed in the different solutions of the Structural Pre-dimensioning Contest. This analysis evidenced how most of the practitioners relied on a limited number of different cross-section, following similar design principles. It is possible to observe that the solutions designed by the Ph.D. candidates were outperformed in their structural performances by those achieved by the proposed learn-heuristic even when considering a limited number of different cross-sections, thus validating the k-means approach described in Section 1.3.3.

Moreover, a comparison was performed to evaluate the readiness of solutions to meet code requirements. It was assessed that in addition to hav-

ing the better performances in terms of objective functions, the solutions of Ph.D. 1, Ph.D. 3 and the described learn-heuristic are those compatible with the codes, while 4 out of 6 practitioners' pre-dimensionings required limited-to-extensive corrections to comply with regulatory codes. This observation emphasizes once again how the pre-dimensioning phase of an irregular structure is a challenging operation that can be accomplished by means of an optimization procedure, while if carried out according to rules of thumb and common sense may require several attempts and subsequent efforts of trial and error. Additionally, finding out that the optimized solution complies with the requirements of regulatory code can suggest, to some extent, that the mathematical formulation originally proposed in Section 1.2 adequately represents the problem of interest.

AI in Construction: Blockchain in structural information flows

2.1 Introduction

In this chapter is proposed a proof-of-concept of the integration of blockchain technology and smart contract into information flows that deploy among different CDEs. The ultimate purpose is to improve transparency and coordination of information flows that relate to structural safety during construction and closeout phases. To this end, this chapter will refer exclusively to the construction process of structural systems.

2.1.1 Problem statement

In detail, structural and civil engineers with the role of project managers (PM) and inspection engineers oversee construction works and ensure the structural safety of works by 1). checking structural materials when they arrive on construction sites; 2). Interpreting and analysing results of tests on structural materials; 3). Inspecting structural systems to ensure compliance with safety standards and project specifications, 4). Overseeing closeout tests. These are mostly manual human-dependent tasks that return reports in PDF format or scanned paper documentation as outputs

which often require the collection of multiple signatures. Nonetheless, this documentation is fundamental to demonstrate the safety and integrity of as-built structural systems therefore it represents an essential component of an asset information model (AIM). Additionally, this documentation is mostly exchanged by email (or certified email) with the additional purpose of collecting signatures. Sometimes, this process is still manually executed when digital approaches are lacking. Consequently, efficiency, consistency, and coordination of structural-safety outputs suffer from these traditional approaches which entail delays, redundancy, loss of documentation, errors caused by human-depended document management.

Research scope arises from the need to overcome inefficiencies and increase reliability and transparency in the management of structural-safety documentation. Consequently, this work proposes a proof-of-concept of the integration of blockchain technology and smart contract into information flows among different common data environments (CDEs). The ultimate purpose is bypassing obsolete and incomplete exchange processes based on email and providing, concurrently, an instrument to create an immutable, trustworthy source that collects the whole storyline of structural-safety information exchanges which occur during the building process. Accordingly, the proof-of-concept introduces smart contracts with different levels of complexity where the advanced level compares exchanged information with data gathered by IoT sensors on site. Improved immutability, transparency, and reliability of structural-safety information and documentation can prevent litigations on construction sites because all significant events are traced on the blockchain, always queryable, and prove themselves as a source of evidence. Adopting blockchain technology can bring other benefits like encouraging the use of digital documentation in place of paper-based one, increasing attention on the construction process of structural systems. Finally, this framework could be used to fully integrate information collection and coordination of in-situ automated construction processes of structural components (for example that one implementing additive manufacturing technologies) and traditional construction processes. This Chapter comprises 5 sections:

- Section 2.1 is the introduction where the problem statement and research scope are described. In this section, we also provide a brief introduction to current blockchain technology applications in the con-
-

struction sector;

- Section 2.2 presents the proof-of-concept of the integration of blockchain technology and smart contracts into information flows among different CDEs;
- Section 2.3 illustrates the first implementation of a decentralised application (DAPP) that deploys a basic level smart contract;
- Section 2.4 introduces the testing of our proof-of-concept by comparison between the proposed and the traditional approaches.

2.1.2 Blockchain technology in the construction sector

Leveraging blockchain technology for renovating work processes in the construction industry is a rather recent academic research field. Figure 2.1 depicts results of a query on the Scopus database with the following attributes: TITLE-ABS-KEY ("Construction" AND blockchain); first documents only date back to 2016 but publications have conspicuously increased between 2018 and 2020. This means that blockchain technology is gaining great attention among researchers of the construction industry.

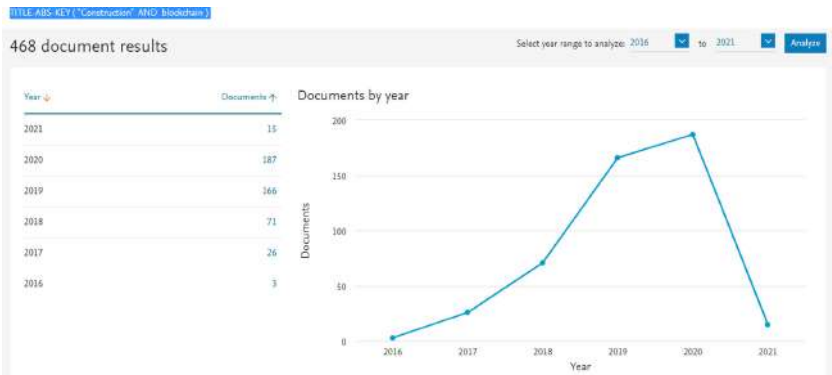


Figure 2.1. Blockchain technology research in the construction industry: publications by year (Scopus).

Looking at the most recent documents, the work of Yang et al. [194] deserves a deeper analysis. It returns an interesting classification of the

application of blockchain in the construction industry. For an in-depth exposition on blockchain adoption in other domains of the Architecture, Engineering, and Construction (AEC) sector such as real estate, smart cities, and smart energy, refer to Li et al. [111]. Yang et al. [194] identify twenty-seven publications among journal papers, conference papers, and book chapters from twelve countries all around the world. The authors provide in-depth analysis of publications that they have also classified with respect to two criteria (blockchain technology) integrated with other digital technologies; digitalization of work process. According to Yang's work, integration between blockchain and BIM technologies is currently the most attractive field of research in the construction domain (the study highlighted 13 publications on the subject) which also includes integration with the internet of things (IoT) and RFID and sensors; moreover, digitalization of work processes mainly affects work processes that relate to information management, supply chain management, smart contract and cryptocurrencies (economic management). In detail, Yang et al. [194] have collected the following work processes: Automatic payments; Contract execution (tendering, etc.); Construction procurement in the supply chain; Supply-chain logistics of construction materials; Management of data and intellectual property rights in the design phase; Recording building performance; Registration of land titles; Information management for all building stages; Equipment leasing. Other work processes can add to this list because this is an open research field. However, Yang et al. [194] have also pointed out that most of the reviewed publications present only inception ideas, while few publications that present proof-of-concept ideas mainly involve cryptocurrencies. This is not surprising because cryptocurrencies have been the first application of blockchain technology which dates to 2008 (Nakamoto 2008). Information management has been addressed by Turk and Klinc [184], Wang et al. [192], and, recently, Sheng et al. [175] and Elghaish et al. [57]. Turk and Klinc [184] first proposed to use blockchain technology to archive operations and changes onto information models created with BIM authoring software. This approach would enhance trace-back processes to establish both intellectual property and responsibilities in the design phase. Currently, there are commercial solutions that are trying to implement this approach like Bluebeam (Available: <https://www.bluebeam.com/>). Wang et al. [188] argue that

blockchain can apply to document management to develop notarization-related applications that eliminate verification time of documents' authenticity. Documents can be stored in a distributed ledger where all creation, deletion and updating are recorded; traceability, immutability, and transparency properties of blockchain technology ensures authenticity of documents. However, authors' contribution mainly consists in highlighting possible benefits of a blockchain-based document management approach; in fact, an application is missing, neither implications nor possible ways of connection with BIM-based information management are discussed. This work focuses on this type of applications and proposes, in section 2.3, a blockchain-based solution for document management in BIM collaborative processes which deploy during the construction phase. Sheng et al. [175] also focus on the construction phase and develop a blockchain-based framework for managing quality information. Their scope consists of providing consistent and secure quality information management to streamline management of nonconformances and determine the party responsible for ensuring that quality standards are ensured. Although authors provide a solution, based on an Hyperledger Fabric architecture Androulaki et al. [6], that could be promoted and applied in practical cases, they also recognise that blockchain technology in the construction industry is still in the exploring stage, thus their work needs further efforts to overcome two fundamental limitations they recognise themselves: the premise that the participants can reach an agreement on applying blockchain to manage quality information; the data on the chain have a strong tamper-proof capacity, but no guarantee exists that fraudulent data will not be uploaded. In this regard, they have also highlighted that improvements can derive from exploring the potential of co-evolution of blockchain technology with BIM and IoT technologies. Finally, Elghaish et al. [57] have developed a framework proposing blockchain technology utilisation in projects that adopt integrated project delivery (IPD) to manage economic flows. The framework would enable core project team members to automatically execute all financial transactions (or automatic payments), through coding the three main transactions of IPD projects - reimbursed costs, profit and cost saving - as functions of an IPD smart contract. The interoperability between proposed framework and 5D BIM is also investigated. In this regard, Di Giuda et al. [50] argue that blockchain can provide a trustworthy

infrastructure for implementing automatic contract executions to support BIM-based processes that relate to tenders and payments in construction phase. Blockchain applications for construction supply chain management are in their infancy, however, considering also other supply chains, there are still few examples of business value being delivered by live solutions Jensen et al. [93]. Wang et al. [192] try to address the applications of blockchain in the domain of the construction supply chain and propose a blockchain-based framework for improving supply chain traceability and information sharing in precast construction. In detail, they substitute fundamental steps in the supply chain for precast construction elements, such as asking, ordering, producing, transporting, and delivering, into functions of a smart contract (named ‘chain-code in the Hyperledger Fabric architecture). However, the proposed solution misses an integration with economic flows and implementation on a pilot project. Kifokeris and Koch [96] try to integrate also economic flows into blockchain applications in the construction sector. Since the very beginning of their research, which is currently going on, they point out Sweden’s construction supply chain as a prolific ground to develop a digital business model because general contractors and suppliers often turn to independent third-party logistics consultants. These assist them in coordinating and handling complex, recurrent, and conflicting flows consisting of deliveries of materials, arrival of incoming goods, and other sub-systems. A digital business model, according to authors, could reduce need of such intermediaries. A completely new utilization is combining blockchain technology and additive manufacturing; according to Zhu et al. [204], this integration can enable cloud additive manufacturing. The authors explore game theory application to establish prices of the 3-D printed component; for estimations, they leverage on-chain data which are automatically updated by IoT sensors that communicate with robotic printing devices to record fundamental data of the printing process.

Blockchain technology

Blockchain technology belongs to the wider family of digital ledger technology that comprises three fundamental types: centralised, decentralised (based on hubs) and distributed. Blockchain technology belongs to the latter: distributed ledger technology (DLT). This is a type of data

structure that resides across multiple computing devices, called nodes, generally spread across locations or regions. The ledger contains records (i.e. transactions) collected into blocks that are linked to each other using cryptography Pilkington [153]. A blockchain (and more generally a DLT) comprises three interdependent core layers: protocol layer, which comprises governance (consensus rules), peer-to-peer (P2P) network and ledger (record of transactions which are grouped into blocks in the case of blockchains); internet layer, which is IP or TCP; application (or data) layer, which contains relations (smart contracts essentially) that allow information to flow through the system. Without going too much into technical details, permissionless blockchains use proof-based consensus algorithms, among which, Proof of Work (PoW) and Proof of Stake (PoS) are the most common ones[15]. Moreover, permissionless blockchains are also a public blockchain, like Bitcoin and Ethereum, because anyone can join the network. On the other side, permissioned blockchains, like the Hyperledger Fabric framework [6], adopt voting-based consensus algorithms [140]. Permissioned blockchain is also called private blockchain because requires pre-verification of the participating parties within the network, and these parties are usually known to each other. A combination of both permissionless and permissioned blockchains is possible and is known as Consortium blockchain. According to the Blockchain and Distributed Ledger Observatory, the main feature of blockchain technology refers to digitizing and transforming data into the digital format. This feature combines with other properties:

- **Distribution:** information is recorded by distributing it among several nodes to ensure IT security and system resilience.
 - **Traceability:** each element (i.e. transaction) on the register is traceable in every part and can be traced back to its exact origin.
 - **Disintermediation:** blockchain platforms allow management of transactions without intermediaries, in other words without the presence of trusted central bodies.
 - **Transparency:** the content of the register is transparent and visible to everybody (in the public blockchain) as well as easily accessible and verifiable.
-

- **Immutability:** once written into the register, the data cannot be changed without the network's consent.
- **Trust:** it is built by the P2P network throughout the consensus mechanism, with no need for intermediaries even though there is no trust among parties involved.
- **Possibility to program transactions:** it is possible to schedule actions that take place when certain conditions occur on the blockchain (i.e. smart contracts).

Smart contract

A smart contract is an agreement, which is written in the machine-readable language, that can execute a part of its function by itself [181]. Self-executed functions consist of predefined actions that initiate when certain conditions (named 'trigger events') are met on the blockchain system. Commonly, smart contracts are used to automate repetitive processes relying on information stored in a blockchain (Hunhevicz and Hall 2020). However, smart contracts have also the role to interact with the blockchain to broadcast transmission and recall data stored in blockchain blocks.

2.2 Integrating smart contracts into BIM collaborative processes

Adopting the BIM methodology involves defining internal processes and collaborative processes among stakeholders to support information management during the entire building process. For a specific project, collaboration happens in the common data environment (CDE) that the ISO 19650-1:2019 defines "an agreed source of information for any given project or asset, for collecting, managing, and disseminating each information container through a managed process", where information container stands for "named persistent set of data and information within a file, system or application storage hierarchy". The same standard has also pointed out that there is at least two CDEs: the appointing party's CDE and the appointed party's CDE, which is also known as distributed CDE. The

distributed CDE is the place where collaboration among stakeholders happens, therefore there are gates to exchange information among CDEs (i.e. diamonds of Figure 2.2). The DIN SPEC 91391-1,2:2019 - Common Data Environments (CDE) for BIM projects – Function sets and open data exchange between platforms of different vendors – Part 1 and Part 2 first provide reference communication strategies among CDEs of different vendors which deploy application programming interfaces (APIs) especially to manage milestones and data drops. Generally, stakeholders that participate in the building process already have, before working on a specific project, a platform (or a database) to manage and archive information; the quality and efficiency of these tools depend on a stakeholder's needs and purchasing power. The split can depend on contractual arrangements, functional needs, and technological necessities. In the construction phase thus, a possible configuration of CDEs can be the one that Figure 2.2 depicts: general contractor, project manager (PM), client, design project team, and suppliers have their own CDE. Information exchanges that concern structural systems can include: - BIM models. - 2D shop drawings. - Technical documentation, such as inspection reports, reports of material acceptance, certificates of testing, etc. - Accounting documentation, such as bills of lading, construction journal, interim payment certificates ('stato avanzamento lavori' in Italian), etc. However, both technical and accounting documentation is generally in the form of pdf files and more often scanned paper documentation, in either case, stakeholders exchange this using certified and non-certified electronic mail in place of APIs. It follows that the sender should upload documentation, from his/her CDE, as an attachment that the receiver would download and then upload in his/her CDE. In the meantime, metadata is difficult to transfer and the trace-back of versions gets complicated. Moreover, PM and inspectors' work gets more difficult because some emails and attachments could easily go unnoticed. It is worth noting that, however, this documentation constitutes a fundamental part of the project information model (PIM, according to ISO 19650) for structural systems. We argue that criticalities we have highlighted can be overcome by introducing a tool based on blockchain technology, named DAPP, that leverages APIs of CDEs and smart contracts to support exchanges of structural-system-related documentation during the production stage of the work, with particular attention to the

execution, testing and closeout phases of the structural system.

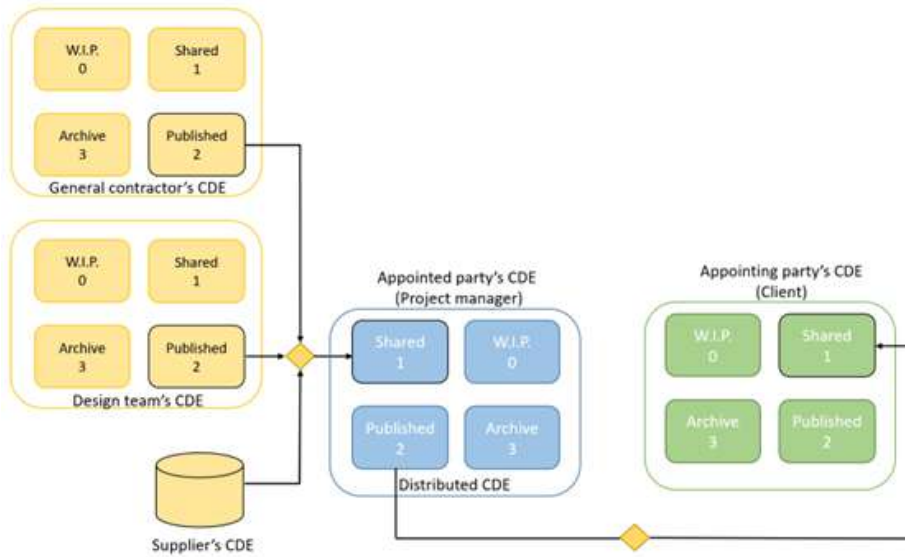


Figure 2.2. Possible configuration of CDEs in the construction stage.

We propose a blockchain-based tool to trace flows of information among CDEs and secure exchanged information containers. In detail, the tool will allow:

- To automatically transfer information containers from a CDE 1 to a CDE 2;
- To create and automatically transfer transmittal documents;
- To create Hash fingerprints of information containers that will be uploaded on the blockchain (this process is also known as notarization of documentation);
- To certify information flows' main metadata (sender, receiver, date, type of information container);
- To recall information from the blockchain to support checking and inspection activities.

Figure 2.3 illustrates the process of transferring an information container.

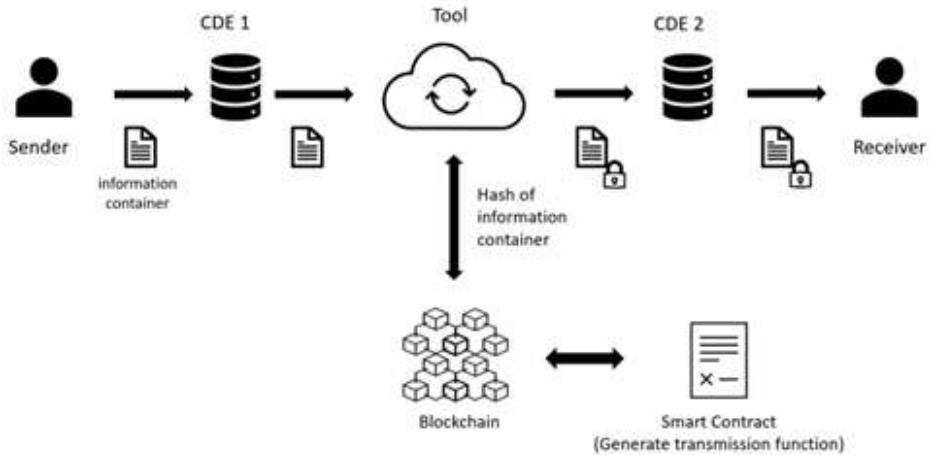


Figure 2.3. Notarization on the blockchain of information flows among CDEs.

The tool leverages APIs of CDEs to automate information exchanges. Before delivering information containers into the receiver's CDE, the tool interacts with a smart contract that generates a transmission, on the blockchain, which contains Hash fingerprints of exchanged information containers. The smart contract also allows verifying exchanged information containers (which can be files in any format: .pdf, .xls, .doc, .ifc, etc.) because this can recall information from the blockchain as Figure 2.4 depicts. We will further deepen the smart contract's capabilities in section 2.3.

Improved immutability, transparency, and reliability of structural-safety information and documentation can prevent litigations on construction sites because all significant events are traced on blockchain and can be retrieved anytime is necessary.

2.2.1 Levels of implementation of smart contracts

In our view, smart contracts can be implemented in information flows among CDEs with an increasing level of complexity and automation of operations:

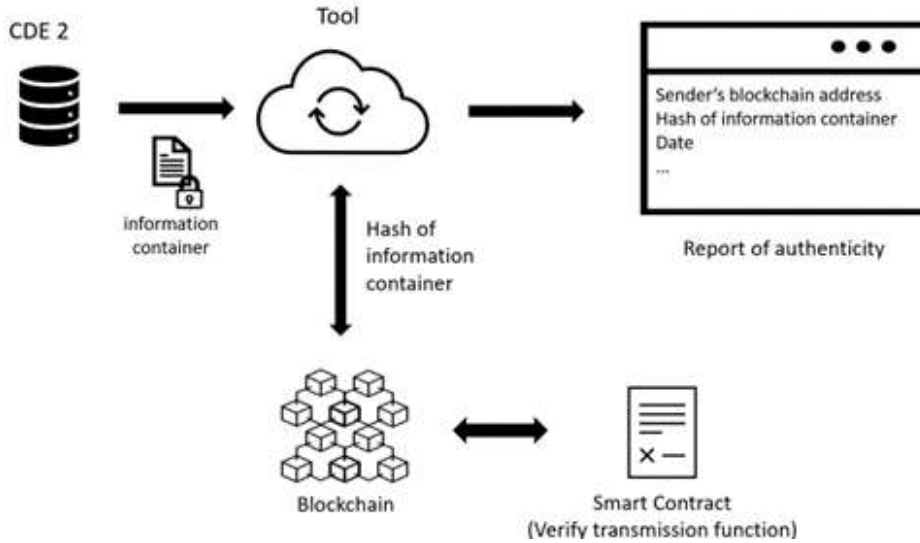


Figure 2.4. Recalling information from the blockchain.

Basic level : a smart contract automatically generates a transmission whenever there is a transfer of information containers from a CDE to another. Additionally, the smart contract records the Hash fingerprint of exchanged information containers. Figure 2.5 depicts an example of this type of implementation for the case of a third-party accreditation (Universities, testing organizations, etc.) that delivers a certificate of testing to the PM's CDE.

Intermediate level : a smart contract collects multi-party consent before exchanging information containers. This functionality can sum to the functionalities described before. Figure 2.6 depicts this type of implementation concerning the case of a PM that delivers documentation for interim payment certificates to the client and concurrently, the general contractor should approve that documentation.

Advanced level : a smart contract performs automatic assessments of exchanged information containers in terms of format, size, and structure, and data content. Figure 2.7 depicts this type of implementation for the delivery of an as-built model for the interim payment

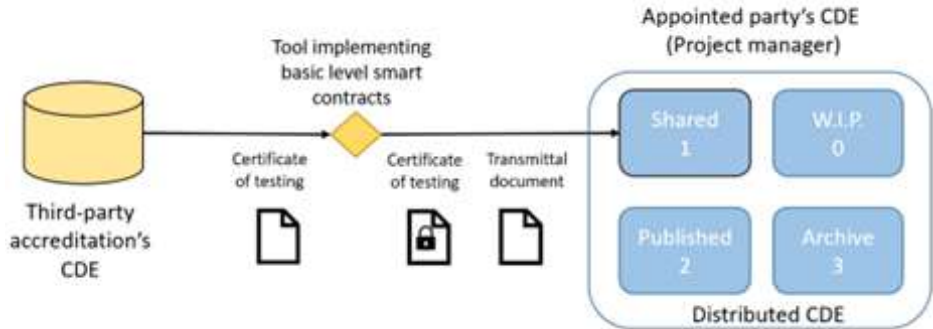


Figure 2.5. Basic level smart contract.

certificates. The implementation of IoT systems on the construction site and Artificial Intelligence algorithms for monitoring the works will allow assessing automatically validity of exchanged information containers, according to the rules set out in the smart contracts. Ultimately, an AI algorithm will be able to verify the correspondence between the as-built model and reality on the construction site, thus approving the interim payment certificates.

Levels I and II can address poor quality management of construction-site documentation that pertains to structural systems. However, we have realised that the purpose of this documentation is collecting sensible information on the construction site that could not be gathered otherwise. This information mostly pertains to temporary tasks therefore documents that contain this are generally signed by multiple stakeholders at a time to ensure sharing of liabilities. The III level addresses renovation of the traditional paper-based approach which, besides, would prove inefficient if in-situ automated construction processes of structural components, like additive manufacturing, were adopted.

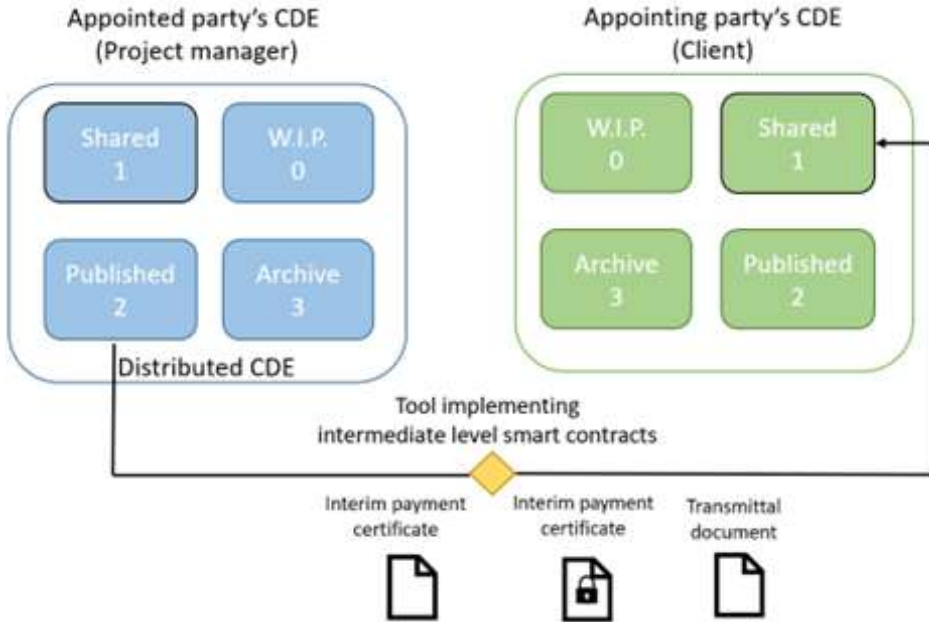


Figure 2.6. Intermediate level smart contract.

2.3 The first implementation of a basic level smart contract

To evaluate the benefits and limitations of the proposed approach, a Decentralized Application (DAPP) was implemented to exchange documents between CDEs. DAPPs are applications able to interact using smart contracts with blockchain and allow users to perform operations through ad-hoc developed user interfaces. We decide to use DAPPs based on Ethereum since this blockchain was the first to introduce smart contracts and its native language solidity is the most used. Moreover, the use of solidity guarantees the possibility to reuse the code even on different blockchains using Ethereum Virtual Machine (EVM), which is an emulator of the Ethereum blockchain that guarantees the portability of the code. In this first application, files were transmitted between two personal cloud environments that allow simulating data passing between generic

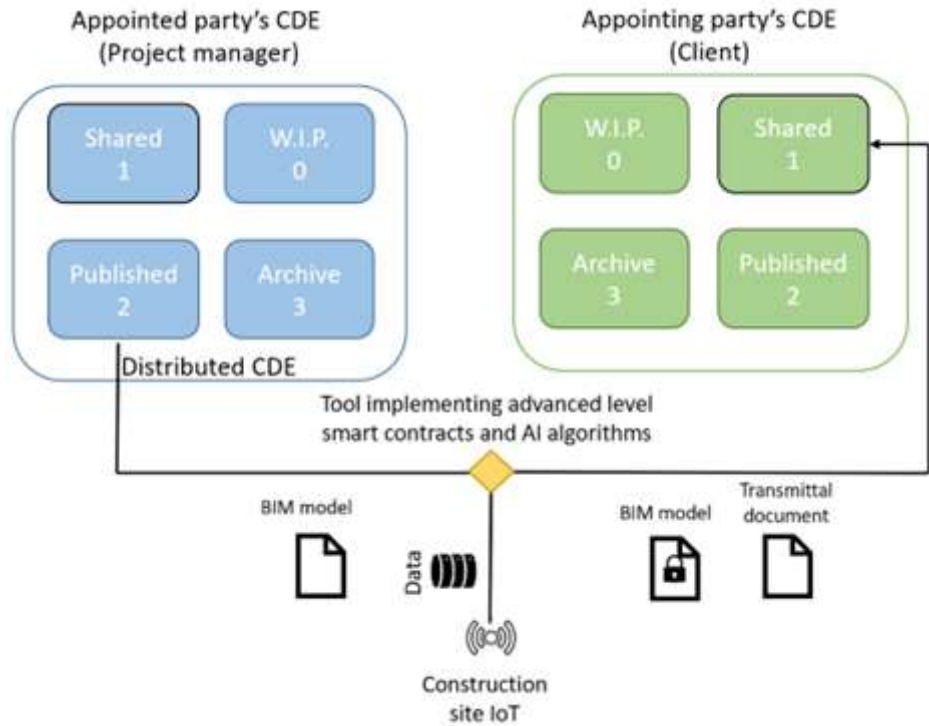


Figure 2.7. Advanced level smart contract.

CDEs. Specifically, the Dropbox API was used for data management by the DAPP.

At the beginning of the smart contract, we have defined the structure of the transmission that comprises: the address of the sender, the address of the receiver, the name of the exchanged information container, the type of exchanged information container, a Hash function of each exchanged information container, the number of the block, the date and traces of a new version of the same information container. Then, we have implemented the methods:

- Generate transmission, which is used to generate a unique code of exchanged information containers and record on blockchain all data that describe the structure of the transmission. This also allows the

management of new versions of the same files.

- Generate register of transmissions.
- Verify transmission, which is used to recall information from the blockchain to check the authenticity of transmissions and exchanged information containers.

The proposed smart contract allows to manage file authenticity and versioning of a generic file: in fact, the Hash verification function allows to verify that a generic file, which was sent in transmission ‘i’, is authentic by comparing a Hash of the file that is generated at the moment with the hash that was uploaded on the blockchain at the moment of the transmission.

2.3.1 An application to the construction process of structural systems

The assembling process of a structural system requires both practical and supervision activities to be done on the construction site. While general contractors materially produce the structure, structural and civil engineers with the role of project managers (PM) and inspection engineers oversee construction works and ensure the structural safety of works by

1. checking structural materials when they arrive on construction sites;
2. Interpreting and analysing results of tests on structural materials;
3. Inspecting structural systems to ensure compliance with safety standards and project specifications;
4. Overseeing closeout tests.

We will show to follow the potential of our blockchain-based tool concerning some of the listed activities. Figure 2.8 presents the user interface of the tool we developed. In detail, there are three areas: CDE (or database) view (1), transmission view (2), sending area, and information container verification (3). In area 1, it will be possible to access one’s information containers, both on CDE and simple database. In area 2 all transmissions have been carried out with the relevant information that refers to the validation on the blockchain (date and block) and version validity.

SQL commands allow filtering the table of transmissions to display only the items of interest. In area 3, we provide tools to calculate the Hashes of information containers; this function is used both when there are information containers to send and when there are information containers to verify once they have been received.

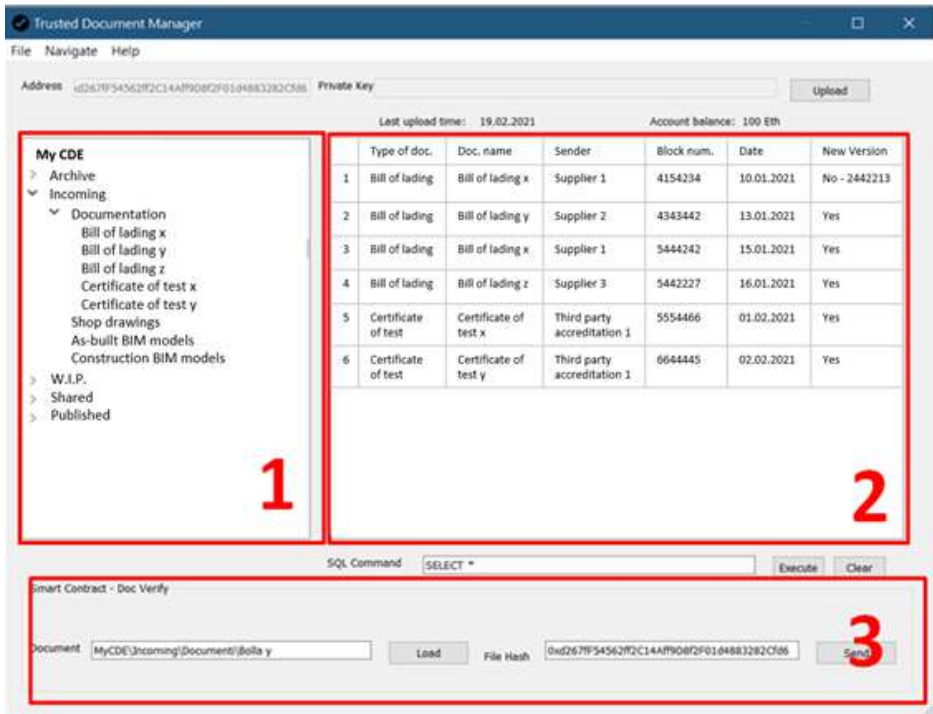


Figure 2.8. Overview of the tool’s user interface.

Concerning the example of Figure 2.5, the tool allows the third-party accreditation to explore his own CDE in the tree menu on the left of Figure 2.9; concurrently, in the table on the right he/she can see all transmissions already done and he/she can filter them with SQL commands. In detail, thus, an employee of the third-party accreditation accesses an information container (1), the tool calculates its Hash (2) and the employee transfers it to the distributed CDE of the PM (3).

For Figure 2.10, the inspector engineer (or the PM) can use the tool

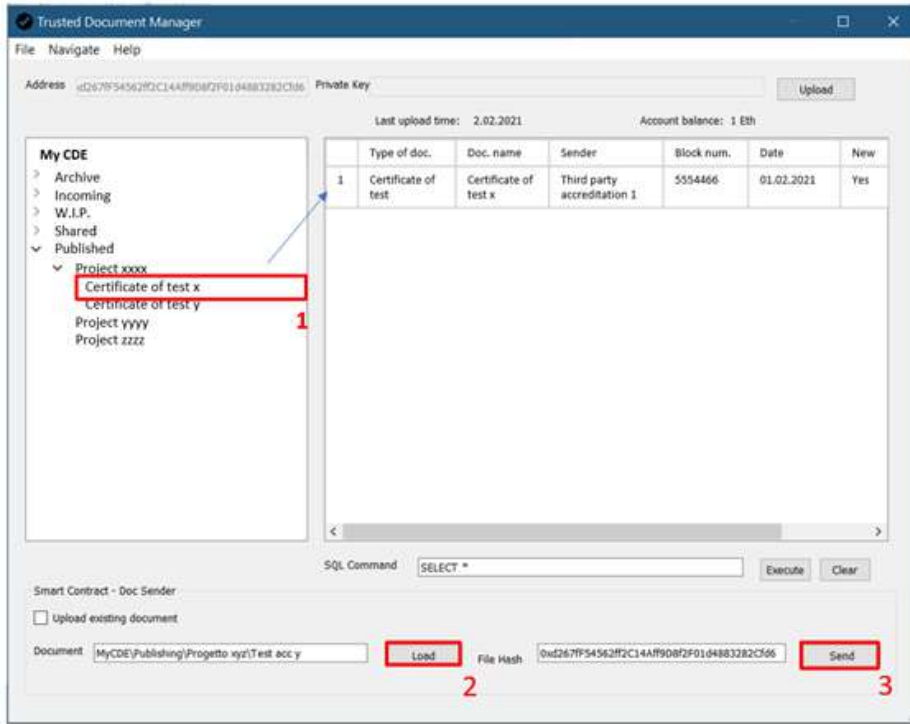


Figure 2.9. Sending information containers.

to see all information containers he/she has received in his/her CDE (the distributed CDE) with specifications of each transaction (on the right). The specifications include the sender, the block where the transmission resides, the date, and the valid version verification. He/she can also export a report of transactions. Additionally, the engineer and the PM can verify whenever the information containers received in their CDE have been certified on the blockchain. Once the structure inspector engineer has received the final report of the works ('relazione a struttura ultimata' in Italian), he/she has to certify the existence of all attachments this contains and their formal and substantial correctness. From the formal perspective, with our tool implementing a basic level smart contract, he/she can use the tool to query the smart contract that will recall information from the blockchain to verify the authenticity and validity of all attached informa-

tion containers.

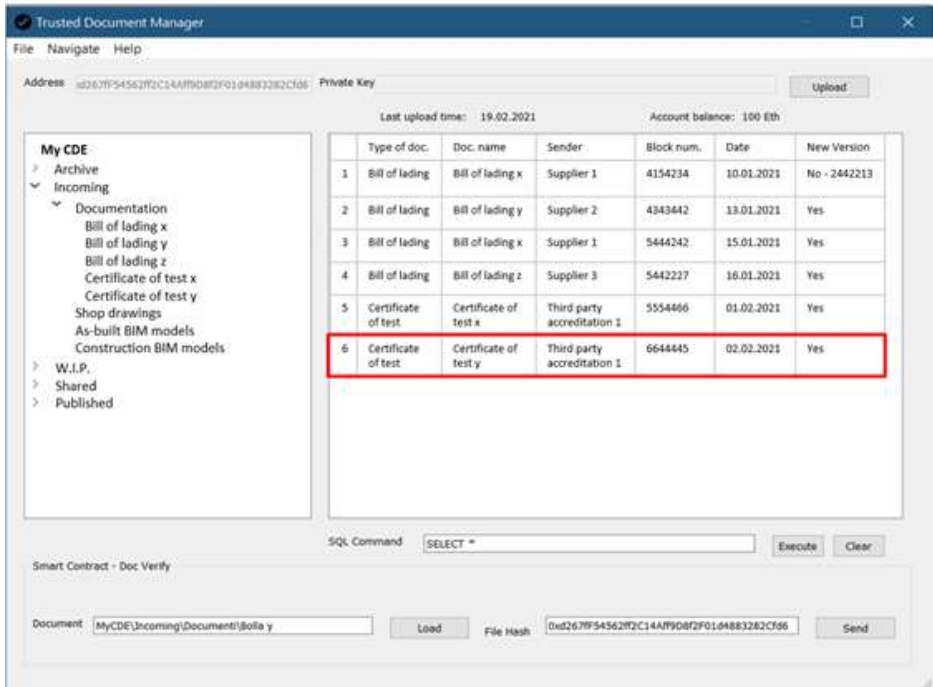


Figure 2.10. Receiving and verifying information containers.

2.4 Discussion

Our proposal aims to bypassing email, certifying on the blockchain any kind of information container exchanged and the corresponding information flow, and providing a common and reliable source of information for inspectors of the structural systems both during and following the construction process of structural systems. Preliminary testing of the proof-of-concept is presented in Table 2.1. In detail, the proposed approach has been compared to the traditional approach in terms of criticalities that arise in the exchange of information, the reliability of the exchanged information, and the transparency of the decision-making process.

Table 2.1. Recap of pointed-out criticalities and benefits implicated by our proposal

Criticalities in information exchanges	Traditional approach	Blockchain-based approach		
		Basic	Intermediate	Advanced
Need for credit to exchange information		✓	✓	✓
Delayed communications		✓	✓	✓
Sending wrong files	✓	✓	✓	✓
Sending the wrong version of files	✓	✓		
Sending to the wrong recipient	✓	✓		
Errors in archiving incoming files	✓	✓		
Reliability of exchanged information	Traditional approach	Basic	Intermediate	Advanced
Information retrievals from the blockchain ledger		✓	✓	✓
Automatic collection of signatures of actors who are involved in the process			✓	✓
Checking the correspondence between exchanged information and IoT recorded data			✓	✓
Transparency of decision processes	Traditional approach	Basic	Intermediate	Advanced
Use of certified and reliable data		✓	✓	✓
Shared and pre-agreed decision-making procedures which are supported by certified data			✓	✓

Although the use of blockchain introduces new criticalities that relate to the timing and availability of credit, traditional tools that require human intervention at several stages present a higher risk of error when transmitting the information.

Moreover, the criticalities of the blockchain-based approach can be mitigated during implementation. On the other hand, the traditional approach is not able to affect the reliability of the information transmitted and the transparency of the decisions made because the activities are mainly manual and left to the discretion of who performs them (project manager, inspector of structures, general contractor, etc.).

On the contrary, the use of an approach based on blockchain technology allows the introduction of smart contracts that perform shared and pre-established procedures to verify the information transmitted. This increases the reliability and quality of the information exchanged and the transparency of decision-making processes.

The levels of reliability and transparency that the proposed approach can ensure are related to the complexity of the smart contracts used, in fact in the case of implementation of advanced smart contracts reliability and transparency are maximized.

Finally, we conducted the first implementation using basic smart contracts. We have found that the availability of open APIs of CDEs is rather scarce, despite the indications of DIN-SPEC 91391-1,2:2019. Besides, we have already seen advantages in drafting the final report of structures, in the closeout phase, because information stored on the blockchain can support both the recovery and the verification of the reliability of construction site exchanged documentation.

AI in Vibration-based SHM: the D²-DTE approach

3.1 Introduction

Several research strands focus on damage detection and location studies. Ensuring the safety of existing structures and infrastructure is one of the most critical engineering challenges, given the aging and deteriorating infrastructure. On the other hand, the development and dissemination of innovative data analysis techniques have provided new opportunities and thus stimulated research activities on new SHM methodologies.

In *visual-based approaches* the detection strategies rely on the analysis of images of the visible surfaces of a structure. Recent contributions in this field are mainly based on the success of convolutional neural networks (CNN) in computer vision, as in [113], [190], [32], [66], and [112]. Although damage identification systems based on the vision-based approach have achieved notable accuracies, they are unable to report on the presence of non-visible structural damages that could severely affect operations and the residual service-life of a structure. In addition to this, most of the methods described in the literature require images captured at standard distances and angles, which can hardly be obtained from a few cameras, and without the intervention of a trained operator, that captures specific images for the different structural elements to be analyzed.

To avoid these limitations, in the *sensor data-processing* the monitoring

process is based on information gathered by sensors placed on a structure, that record measurements of both static and dynamic physical quantities. Within this context, the data-collection scheme can be accomplished according to a wide variety of paradigms, ranging from the classical study of static displacements measured by means of fiber optics, GPS, or corrosion sensing ([91, 119]), to the development of innovative sensing materials, that enable the continuous recording of the physical response of the structure [53, 54, 193, 68].

More generally, whenever sensors are used to detect information regarding the dynamic behavior of the structure, *sensor data-processing* methods are also denoted as *vibration-based approaches*. In the approaches of this class, data is either analyzed in the form of time-history, such in the case of acceleration data, or pre-processed by dynamic identification techniques, that enable the extraction of predictive features to be subsequently analyzed.

As instances of the former approach, Chun et al. [39] use acceleration time-histories to train an artificial neural network, the aim of which consists in the detection of thickness reductions of steel elements in a bridge. Analogously, de Almeida Cardoso et al. [43] devise an unsupervised method to directly process raw dynamic data, and identify structural novelties, validating their approach studying a railway viaduct. Abdeljaber et al. [2] use a 1-D CNN to detect damage to the connections of a steel structure, training the model to identify joint damages directly using acceleration time-histories experimentally acquired from the structure. Remarkably, the authors distribute their dataset, that can be used for benchmarking purposes in the testing of damage localization algorithms. Conversely, other approaches start from a feature extraction pre-processing phase, that allows the elaboration of raw signals, obtaining significant quantities that are then used in the monitoring of the structure. Rafiei and Adeli [158] embed a restricted Boltzmann machine within a framework that is based on a neural dynamic classification algorithm to detect damages in high-rise buildings; even in this example, the validation of the approach is made through the analysis experimentally recorded data. Notably, the same structural typology – addressed in the seminal work of Jiang and Adeli [94] – is considered in Rafiei and Adeli [159], that describe a novel unsupervised methodology that does not require the costly experimental

simulations of damages on a scaled version of the structure. In Chong et al. [37] features are extracted by a multi-phased process that integrates a wavelet decomposition and wavelet-based autoregressive models; then, the damage detection is obtained exploiting a non-linear multi-class support vector machine. Lin et al. [116] use an automatic feature extraction algorithm coupled with a CNN to localize simulated damages on a numerical model of a simply supported Euler-Bernoulli beam. Cabboi et al. [27] adopt a two-step approach - combining a principal component analysis (PCA) with a novelty-detection system - to cleanse monitored data and localize numerically simulated damage on a finite element (FE) model. Sajedi and Liang [167] define the concept of a grid environment, that allow the flexibility of taking into account different structural typologies within the same methodological framework. This environment is coupled with a CNN whose input consist in cumulative intensity measures. Finally, Azimi and Pekcan [10] implement a CNN that identifies and localizes damages considering three possible inputs: time-domain data –i.e. raw accelerometer signal –, discrete histograms to compress acceleration data, and three-parameters data that represent a continuous distribution in an extremely compressed form. Notably, the authors validate their approach considering FE models and publicly available data: both from numerical simulations and experimental recordings.

On the other hand, a widespread feature extraction approach consists in the processing of acceleration time-histories through operational modal analysis (OMA). The diffusion of this approach is founded on the observation that the extracted dynamical properties are extremely sensitive to changes in the stiffness of structures, and can so be used as predictors in damage detection systems. OMA represents a research topic of interest, given the challenges that it presents, such as: full or partial references, multiple sensors setup, non-stationary excitation, structural mode sorting, bias and modal shape scaling (Zhang and Brincker [201]). Notable examples of recent contributions in the integration or automation of OMA within continuous SHM frameworks can be found in Magalhães et al. [123], Gentile and Saisi [70], Oliveira et al. [146], Zhang et al. [199, 200].

A significant portion of scientific literature attempts to take advantage of combined OMAs and damage localization methods based on learning algorithms. In particular, this combination aims to provide robust dam-

age detection methods that make use of natural frequencies, mode shapes, and damping, or in general features extracted by OMA as input. In Zhou et al. [202] damage identification on long-span bridges is obtained through a probabilistic neural network which uses only the modal frequency information as inputs. This approach is numerically validated considering the introduction of damages to cable, bearings and main girders of two distinct FE models: the suspension Tsing Ma Bridge, and the cable-stayed Ting Kau Bridge.

Lam et al. [105] employ an artificial neural network (ANN) to localize and quantify damage from a numerical model of a steel truss system. The network is trained with a set of Ritz vectors associated with numerically simulated damage scenarios and evidences good flexibility when it came to identifying the stiffness reduction in the structure's truss elements. Similarly, Chang et al. [34] train an ANN model to localize and quantify damages, specifying the affected story, of a seven-story building.

Reviewing the contributions proposed in the scientific literature, it can be pointed out that most of the cited research efforts provide only limited details about the occurred damage in the case of complex structures; or, alternatively, an in-depth characterization of the occurred damage is achieved only simple structures (e.g. a few structural elements) analyzed as independent structural systems.

In addition, most of the proposed approaches are based on the hybridization of multiple interacting numerical procedures. The resulting intrinsic complexity makes often challenging the effective implementation of a given solution method. In this context, the *less is more approach* (LIMA) – originally proposed in optimization literature [138, 137, 24] – attempts to make a methodology as simple as possible, but at the same time, more effective than the current state-of-the-art.

Following this consideration, this chapter proposes a SHM framework, named Damage-Detection Decision Tree Ensemble (D²-DTE), based on a vibrational approach coupled with a decision trees ensemble (DTE [69]) learning method, able to respond to LIMA needs. In details, following a vibration-based feature acquisition, the learning algorithm infers the relationship between the dynamic structural properties of a given complex structure and the corresponding detected single and/or multiple damage, with an high level of accuracy. Within the proposed framework, FEM

is used to: create a database of "pathological" (damaged) structural responses; test the performances of the DTE learning method; and simulate the occurrence of damage to real case structures. Hence, the main research objectives are:

- to investigate the possibility of identifying damage with different localization accuracy and extent, down to the scale of a single structural element;
- to explore the learning capabilities of DTEs, tailoring their algorithmic procedures to the SHM objectives;
- to assess DTE performances in terms of classification agreements between the damage prediction and the real assessment, the confidence of probabilistic predictions, and damage localization distances.

3.2 D²-DTE methodology

The basic idea behind the proposed D²DTE SHM methodology here is that, for any single structure, it is possible to create a large database of virtual 'pathological' and 'non-pathological' structural responses, gathered either from a calibrated FE model, or laboratory tests, through which, numerous damaged scenarios of the structure are generated and recorded. Then, this large database can be used to train an ML model that is able to process sensor data from an actual structure and identify any pathological responses, highlighting the position and extent of occurred damage on structural elements.

In particular, as depicted in Figure 3.1, the methodology is divided in two main phases: a set-up phase, and the deployment phase. During the set-up, preliminary operations are performed on the target structure to be monitored, i.e.: *FE modelling*, *damage simulation*, and *data preparation*, leading to the *DTE training* and *testing outcome*. The deployment phase consists in the application of the trained learning model to analyze data recorded on the monitored structure in order to timely produce health assessments.

The set-up phase is thoroughly described in this Section, and it is composed by:

- 1) *FE modelling*;
- 2) *damage simulation*;
- 3) *data preparation*;
- 4) *DTE training*;
- 5) *DTE performance evaluation*.

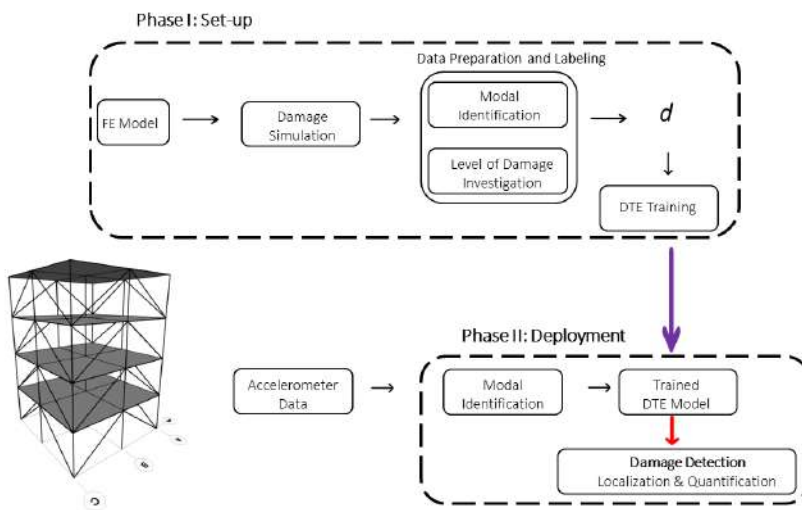


Figure 3.1. Depiction of the D²-DTE methodology.

The first two steps – Section 3.2.1 – consist in the modelling of a structural system of interest and in the choice of a simulation strategy to introduce in the model several damage conditions. In the *data preparation* step – Section 3.2.2 –, based on the FE model and *damage simulation* strategy defined in the first two steps, the structural response of the system is recorded in the form of a vector of dynamic properties \mathbf{d} corresponding to each damage scenarios generated; the locations of those damages are then labelled according to a pre-defined level of detail. In the *DTE training* – Section 3.2.3 –, the vectors of dynamic properties obtained from the damage scenarios are used as samples to let the DTE learn the association rule

between a specific dynamic structural response \mathbf{d} (denoted as *input*) and the corresponding health assessment of the structure (denoted as *output*).

To evaluate the reliability of the performances achieved by the trained DTE (using the metrics described in details in Section 3.2.4), the testing phase considers a "new" dynamic structural response vector \mathbf{d} along with the corresponding actual damage configuration a^d (damage location and extent), and compares the predicted damage configuration a_{pred}^d with a^d . The "new" dynamic structural responses used in this step can either gathered by a different generated (damaged) FE model of the target structure, or by data collected from a physical structure, as done in the deployment phase. This validation phase represents a common practice in the context of ML for SHM, and its goal is to assess the accuracy and robustness of the predictor. It is duly noted that the validation represents a similar situation of a possible SHM scenario, with the main difference being that in a real deployment phase the actual damage configuration a^d is not known a-priori.

To this aim, the learning method validation step reported in Section 3.3 includes three different test cases: (i) damage localization accuracy determination based on FE numerical models (ii) damage identification and quantification using the IASC-ASCE benchmark [95, 28], and (iii) damage localization and quantification using the Qatar University Grandstand Simulator (QUGS) [2, 9]. In particular, the three test cases are designed to account for the variations of performances with respect to: different damage localization scales, source of data (numerical or physical) and analysis of input data derived from increasing levels of structural complexity.

3.2.1 Structural modeling and Damage simulation

The structural typologies investigated in this work include two reinforced concrete (r.c.) frames (2D and 3D frames) and a 3D steel truss frame, belonging to IASC-ASCE benchmark and the testing cases from QUGS. These structural typologies are considered mainly for two reasons: the importance of traditional construction paradigms with concrete, and the possibility to highlight differences between them in the D²-DTE validation process. The corresponding FE structural models are generated by means of the FE code OpenSees [130]. Each one of the structural elements in the r.c. frames or steel truss is modeled using native elastic beam

or column elements [129]; further details of the structural FE models are given in the description of each testing case reported in the corresponding subsections. With the aim of generating a suitable training data-set for the DTE learning algorithm, it is firstly necessary to incorporate damage scenarios in the target structure modeled using FE; this can be achieved either using (i) an appropriate FE damage modeling strategy, or (ii) by adopting available sensor recordings measured during laboratory testing.

In particular, different FE modeling strategies were adopted in this study according to the structural typology considered. In the case of the r.c. structures, the simulated damages belong to two different classes: concrete cracking and joint damages. Cracking phenomena are implemented in the model by introducing a reduction factor related to the cross-section inertia of each damaged element, α_{rc} ; in this way, the "local" stiffness (of the structural element) is reduced and, as a consequence, the global dynamic structural behavior changes accordingly. The extent of cracking is taken into account through three different damage levels (i.e. corresponding to three element stiffness reductions): undamaged, moderate cracking, and severe cracking. A set of α_{rc} factors is defined for each level, and it is assumed that the element is: undamaged when the local stiffness reduction is between 0% and 15%; moderately damaged with a local stiffness reduction between 15% and 75%; and severely damaged when the local stiffness reduction is greater than 75%. The relationships between the reduction factors and damage levels are set out in Table 3.1.

The damage affecting r.c. beam-column connections is not categorized in terms of severity and is introduced as perfect hinges into the structural joint. In order to evaluate the damage affecting the endpoints of each structural element converging into a given joint, a generic node N is modeled as four different connecting nodes (N^I , N^{II} , N^{III} , and N^{IV}) linked by a rigid body constraint to N (see Figure 3.2). Regarding steel structures, damage often can occur due to corrosion phenomena: for these cases the damage is introduced as a reduction in the cross-section of the structural element. The adoption of this kind of damage for the steel structure is mainly related to two observation: 1) steel is characterized by higher mechanical performances, meaning that the cross-sections of common commercial profiles are relatively small. As a result, minor variations in the cross-section of an element could correspond to major changes in its structural behavior;

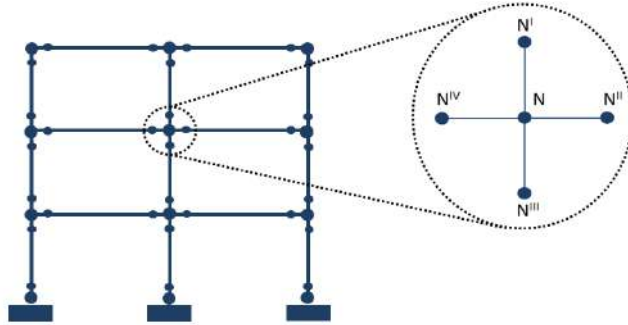


Figure 3.2. Representation of the joint, modeled as four constrained connection nodes.

and 2) changes in cross-sections have a significant effect on the structural performances of truss structures (a widespread standard in steel constructions), whose stresses are mainly due to axial forces. As for the cracking damage in the r.c. structures, the reduction in the steel elements' stiffness is again defined using a reduction factor α_{st} , in accordance with Table 3.1.

Table 3.1. Summary of Element stiffness reductions for damage simulation in r.c. and steel structures.

α_{rc}, α_{st}	Local reduction (%)	Damage severity
1	0%	Undamaged
0.9	10%	Undamaged
0.85	15%	Undamaged
0.55	45%	Moderate damage
0.45	55%	Moderate damage
0.25	75%	Severe damage
0.20	80%	Severe damage
0.10	90%	Severe damage

3.2.2 Training data generation

Given a specific structural model, the *training data generation* phase simulates a broad set of damage configurations, recording the resulting dynamic response of the system. The recorded vector of dynamic properties of the system, \mathbf{d} , consists of modal analysis outcomes associated to the first three mode shapes and frequencies.

This decision is related to the observation that the higher the mode shape, the less influence it has on the dynamic behavior of the structure. Consequently, selecting data from the first three mode shapes and frequencies aims to balance the trade-off between computational effectiveness and the use of a denser dataset, i.e., a higher number of mode shapes and frequencies. Section 3.3.1 contains a brief discussion relating to the accuracy of the DTE in this regard. In particular, denoting the i^{th} period with T_i , the k^{th} mode shapes related to the j^{th} set of recorders (placed on the frame structure) with ϕ_{kj} , and \mathcal{L} the number of different set of recorders, then \mathbf{d} is obtained as

$$\mathbf{d} = (T_1, T_2, T_3, \phi_{11}, \phi_{21}, \phi_{31} \dots, \phi_{3\mathcal{L}}). \quad (3.1)$$

For element cracking (in r.c. frame) and cross-section reductions (in steel truss), the number of possible damage configurations depends directly on three factors: the number of structural elements in the system (N_{el}), the possible α values (N_α), and the number of simultaneous damages (N_{sim}) on the structure. The total number of damage configurations, Dmg_{tot} , is then obtained as the product of the number of N_{sim} -permutations with repetitions of N_α elements, times the number of N_{sim} -combination without repetitions of N_{el} elements, thus giving:

$$Dmg_{tot} = N_\alpha^{N_{sim}} \cdot \frac{N_{el}!}{(N_{el} - N_{sim})! \cdot N_{sim}!}. \quad (3.2)$$

Differently from crackings and section reductions, damage severity stands undefined for joint damages. Consequently, Dmg_{tot} can be obtained as

$$Dmg_{tot} = \frac{2 \cdot N_{el}!}{(2 \cdot N_{el} - N_{sim})! \cdot N_{sim}!}, \quad (3.3)$$

considering that the number of connections nodes is twice the size of N_{el} ,

as depicted in Figure 3.2.

Hence, while generating training data, each one of the Dmg_{tot} damage configuration is modelled according to the specific structural typology (r.c. or steel) and with respect to the simulation paradigm discussed in Section 3.2.1. To each of such damage scenarios, the structural model associates a dynamic response that is then recorded in a vector \mathbf{d} (as in (3.1)) to be used as input in the training of the DTE.

The training of the DTE – and in general of all supervised learning methods – is based on the principle of gathering the relationships connecting input and output pairs of a training set, in order to automatically produce a predicted response in presence of new (real, recorded) input data. In the context herein described, the input is given by the vector \mathbf{d} of dynamic properties resulting from a given damaged configuration, and coherently, the output corresponds the health assessment of the structure, a^d . Such an health assessment can be formulated in many ways: detecting different damage localization scales and/or including damage severity.

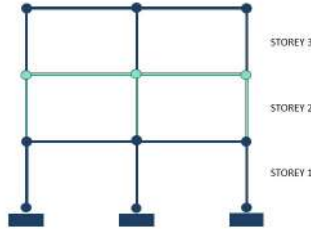


Figure 3.3. Representation of the story localization scales for the cracking phenomena and joint damage.

Unlike available approaches in which the damage detection is often limited to the story level (as in the case of complex structures, e.g. Lin et al. [116]), or it is very accurate but limited to simple structural elements (e.g. Cabboi et al. [27] and Chang et al. [34]), the localization attempts performed in the D²-DTE aim to identify the occurred damage according to different levels of detail. In particular, the overall D²-DTE outcome ranges from the identification of the story at which the structural element damage has occurred – especially in multi-story r.c frames –, to the single structural element affected.

Three different levels of detail are thus considered for damage detection in D²-DTE training data generation for the two damage types (i.e. element cracking and joint damage). In the case of the cracking phenomena, the levels are:

- the **story extent**: indicates the story to which the damaged element belongs (Figure 3.3);
- the **floor – beam level**: indicates the single damaged element (if it is a column) or the floor beam to which the element belongs (Figure 3.4, a);
- the single **structural element**: indicates the affected element (Figure 3.4, b).

For the joint damage type, the three levels are:

- the **story extent**, indicates the story to which the damaged joint belongs (Figure 3.3);
- the single **node** scale: indicates the node affected by the damage (Figure 3.5, a),
- the **hinge** scale which identifies the joint which is responsible for plastic hinge activation (Figure 3.5, b).

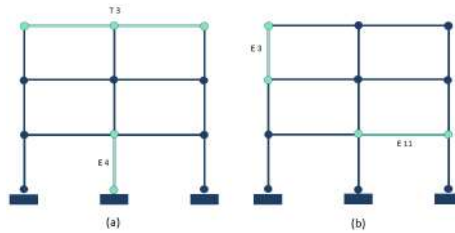


Figure 3.4. Representation of the column and floor-beam (a) and element (b) localization scales for the cracking phenomena.

Additionally, the health assessment can possibly include an estimation regarding the damage severity.

The last step of the *training data generation* focuses on a data augmentation procedure to reduce overfitting and test the performances of the DTE in common applications where uncertainty and errors affect the acquisition data. More specifically, each vector of dynamic properties \mathbf{d} is modified by adding random Gaussian noise. In this phase, noise is added according to a normal distribution, with a mean of zero and a standard deviation of $\sigma > 0$, $N(0, \sigma)$.

In particular, starting from an arbitrary vector \mathbf{d} , the corresponding noisy data, $\tilde{\mathbf{d}}$, is obtained as

$$\tilde{\mathbf{d}} = \mathbf{d} + \mathbf{d} \cdot \tilde{X}, \quad (3.4)$$

where \tilde{X} is a diagonal matrix whose non-zero components are independent realizations of a random variable distributed as $N(0, \sigma)$.

This procedure is conducted in such a way that each single dynamic property is affected by a variation around its normalized value, with an expected maximum magnitude of either 3%, 6%, or 9%. This strategy successfully defined three different levels of disturbance in the analyses.

Additionally, the Gaussian noise considered in the data augmentation phase is used to obtain the samples belonging to Training and Testing sets. Since eq. (3.2) and (3.3) generate different number of damage configurations in each scenario, sets of total records (Testing plus Training) of proportional size are populated with a number of samples equal to $50 \cdot Dmg_{tot}$. More specifically, the samples are divided into two disjoint groups, Training and Testing, and then the two groups are perturbed introducing the Gaussian noise as specified by equation (4.4). As a fortiori sanity check, the numerically simulated datasets obtained through data subdivision and augmentation present analogous relative differences and cosine similarity values to those extracted from the experimental dataset discussed in Abdeljaber et al. [2], and Avci et al. [9]. In particular, the testing reported in Sections 3.3.1-3.3.1 considers a 50% – 50% Training-Testing split. Differently, throughout the whole numerical experiments of Sections 3.3.2 and 3.3.3, the testing process follows a 5-fold validation approach, thus implying that the Training-to-Testing size ratio is 4 to 1. To investigate the damage localization capability of the D²-DTE, the numerical validation of Section 3.3 reports on the achievable levels of responsiveness in structural health assessment.

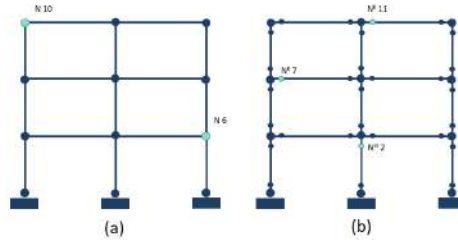


Figure 3.5. Representation of the node (a) and hinge (b) localization scales for the joint damage.

3.2.3 DTE Training

Decision tree ensembles belong to the class of supervised learning approaches. As such, starting from a set of known input/output pairs (the training set), their goal is to produce a function that maps a certain input into its associated output. In the learning paradigm discussed here, the input \mathbf{d} is an m -dimensional vector of structural dynamic properties, and the output is a predicted health assessment for the structure, a^d .

In addition, according to the ensemble learning paradigm, a collection of weaker learning models should be aggregated to obtain a combined version with a better predictive performance [163]. In the present Chapter, the ensemble is obtained by aggregating classification trees with the bagging meta-algorithm, depicted in Figure 3.6. This technique, discussed in Breiman [21], starts by generating L different samplings – uniformly at random –, $\{D_i\}_{i=1}^L$, of the training set, D .

In the SHM context here embraced, D_i is a collection of pairs $D_i = \{(\mathbf{d}_1, a^{d_1}), \dots, (\mathbf{d}_h, a^{d_h})\}$, where each single \mathbf{d}_j , $j = 1, \dots, h$, is as in (3.1), and a^{d_j} is its corresponding health assessment. Subsequently, each sample D_i is used to obtain a classification tree, \mathcal{T}_i [22]. After this training phase, the DTE is obtained by aggregating the \mathcal{T}_i s: given a new vector of dynamic properties $\bar{\mathbf{d}}$, the ensemble model returns the assessment provided by the majority of the \mathcal{T}_i s.

The hyper-parameters characterizing the DTE are obtained through a preliminary tuning. As a consequence, the total number of trees in the ensemble is set to 30 while each single tree makes use of Gini purity index and a *best-splitting strategy*. Additionally, each set D_i is obtained sampling

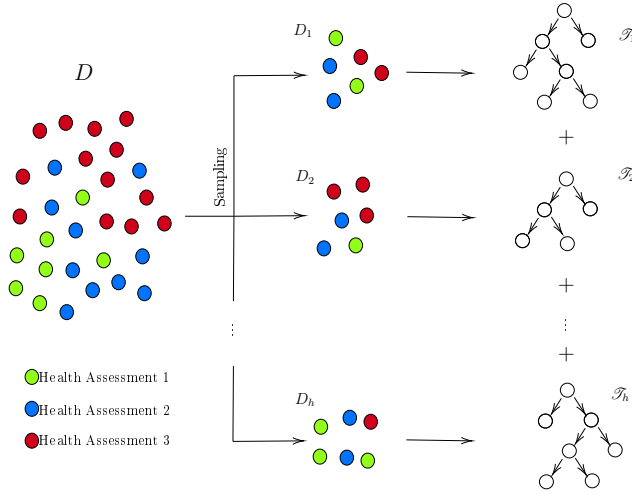


Figure 3.6. Depiction of the decision tree ensemble obtained with the bagging meta-algorithm.

uniformly with replacement from D exactly N elements, with $N = |D|$. Thus, for large values of N , each sampling D_i is expected to have the fraction $(1 - 1/e)$ ($\approx 63.2\%$) of the unique examples of D , with the rest being duplicates [8].

3.2.4 DTE performance estimation metrics

The prediction capabilities of the DTE are evaluated considering three different classes of evaluation criteria: *accuracy*; *confidence of probabilistic predictions*; and *localization errors*. The goal of accuracy is to appraise the degree of agreement between the output provided by the D²-DTE and the real health assessment, which is achieved by counting the percentage of correct predictions over the total number of cases tested.

In particular, *Accuracy* counts the percentage of cases in which a_{pred}^d is equal to a^d . Consequently, this accuracy evaluation follows the levels of detail described in Section 3.2.1.

In contrast, in terms of the confidence of the probabilistic predictions, the goal is to evaluate the confidence levels of the different assessment by the set of \mathcal{T}_i s. More specifically, given a certain damage scenario, the

Tree Ensemble associates a confidence value $P_a \in [0, 1]$ to each possible assessment a^d . The confidence of probabilistic prediction consists in the comparison of the relative frequency (in the Tree Ensemble) of the correct assessment (PT in Section 3.3) to that of the output assessment, i.e., the most common among the \mathcal{T}_i 's (PP). The higher and closer are the two values, the better is the prediction. These values can then be used as likelihood estimates for each possible assessment outcome.

Lastly, the prediction of the DTE is evaluated from a damage localization accuracy standpoint. For each test case that involved damage, the distance (in meters) between the actual damage location in the structure and that produced by the tree ensemble is measured. In particular, as set out in Figure 3.7, in the case of single damage, it is evaluated the distance d' between the center of mass of the structural element identified as "damaged" by the predictive model (E2-5 in Figure 3.7, a) and the actual damage position (element E1-4 in Figure 3.7, a). Similarly, in the case of more than one site of damage, the distances are computed with respect to the closest predicted damage location from each center of mass of an element with actual damage. As shown in Figure 3.7 (b), the computed distances are, respectively: d''_1 and d''_2 , separating E1-4 (actual location) and E2-5 (predicted location); and E10-11 (actual location) and E7-8 (predicted location). It is duly noted how this metric is strongly scale dependent. In the case of damage localization at the story level, the error distance is computed between the center of mass of the predicted and the actual position of the story affected by the damage. In the numerical validation, the localization error is denoted as Error-DIST.

3.3 Numerical Validation

The validation of the D²-DTE framework herein adopted is organised through three test cases, characterized by the analysis of three corresponding data-sets: (i) damage simulated using FE models of r.c. and steel truss frames, (ii) the IASC-ASCE structural health monitoring benchmark problem [95, 28], and (iii) the QUGS dataset.

The first test case consists in the simulation and subsequent localization of a diverse set of damage configurations introduced in the numerical models of three different structural typologies, namely: a 2D r.c. frame, a

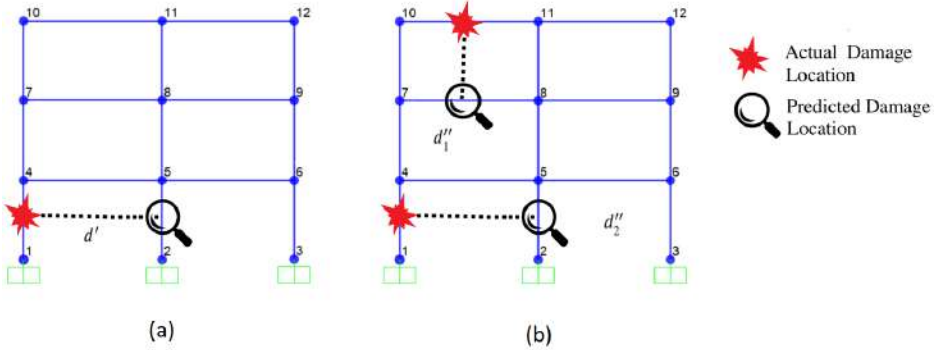


Figure 3.7. Depiction of the error estimation in relation to the damage localization.

3D r.c. frame, and a 3D steel truss structure. The aim of this first test case is to appraise the localization performances with respect to the definition of the three different levels of details described in Section 3.2.2.

On the other hand, the test case of the IASC-ASCE benchmark allows the evaluation of damage detection effectiveness in two well-established numerical models characterized by 12 and 120 DOFs. The aim of this test case is two-fold: the first is to localize damages with respect to models characterized by a different number of DOFs, and the second is to use a well-established benchmark that allows the direct comparison of the performances with other research efforts.

Lastly, the use of the data recorded on the QUGS enables the testing of the framework in a set-up closer to the deployment phase, in which the data used for both the training and the testing of the DTE are obtained as two distinct sets of measurements recorded on a physical structure. As an additional value, just as for the IASC-ASCE benchmark, the diffusion of the QUGS allows for a direct comparison of the damage localization performances of our framework with other damage localization approaches.

3.3.1 R.C. frames and 3D steel truss system

The structural models adopted in the first tranche of numerical tests are developed using the FE code OpenSees [130] and include two r.c. frames

(2D and 3D) and a 3D steel truss structure. For each structure, the modal properties are obtained simulating the presence of three axis accelerometers in a set of measurement points.

The 2D r.c. frame is characterized by three storeys (height 3 m) and two spans (length 4 m). The rectangular sections for the beams and columns are 30×50 cm and 30×30 cm, respectively, as depicted in Figure 3.8.

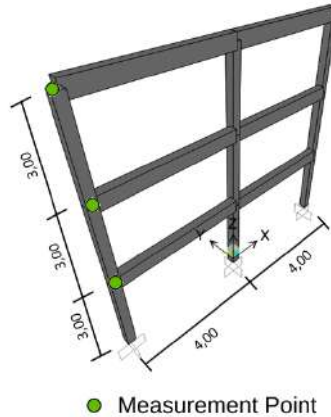


Figure 3.8. 2D r.c. frame considered in the numerical validation.

The 3D r.c. frame is composed by three storeys (height - 3 m) and two spans along the x direction (length - 5 m), and three spans (length - 4 m) along the y direction. The rectangular cross-sections of the beams and columns are 30×50 cm and 30×30 cm, respectively, as depicted in Figure 3.9.

As shown in Figures 3.8 and 3.9, in both r.c. frame structures the modal properties are obtained in correspondence of three different measurement points, one per each storey, taken on corner pillars belonging to a same vertical axis.

Each one of the structural elements in the r.c. frames are modeled using OpenSees' native elastic beam column elements [129], while the columns are clamped to the base. Additionally, diaphragm constraints are separately applied on the set of nodes lying on each story, according to a rigid-floor assumption by means of the native OpenSees command *equalDOF*.

Lastly, the 3D truss is a 8 m-high triangular truss structure, with equal-

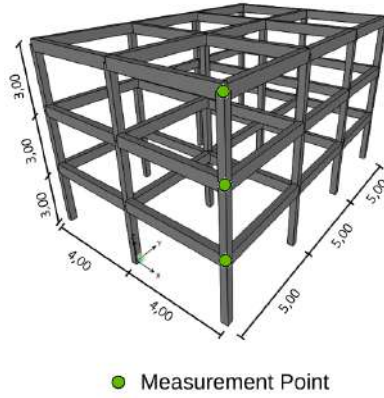


Figure 3.9. 3D r.c. frame considered in the numerical validation.

sided L-section elements with the dimensions $30 \times 30 \times 3$ mm, as represented in Figure 3.10.

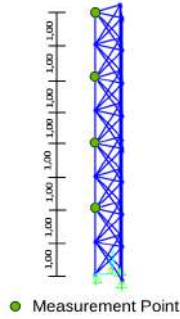


Figure 3.10. Depiction of the 3D truss structure.

For the case of the triangular truss structure, the modal properties are obtained considering a total of four measurement points placed every 2 meters of a same vertical direction (see Figure 3.10).

Preliminary analysis of the input features

As detailed in Section 3.2.2, the input features of the D^2 -DTE are first three vibration modes of the structure. From a methodological point of

view, different input combinations, as a function of occurred damage, can be considered, and these either reduce or enrich the complexity of the input dataset. To evaluate the effect of different combinations of periods and mode shapes, on the overall accuracy (the relationships connecting the input features with the predicted damage performances), a preliminary test case is generated on the 2D r.c. structure considering a single-cracking damage type.

The numerical results reported in the following refer to the floor-beam scale damage localization, with 6% random Gaussian noise. Table 3.2 reports the results of this comparative analysis, with "X" implies that the single feature has been considered in the input, "-" otherwise. Analyzing the results, it should be noted that the configurations that consider only one of the vibration modes (either I, II or III) make inaccurate predictions (between 50% and 59%). Similar performances, although less remarkable, occurred in the case of an arbitrary combination of two of three vibration modes, which produced an accuracy of 73.9%, 78.4% and 77.7%, respectively. It is possible to observe that the vibration periods alone are unable to represent the statistical variability of the input/output relationship (33.6% accuracy), but the modal shapes are more sensitive regarding damage localization (86.4% accuracy), given their spatial interpretation. This difference in predictive quality was expected, as periods aggregate the structural behavior in a "global" measure, while modal shapes provide "local" and geometrical information, in line with the requirements of a localization problem. Ultimately, the highest accuracy is obtained when including the complete set of input features, and this will therefore be considered in the numerical validations set described in Section 3.3. In contrast, the different effectiveness of the modal shapes as input feature is of particular interest in terms of their potential use in real-case scenarios (as identifications from the sensor data).

2D concrete frame

The first step in the numerical validation consists of damage detection, localization and estimation in the 2D r.c. frame.

This test case includes four different types of damage scenarios: the

presence of a single cracked element, the presence of two cracked elements, single joint damage, and damages affecting two joints. The results achieved for the detection of a single cracked element are reported in Table 3.3, highlighting that the D²-DTE exhibits a very high accuracy for the story scale and low noise level, while, as expected, higher levels of both detail and noise are correlated with reduced accuracy.

In the case of 6% noise, the detection of a single cracked element is managed properly by the DTE, which produced an accuracy of 83% on the element scale (with damage). This performance is encouraging, detecting that the average distance separating the predicted and the actual damage location (Element scale) is less than 0.74 m for 6% noise, and less than 0.01 m and 1.14 m for 3% and 9% noise, respectively. This behavior suggests that, in a monitoring scenario, it may be possible to define a relatively small area in which the damage is probably localized, even when there are prediction errors.

Finally, the prediction output of the single trees in the ensemble can be evaluated by studying the distribution of the confidences for each health assessment (as referred to in Sections 3.2.3 and 3.2.4). A comparison of the PP and PT values revealed that, as expected, when the prediction confidence is high, the corresponding accuracy is also satisfactory, while lower confidences are correlated with a greater number of errors. In terms of the detection of the joint damage, Table 3.4 reports accuracy of over 92% for all noise levels. These results are supported by the observation that joint damages severely affect modal shapes and are thus easier to detect and localize. In fact, considering the Hinges localization scale, the average localization error is lower than 0.5 m. The quality of the performances exhibited by the DTE is consistent, including in terms of label ranking and the difference between the confidence of the true assessment (PT) and the predicted assessment (PP).

The next two analyses are characterized by the simulation of two different simultaneous damages in the structure ($N_{sim} = 2$): the first considers two cracked elements and the second two joint damages. In contrast to the single damage case, the study of a two-damage-site configuration introduces a degree of difficulty related to the more complex interactions between the dynamic properties and the health assessment. As reported in Table 3.3 concerning the classification of two cracked elements, the DTE

achieved lower accuracy (in percentage), ranging from 95% in the easiest case (story scale, 3% noise level) to 49% (element scale with damage intensity, 9% noise). The worse performances can be related to the high number of possible assessments generated by the likely damage locations and intensities. A further indication of this change in performance is the fact that increasing the level of specificity in the localization and damage scales, significantly reduces the PT and PP values, and so the confidence level of the DTE.

As set out in Table 3.4, the results obtained for the two joint damages evidence behavior that is consistent with that observed in the single case. Regarding the cracking phenomena, however, the algorithmic performances did not produce the same reduction in accuracy. The greater confidence in the results is reflected in the fact that the PP and PT values are close and higher than those reported in Table 5. Notably, these performances are not reasonably affected by the noise levels.

3D concrete frame

The D²-DTE simulation results are divided based on the type of damage considered and regard either the presence of a single cracked element in the structure or the activation of a single plastic hinge in the joint connection. As also done for previous simulations, the experiments account for three noise levels: 3%, 6%, and 9%. The results are summarized in Tables 3.5 and 3.6. It is notable that the accuracy for the detection of a single cracked element is 86% for the 9% noise level and also for the element with the damage scale. Conversely, in the numerical experiments, the accuracy is reduced for the simplest case of the story scale with the 3% noise level. This behavior can be related to the different number of input examples in the training dataset, which may have led to an underfitting phenomenon.

As for the 2D frame, these performances suggest that, even in the case of an erroneous localization, the actual damaged element will be close enough to enable the predicted locations to be used to define a small area where the damage is most likely to be found.

The results obtained on the detection and localization of a single joint damage in a 3D r.c. frame (Table 3.6) show a high reduction in performance for the hinge scale localization compared to the 2D frame. This is because the modal shapes, in the presence of 12 columns per story and,

Table 3.3. Summary of performances on 2D r.c. frame, cracking damage.

Level of detail Damage severity Noise Level	Story				Floor beam			Element							
	No 3%	6%	9%	3%	No 3%	6%	9%	No 3%	6%	9%					
Single cracked element:															
Accuracy	96%	90%	85%	96%	90%	89%	93%	87%	80%	90%	83%	76%	91%	83%	76%
PT	0.92	0.83	0.75	0.97	0.80	0.79	0.86	0.77	0.71	0.95	0.72	0.64	0.95	0.72	0.64
PP	0.94	0.88	0.82	0.97	0.85	0.84	0.87	0.82	0.78	0.95	0.78	0.73	0.95	0.78	0.73
Error - DIST [m]	0.01	0.05	0.11	-	-	-	0.46	0.86	1.10	0.01	0.74	1.14	-	-	-
Two cracked elements:															
Accuracy	95%	88%	82%	74%	86%	76%	-	-	-	90%	60%	48%	76%	62%	49%
PT	0.89	0.79	0.71	0.60	0.72	0.64	-	-	-	0.75	0.42	0.29	0.67	0.48	0.32
PP	0.92	0.84	0.77	0.67	0.78	0.72	-	-	-	0.79	0.52	0.43	0.74	0.58	0.46
Error - DIST [m]	0.16	0.33	0.52	-	-	-	-	-	-	0.71	1.26	1.48	-	-	-

Table 3.4. Summary of performances: 2D frame, joint damages.

Level of detail	Story			Node			Hinges		
Damage severity				n.d.					
Noise Level	3%	6%	9%	3%	6%	9%	3%	6%	9%
Single joint damage:									
Accuracy	97%	97%	95%	97%	94%	92%	98%	97%	96%
PT	0.95	0.94	0.92	0.92	0.90	0.87	0.91	0.88	0.85
PP	0.96	0.95	0.94	0.94	0.92	0.89	0.97	0.94	0.91
Error - DIST [m]	0.09	0.11	0.21	0.37	0.48	0.71	0.34	0.43	0.62
Two joint damages:									
Accuracy	91 %	86 %	82 %	88 %	83 %	77 %	89 %	84 %	78 %
PT	0.81	0.69	0.64	0.76	0.66	0.57	0.76	0.58	0.56
PP	0.84	0.74	0.70	0.79	0.71	0.63	0.79	0.64	0.61
Error - DIST [m]	0.66	0.76	1.43	1.01	1.31	1.91	0.91	1.15	1.67

therefore, 24 hinges, are less sensitive to damage to single hinges.

3D truss system

The final analysis of the first type of test cases is conducted with a 3D steel truss structure. As reported in Table 3.7, D²-DTE achieved good performances in the localization of the section reduction in the 3D truss. Indeed, the predictive model had very high accuracy across the entire dataset and for all noise levels. Good performances could also be noted when comparing the PT and PP values, which are similar and high. These achievements can be related to the specific geometry of the truss, which increases in height, meaning that the modal shape is defined by eight displacement values, thus presenting a rich vector of input data.

3.3.2 IASC-ASCE benchmark

The IASC-ASCE benchmark is a well-known problem initially described in Johnson et al. [95] and numerically simulated in Caicedo et al. [28]. The structure is a four-story quarter-scale (grade 300W) steel frame, characterized by a height of 3.6 m and a 2.5 m \times 2.5 m squared plan. The sections are specifically designed for the scale model: the columns are B100x9 sections and the floor beams are S75x11 sections. The bracing system is

Table 3.5. Summary of performances: 3D frame, single cracked element

Level of detail	Story						Element					
	Damage severity		No		Yes		No		Yes		Yes	
Noise Level	3%	6%	9%	3%	6%	9%	3%	6%	9%	3%	6%	9%
Accuracy	83%	79%	75%	88%	85%	85%	88%	87%	87%	93%	87%	86%
PT	0.80	0.76	0.60	0.87	0.68	0.70	0.87	0.86	0.85	0.84	0.86	0.86
PP	0.83	0.81	0.75	0.89	0.72	0.74	0.89	0.89	0.88	0.85	0.88	0.88
Error - DIST [m]	0.53	0.71	1.93	-	-	-	0.39	0.40	0.41	-	-	-

Table 3.6. Summary of performances : 3D Frame, single joint damage

Level of detail Damage severity Noise Level	Story			Hinges		
	3%	6%	9%	n.d.		
Accuracy	81 %	82 %	77 %	73 %	57 %	52 %
PT	0.76	0.74	0.72	0.67	0.47	0.41
PP	0.81	0.81	0.78	0.75	0.60	0.54
Error - DIST [m]	0.83	1.09	1.28	0.42	0.74	1.12

Table 3.7. Summary of performances: 3D truss, single section reduction damage.

Level of detail Damage severity Noise Level	Element					
	3%	No			Yes	
	3%	6%	9%	3%	6%	9%
Accuracy	99 %	98 %	96 %	99 %	98 %	97 %
PT	0.97	0.96	0.94	0.99	0.97	0.96
PP	0.98	0.96	0.95	0.99	0.98	0.97

composed by two 12.7 mm diameter threaded steel rods placed diagonally. The damages introduced in this benchmark are obtained either removing or reducing the cross sections of diagonal bracing members present at each floor.

The dynamic behavior of the structure is numerically simulated through two different FE models, introduced by Caicedo et al. [28]. More specifically, the first model consists of a 12-DOF shear-frame, in which each single floor is described by three degrees of freedom. The second model is more complex and includes out-of-plane motion and rotations in the floor slabs; the resulting DOF are 120. It is worth noting that the difference in terms of DOFs – and thus complexity of the numerical model – is used to simulate the possible disagreement existing by a simple numerical model (12DOF) and the complexity of a real-world structure (120DOF). As reported in Johnson et al. [95] the numerical models simulate the presence of sixteen mono-axial accelerometers, two each in the x- and y-directions per floor. Accordingly, the data representing each simulated case is composed by 51 scalars: 3 Periods, and 48 modal shapes (3 modes for each accelerometer).

In order to validate the D²-DTE approach here presented, in addition to the undamaged scenario, the same 8 different damage patterns considered in Azimi and Pekcan [10] are introduced in the numerical model, and consequently grouped into 8 different cases to be analyzed. The damage patterns P1-P8 are shortly described in the following, and depicted in Figure 3.11.

- P1: a brace of the first floor is damaged by 30%;
- P2: a brace of the first floor is damaged by 100%;
- P3: a brace of the first floor and a brace belonging to the second floor are damaged by 100%;
- P4: two braces at the first and second floor are completely damaged. Two of the floor beams are released from their endpoints;
- P5: all the braces of the first floor are damaged by 100%;
- P6: all the braces of the first and third floors are damaged by 100%;
- P7: the braces from the same facade of the first and second floors are damaged by 100%;
- P8: all the braces belonging to a facade are 100% damaged. Additionally, two floor beams (1st and 2nd story) are released from their endpoints.

The resulting cases to be analyzed are reported in Table 3.8.

Table 3.8. Cases analyzed in the IASC-ASCE benchmark.

Case	Excitation	Model	Damage patterns
1	Wind	12 DOF	Intact, P1, P2
2	Wind	12 DOF	Intact, P3, P4
3	Wind	120 DOF	Intact, P1-P4
4	Wind	12 DOF	Intact, P5, P6
5	Wind	120 DOF	Intact, P5, P6
6	Shaker	12DOF	Intact, P5, P6
7	Wind	120 DOF	Intact, P7, P8
8	Wind	120 DOF	Intact, P1-P8

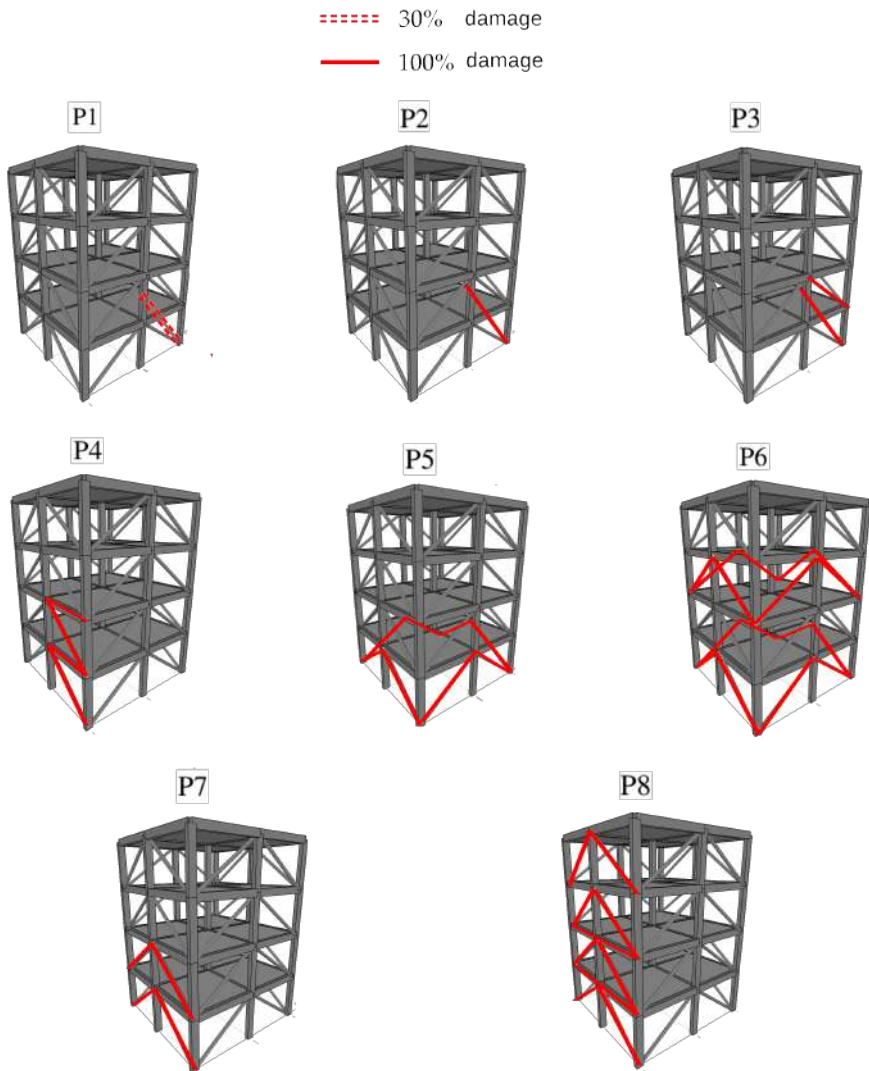


Figure 3.11. Damage patterns considered in the IASC-ASCE benchmark.

As done in Azimi and Pekcan [10], the simulated dynamic behavior of the structure is obtained for the undamaged condition, and thus introducing the patterns P1-P8 by means of the Matlab code available in Dyke [56]. The generated samples are collected according to 8 different cases summarized in Table 3.8.

As discussed in Johnson et al. [95] the damage patterns P1-P8, and their grouping in cases, are not necessarily intended to directly represent the complexity of a frequent or physically realistic damage mechanism, but their variety is introduced to test the capability of Machine Learning methods with different damage typologies, DOFs in the numerical model, and actions (wind, shaker).

The data obtained by means of the Matlab code simulation is generated in terms of acceleration time history, thus the modal properties are derived through the FDD algorithm [25]. For each of such cases, the generated data are then split in training and testing according to a 5-fold cross-validation approach. The performances of the D²-DTE are reported in the confusion matrices of Figures 3.12 - 3.13.

With the aim of testing the D²-DTE, the present Section reports a comparison with the damage classification approaches originally discussed in Azimi and Pekcan [10] and tested on Cases 1 - 8 by the authors.

In particular these damage classification approaches rely on a finely-tuned Convolution Neural Network that analyzes acceleration data, the source of which is either conventional sensors (MEMS raw data) or compressed data. In particular, compressed data is obtained ideally sampling acceleration time-histories at discrete time interval, as done by self-powered sensors. The result of this sampling operation is thus a discrete histogram representing the dynamic information in a compressed form.

The main differences distinguishing the method presented in the present Chapter with respect to the approaches discussed in Azimi and Pekcan [10] lie in the fact that the D²-DTE relies on a different base-classificator, Decision Tree Ensembles, and the damages are assessed on to assess damages based on the dynamic proprieties of the structure.

For the sake of comparison, Table 3.9 collects the results gathered on Cases 1 - 8 by the D²-DTE and the two methods described in Azimi and Pekcan [10]. For each case, the methods achieving the best accuracy are reported in bold.

Case 1: Confusion Matrix (Acc. 99 %)

		Predicted			Acc.
		0	1	2	
Actual	0	199	1		99.50%
	1		200		100.00%
	2			200	100.00%

Case 2: Confusion Matrix (Acc.100 %)

		Predicted			Acc.
		0	3	4	
Actual	0	200			100.00%
	3		200		100.00%
	4			200	100.00%

Case 3: Confusion Matrix (Acc.100 %)

		Predicted					Acc.
		0	1	2	3	4	
Actual	0	200					100.00%
	1		200				100.00%
	2			200			100.00%
	3				200		100.00%
	4					200	100.00%

Case 4: Confusion Matrix (Acc.100 %)

		Predicted			Acc.
		0	5	6	
Actual	0	199	1		99.50%
	5		200		100.00%
	6			200	100.00%

Case 5: Confusion Matrix (Acc.100 %)

		Predicted			Acc.
		0	5	6	
Actual	0	200			100.00%
	5		200		100.00%
	6			200	100.00%

Case 6: Confusion Matrix (Acc.100 %)

		Predicted			Acc.
		0	7	8	
Actual	0	200			100.00%
	7		200		100.00%
	8			200	100.00%

Case 7: Confusion Matrix (Acc.100 %)

		Predicted			Acc.
		0	7	8	
Actual	0	200			100.00%
	7		200		100.00%
	8			200	100.00%

Figure 3.12. Confusion matrices for cases 1-7.

		Case 8: Confusion Matrix (Acc.100 %)									
		Predicted								Acc.	
		0	1	2	3	4	5	6	7	8	
Actual	0	200									100.00%
	1		200								100.00%
	2			200							100.00%
	3				200						100.00%
	4					200					100.00%
	5						200				100.00%
	6							200			100.00%
	7								200		100.00%
	8									200	100.00%

Figure 3.13. Confusion matrices for case 8.

Table 3.9. Comparison of the performances achieved by D²-DTE , and the two methods described in Azimi and Pekcan [10].

Case	Accuracy [%]		
	MEMS	Self-powered Sensors	DTE
1	98.6%	99.8%	99.8%
2	99.9%	99.9%	100%
3	97.6%	100%	100%
4	100%	91.6%	99.8%
5	100%	94.4%	100%
6	100%	96.3%	100%
7	100%	100%	100%
8	96.5%	98.1%	100%

3.3.3 QUGS

The third dataset considered in the validation process is composed by experimental data, and its purpose is to appraise the performances of D²-DTE when applied in the analysis of a real physical structure. The dynamic properties used in this experiment were obtained processing acceleration time-histories recorded on a steel frame structure named Qatar University Grandstand Simulator (QUGS) [2, 9]. This grandstand is made by IPE 220 hot rolled elements, and designed to hold 30 spectators. The frame is made up of 8 main beams and 25 secondary beams supported by 4 columns. The main beams are 4.6 m long, the secondary beams measure 77 cm, while the height characterizing the two columns is 1.65 m. The main beams and the 25 secondary beams are connected by 30 joints, each of which is equipped with an accelerometer. The damages on the frame are simulated loosening the bolts of one connection at a time. For each damage pattern – 30 in total – the acceleration is recorded in a time history.

For each scenario, the acceleration signals were recorded in correspondence of each one of the 30 joints under a white noise shaker excitation at a sampling frequency of 1024 Hz. The signals were recorded for 256 s. This process was conducted twice for each scenario, resulting in two datasets: Dataset A and Dataset B. Then, the former data set is used in the training phase, while the latter is employed in the testing phase of the D²-DTE .

In order to apply the D²-DTE methodology herein proposed, the modal properties of the structure are obtained, for each pattern, by means of dynamic identification. The dynamic identification is then obtained from the acceleration time-history applying the FDD technique.

In order to reduce over-fitting in the training process, a data augmentation strategy is adopted, adding a 5% Gaussian noise to the dataset. The results of a 5-fold cross-validation approach are reported in Figure 3.14, evidencing an accuracy of 98.3%.

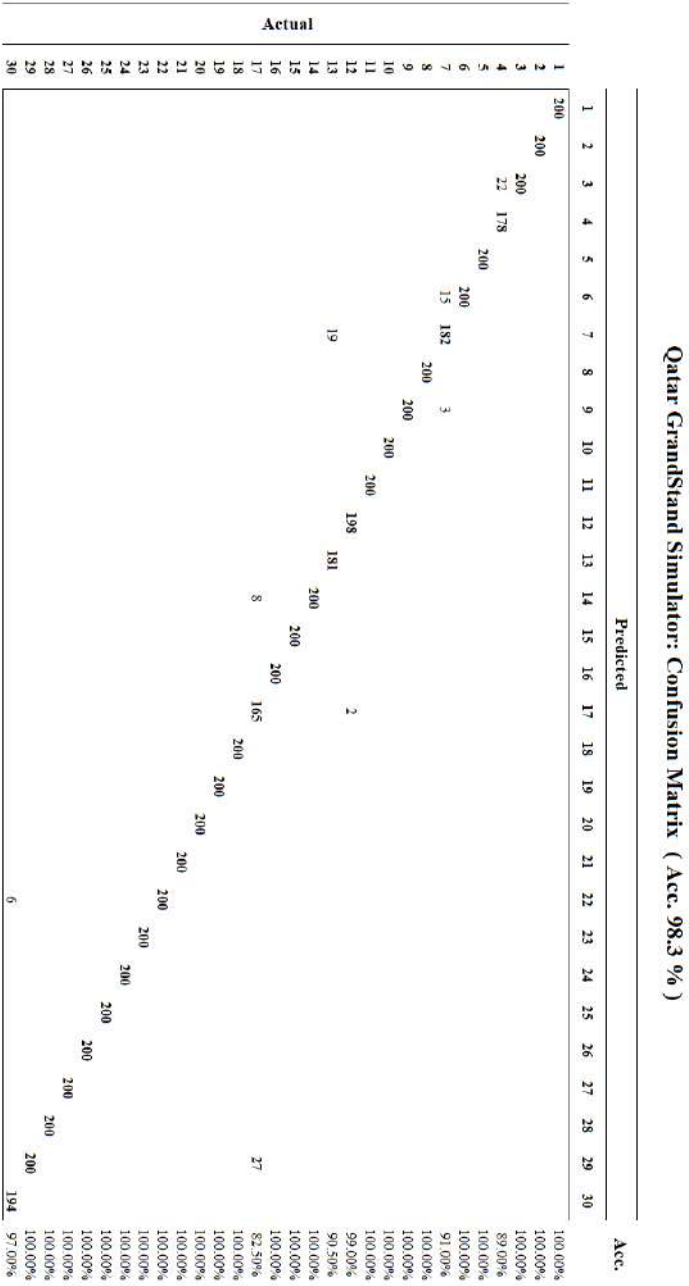


Figure 3.14. Confusion matrix QUGS dataset.

3.4 Discussion

The numerical experiments presented in Section 3.3 are aimed to analyzing the performances achieved through the D²-DTE in assessing a wide variety of damage scenarios in a diverse set of structures, being either FE simulations or real cases. In particular, the validation process tackles three different test cases: damage localization on numerical models, damage identification on the IASC-ASCE benchmark, and damage localization on the QUGS.

The aim of the first test case consists in the study of damage detection performance on simulated numerical models, with respect to the definition of different levels of details according to the proposed classification of section 3.2.2. In the detection of a single damage (either single element cracking or joint failure), DTE attained 91%, 87%, and 84% mean accuracy (for 3%, 6%, and 9% noise), with standard deviations of 0,07, 0,10, and 0,11, respectively. Moreover, as expected, DTE achieved its lower values when the noise levels are higher and the damage configurations are more complex. Nonetheless, to evaluate the performances in terms of the different levels of detail considered, encouraging insights are gathered by the determination of the distance metric (Error - DIST [m]). Analyzing the results reported in Tables 3.3– 3.6, it is possible to notice how, even in the case of significantly reduced damage detection accuracy (in percentage), the localization error in terms of physical distances is limited. A notable example of this behavior can be observed for the localization of two simultaneous cracking damages in the 2D frame with a 9% noise level (Table 3.3): in this scenario DTE exhibits the lowest accuracy (48%), while achieving a relatively small average localization error (1.48 m). The duality between these two metrics suggests that in the evaluation of the performances with respect to different levels of detail, accuracy alone can only give limited information concerning the robustness of the DTE, while distances can be used to estimate the magnitude of localization errors.

The results gathered testing the D²-DTE on the IASC-ASCE benchmark, point out the robust and accurate prediction across the whole set of cases 1-8. In fact, out of the 8 cases analyzed, the adopted DTE learning algorithm of the SHM framework was able to achieve exact matching in 6 cases, while registering a single misclassification in the remaining 2 cases

(case 1 and 4). Interestingly enough, both cases 1 and 4 are simulated with the 12DOF model; nevertheless, the magnitude of the error is negligible and does not allow to draw conclusions. For the sake of comparison, the performances of the DTE are measured against those achieved by the methods described in Azimi and Pekcan [10]. As reported in Table 3.9, it can be seen that all of the three approaches scored an accuracy value higher than 90% for the simulated damages. Additionally, it can be noted how the CNN based on MEMS is characterized by the best performances 4 out of 8 times; the CNN based on Self-powered sensors 3 out of 8 times, while the DTE characterizing the present framework achieves the best accuracy in 7 out of the total 8 cases.

Lastly, the application of the D²-DTE framework to the QUGS benchmark data shows high prediction capabilities also in a real application environment. In particular, as reported in the confusion matrix of Figure 3.14, the DTE achieved 98.3% accuracy while recording limited localization errors for a very small subset of damage configurations. On the contrary, for example, in the analysis of the QUGS, the CNN coupled with self-powered sensors of Azimi and Pekcan [10] achieved an accuracy of 91.9%.

Chapter 4

AI in Stress-based SHM: the LA-ELM approach

4.1 Introduction

The study of damage-detection strategies for bridge structures defines a well-established field in scientific literature [169, 191, 171]; within this context, several works specifically refer to the possibility of detecting – through physical measurements – the presence of damages affecting the prestressing systems of bridge decks. These studies involve both experimental analyses and numerical computations, and can be broadly classified according to the measurements considered in the assessment process, which are either dynamic, static, or nonstructural. The following paragraphs summarize the main research streams on the subject, yet a full review is beyond the scope of this chapter; the reader is instead referred to Bonopera et al. [20].

The sensitivity of dynamic properties to damages affecting the prestressing system has been evaluated both with numerical experiments and by studying real-world structures. Conducting laboratory experiments, Hop [85] found a cause-effect relationship between increased prestressing force and increased vibration frequency. This correlation has also been observed in other studies [166, 97], yet evidencing how after a certain threshold of the prestressing force the increase in frequency is reduced. Conversely, the findings of numerical studies partially contrasted these results, but this behavior is possibly due to the fact that the simulations only included

damages affecting the prestressing system, without taking into account the effects of concrete crackings. Using a transformation method to process vibration data, Tuttipongsawat et al. [185] proposed to use change of phase space topology (CPST) index to detect damages, studying experimentally measured acceleration histories. In their work, the authors observed a correlation between the increase of damage severity with the increase of the CPST index, noting a higher sensitivity to damages in comparison to modal properties.

Allegedly, there is not a consensus in scientific literature concerning the inter-relations of prestressing force and structural dynamics. For example Chan and Yung [33] and Law and Lu [108] described that, as the prestressing force increases, there is a reduction of the natural frequency of the deck, while Vera et al. [186] find an opposite trend. Instead, Hamed and Frostig [80] and Limongelli et al. [115] observed only marginal influences of prestressing force over structural dynamics.

Differently from dynamic analyses, static tests for the evaluation of prestress levels can be either destructive or non-destructive. The former provide excellent results in terms of measurements but imply damaging the structure and are thus not suitable for real-time assessment. Halsey and Miller [79] evaluated stress levels in cables by cutting them and measuring deformations with a strain gauge, Baran et al. [16] have instead performed tests evaluating cracking loads while back-calculating prestress levels. In their findings the authors assessed that prediction of losses based on the study of crackings and standard theory of mechanics results in an overestimation of prestress losses. Otherwise, the implementation of a real time system requires the measurements to be non-destructive like those proposed by Bagge et al. [12] and Azizinamini et al. [11], that correlate local deformations to prestress level. An alternative is the evaluation of deflections in the presence of known loads, which could be produced by closing the structure for a few minutes and allowing the transit of vehicles with a known weight [40].

Lastly, a related stream of scientific research proposed tendon-evaluation techniques based on non-structural measurements. Among others, acoustic evaluation can be used to assess failures. For instance, this approach is used by Yuyama et al. [197], which measured how the rupture of a tendon generates an acoustic emission that exceeds 100dB. The authors

used such emissions to detect ruptures in their laboratory experiments, finding an 80% accuracy. A further set of experiments assessed the performance of this method in a real-world context, studying two operating bridges. The goal of the experiment was to appraise acoustic emissions related to ruptures in presence of high ambient noise (e.g. traffic). Emissions compatible with those measured in the laboratory experiment were generated by a rebound hammer. The authors found detection accuracies between 80% and 90%. Another application based on the use of acoustic waves is described by Salamone et al. [168]. Using guided ultrasonic waves transmitted through the prestressing tendons, the authors aimed to detect defects or changes in prestressing force. The experimental results presented indicated that the nonlinear ultrasonic parameter – the ratio between higher-order harmonics and the fundamental generated harmonic – is a suitable feature for monitoring prestress levels in posttensioned concrete beams. Differently, Oh et al. [145] developed and applied a movable yoke system, coupled with a denoising algorithm, to detect the reduction of cross-sectional area in corroded external prestressing tendons. The proposed method correctly detected corrosion events characterized by less than 3% cross-section reductions. In line with the importance of continuous and accurate structural monitoring, in the past few decades a growing amount of research was devoted to the development of Structural Health Monitoring (SHM) systems based on the use of Artificial Intelligence (AI) and Machine Learning (ML) techniques; see [63] for a recent survey on the subject.

Nevertheless, despite the interest in the study of PSC bridges, only few works directly relate AI to these structural specimens. Cancelli et al. [31] proposed a method to localize and quantify cracking damages using vibration data. The authors described a methodology consisting of a model-updating framework based on a Particle Swarm Optimization algorithm, tested with both numerical simulations and a laboratory experiment, in which the data is collected on a single full-scale bridge girder. Supported by the visual observation of crack locations registered during the laboratory test, the authors demonstrated that the model-updating algorithm was able to identify the location of damages. Using structural dynamics as input of an algorithmic methodology, Lee et al. [110] presented a novelty detection approach to identify tendon damages in PSC bridges, based on

the numerical analyses of acceleration histories of the deck as one or more vehicles pass by. Using a convolutional autoencoder the authors modelled the structure in the undamaged state and in three significant damage conditions, in which the tendons were affected by loss of tensions of 50%, 75%, and 100%, respectively. Additionally, in their numerical simulation, random noise between 0% and 10% was added to simulate the possible presence of measurement errors. The results of the numerical experiments reported accuracies $> 79.5\%$ in the case of severe damages (100% and 75%) with all error levels, and 50% damage severity with no error. Differently, the authors report reduced accuracies in case of 50% damage severity with 5% and 10% error levels.

Reviewing the contributions proposed in the scientific literature, it can be pointed out that just few of the cited research efforts describe ML approaches to monitor PSC bridges and detect tendon malfunctions. Moreover, often the corresponding health assessment produced by such algorithms mostly consists in limited details about the occurred damage, rather than a precise quantification and localization of the prestress loss in the structure.

Finally, many application scenarios require model updating procedures to yield reliable estimations of the structural performance [82]. Accordingly, ML algorithms in these SHM scenarios may require frequent training phases, subsequent to each model updating procedure. Henceforth, the training time required by the ML algorithms is a key aspect to be considered as it can often be a bottleneck aspect in the applicability of proposed algorithmic methodologies.

In this context, this chapter proposes a novel framework based on the Extreme Learning Machine (ELM) model, a recent ML approach that in many studies achieved high accuracies with reduced training times in comparison to classical deep learning techniques [89]. The aim of the present work is to describe an innovative algorithmic methodology to provide a precise detection and quantification of damages affecting the prestressing system of a PSC bridge, using local stress data. The proposed framework is characterized by a layout-aware weight generating model (LA-ELM), that accounts for the positioning of the sensors to guide the learning model towards a spatially-consistent network topology.

According to the supervised learning paradigm, the described approach

builds a training dataset simulating stress data in different damage scenarios, and trains the LA-ELM to precisely recognize the damage affecting the prestressing system analyzing stress data. This proposal is tested in a diverse set of computational experiments that evaluates its performance in the analysis of the numerical models of three PSC bridges.

The main contributions of this chapter are: (i) study of the efficiency and applicability of ELM in the context of SHM, (ii) implementation of a problem-specific layout-aware weight assignment procedure for the detection of tendon malfunctions in PSC bridges, and (iii) achievement of high accuracies in short computational times and statistically significant improvements when compared to the classical ELM implementation.

The chapter is structured as follows: Section 4.2 reports the outline of the proposed approach and a formal description of its components. Numerical tests are described and discussed in Section 4.3 while Section 4.4 deals with the limitations of the numerical experiments.

4.2 Methods

The objective of the proposed methodology is the detection, localization and quantification of damages affecting the prestressing system of a PSC bridge with n longitudinal beams. In this context, the developed algorithm allows to evaluate n damage indices, related to the prestress load of each beam, thus providing identification, localization and quantification of the damage.

The work described in the present chapter employs an ELM-based algorithm – named LA-ELM – embedded with a problem-specific weight generation procedure. According to this paradigm, for any single structure of interest, it is possible to train the learning model on a datasets composed of simulated structural responses – including both “pathological” and “non-pathological” scenarios – to extract the intrinsic mathematical relations connecting a set of physical input features to a specific assessment on the health of the bridge.

The proposed methodology is based on the analysis of normal stresses at different points of the structure.

Currently, the estimation of stresses in structural elements is a major R&D challenge for sensor manufacturers, and in the past years, many

patents were filed on the topic (e.g. see [61, 178]). Although a general evaluation of stresses presents several difficulties, in the linear-elastic region of the stress-strain curve, Hook's law allows them to be easily derived from strains. In civil engineering, several solutions have been described while surveying passive wireless sensor networks [45]. Additionally, Lee et al. [109] proposed the use of a novel design for a tri-axial piezo-resistive sensor, based on a vertically integrated double-bridge scheme, and Gallucci et al. [65] described a setup based on wireless communication and power systems to evaluate the stresses in structural elements with a load cell.

In this work we refer to innovative parallel-plate capacity sensors – as patented in [78] – that allow to precisely estimate local stress values in structural elements by measuring changes in the electric signal due to contraction or the expansion of the dielectric material. This sensing unit is able to adjust the measurement using data acquired from thermocouples. Currently, different studies are investigating the quality of the measurements for different structural types [102].

For the sake of simplicity, in line with what found in the literature, in the remainder of the chapter such sensing system will be referred to as *stress-sensors*.

With these recent findings in mind, the proposed methodology considers as input features the normal stresses evaluated at different points of the longitudinal beams of the deck. The use of normal stresses as input features is justified by the observation that variations of tension in the prestressing tendons should induce a variation of the normal stress on the beam.

This methodology can be applied to both new and existing bridges. The main differences distinguishing these two cases are related to the two following aspects: ease of installation, and the capability of the sensors to evaluate the stress levels for deadweight loads.

Indeed, while the capacity sensors patented by Guidetti et al. [78] are straightforward to install on new structures, their use in existing bridges is being currently tested. Alternatively, many sensing systems can be used for the estimation of stresses while measuring strains. To this end, different typologies can be considered, yet, in practical applications, each one of these needs to be coupled with denoising strategies to isolate the effects that external factors – e.g. temperature – have on the strain field.

For their widespread diffusion in the measurement of strains, fiber optics represent one of the reference technologies [92], and can be used for both distributed or local measurements – when coupled with fiber Bragg grating [195].

Recent research efforts proved that soft elastomeric capacitive sensors can be used to evaluate strains by assessing changes in the electrical characteristics of the device [104]. In fact, the deformations alter the capacitance of the sensor, and this can be correlated to strains, estimating stresses accordingly. Notably, this technology can be used to measure strains over large surfaces [103]. Further type of surface sensors for large areas are based on Large-Area Electronics [75, 101].

For what concerns the capability of evaluate stresses, while in a new structure the sensors measure the actual stress values, in an existing bridge the sensors can only measure stress variations with respect to the conditions assessed at installation. Therefore, the analysis of existing structures requires an estimation of the initial stresses via a numerical model. Accordingly, the input of the predictive model – σ_{ML} – will have the following formulation:

$$\sigma_{ML} = \sigma_{RM} + \sigma_{SS} \quad (4.1)$$

where σ_{RM} is the numerically estimated deadload stress at the time of sensor installation, and σ_{SS} is the stress value estimated by the sensing system.

In this context, the problem of interest is formulated as a regression analysis for each beam of the bridge, in which the numerical output to be predicted gives an estimate of the stress levels of the prestressing cables.

Figure 4.1 presents a graphical representation of the methodology described in this chapter. Ideally, the workflow is divided in two main phases: a set-up phase, in which the preliminary operations are performed, and a second phase that takes on the actual monitoring of the structure.

The first two steps of the Set-up phase consist in the Finite Element (FE) modelling of the structural system of interest and in the simulation of a wide variety of damage conditions. These two operations allow to collect numerically simulated stress data that can be then used in the training of a LA-ELM algorithm for each beam of the bridge. In this training process, the aim of the algorithmic model is to learn the association rule between a specific stress vector – *input* – and the corresponding health assessment

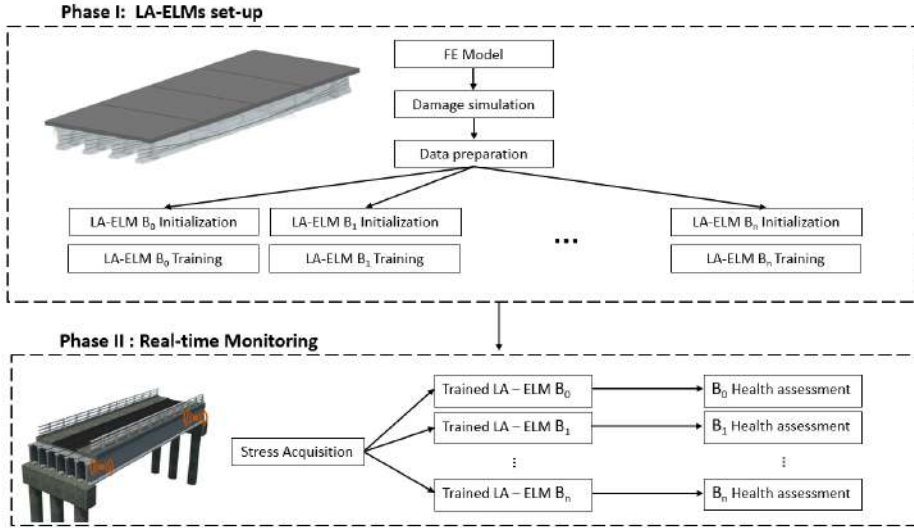


Figure 4.1. Graphical depiction of the proposed methodology.

of the prestressing system – *output* –.

Subsequently, the performance of the trained models are evaluated in a testing phase. Such phase considers unseen vectors of stress values along with their corresponding health assessment of the prestress cables, and compares the regression of the LA-ELM with the actual health assessment of each beam. The unseen vectors of stress data used in this step can either be by new numerical simulations of the target structure, or by data collected from a physical structure, as done in real-time monitoring. This validation phase represents a common practice in the context of ML for SHM, and its goal is to assess the accuracy and robustness of the predictor.

4.2.1 Structural FE Modelling

The first step of the Set-up phase aims to build a benchmark database of structural responses. To this extent, a fitting FE model allows to simulate the behavior of a structural system of interest in a wide variety of damage configurations. This dataset will be used to train the LA-ELM. In this context, the structural elements will be modelled with linear and elastic materials, to simulate a scenario that aims to the detection of dam-

ages affecting the prestressing system in absence of visual cues, such as crackings and spalling phenomena. The structural specimens modelled in this study are three PSC bridge decks characterized by common geometric features, as reported in Table 4.1.

The bridge decks have been modeled in SAP2000 using a plate with eccentric beam (PEB) modelling approach [3] as depicted in Figure 4.2. This structural simulation strategy requires the use of one-dimensional elements for beams, two-dimensional elements for deck slab, and rigid links for the geometric offset of the structures. The 2D continuous deck modelled in the PEB approach enforces compatibility between girders and allows the transfer of longitudinal shear forces between them, avoiding the need to use approximating schemes based on effective widths and modular ratios. In the modelling phase, more detailed 3D elements could also be used, but this choice would result in a higher computational burden implied by the increase in DOFs. Consequently, for the purposes of this work the PEB approach has been identified as an adequate trade-off between model fidelity and computational efficiency.

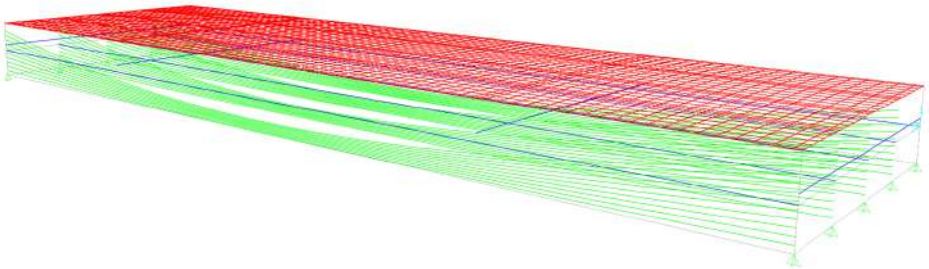
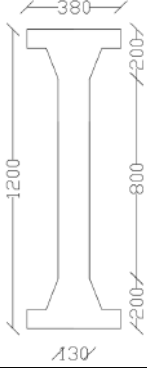
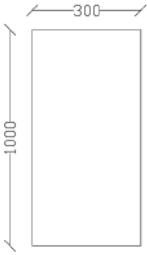
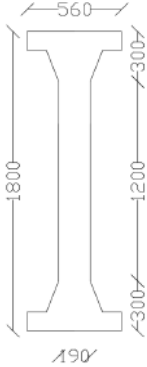
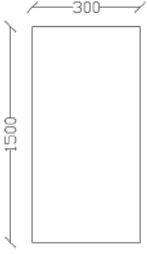
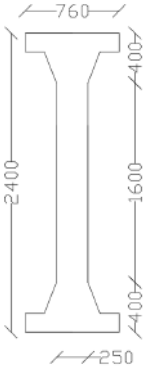
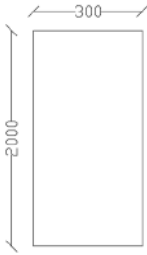


Figure 4.2. Numerical Model of a PSC bridge modelled using PEB approach.

In the reference models the bridge deck slabs are supported by 5 I-shaped longitudinal prestressed beams and 2 rectangular-shaped transverse beams. Table 4.1 shows beam sections for each one of the bridges modelled.

Lastly, the action of the prestressing system is modelled using the SAP2000 native tendon elements. Tendons are adopted to simulate the effect of post-tension in longitudinal beams. In particular, the native element permits to consider the effective tendon geometric shape and prestress load.

Table 4.1. Characteristic features of PSC bridges considered.

Deck length [m]	Deck width [m]	Deck slab thickness [mm]	I-shaped beams [mm]	Transverse beams [mm]
20	12	250	 $\begin{matrix} \text{---} 380 \text{---} \\ \text{---} 1200 \text{---} \\ \text{---} 200 \text{---} \\ \text{---} 800 \text{---} \\ \text{---} 200 \text{---} \\ \text{---} 130 \text{---} \end{matrix}$	 $\begin{matrix} \text{---} 300 \text{---} \\ \text{---} 1000 \text{---} \end{matrix}$
30	12	250	 $\begin{matrix} \text{---} 560 \text{---} \\ \text{---} 1800 \text{---} \\ \text{---} 300 \text{---} \\ \text{---} 1200 \text{---} \\ \text{---} 300 \text{---} \\ \text{---} 190 \text{---} \end{matrix}$	 $\begin{matrix} \text{---} 300 \text{---} \\ \text{---} 1500 \text{---} \end{matrix}$
40	12	250	 $\begin{matrix} \text{---} 760 \text{---} \\ \text{---} 2400 \text{---} \\ \text{---} 400 \text{---} \\ \text{---} 1600 \text{---} \\ \text{---} 400 \text{---} \\ \text{---} 250 \text{---} \end{matrix}$	 $\begin{matrix} \text{---} 300 \text{---} \\ \text{---} 2000 \text{---} \end{matrix}$

4.2.2 Damage simulation

To simulate the conditions characterizing a deteriorated bridge, this work employs a strategy to stochastically introduce diffused damages in the FE models of Section 4.2.1. This strategy consists in the simulation of different damage levels for each tendon of the I-shaped longitudinal beams according to a statistical distribution. The simulation process – depicted in Figure 4.3 – is divided in two fundamental step: (i) main damage simulation, and (ii) damage diffusion.

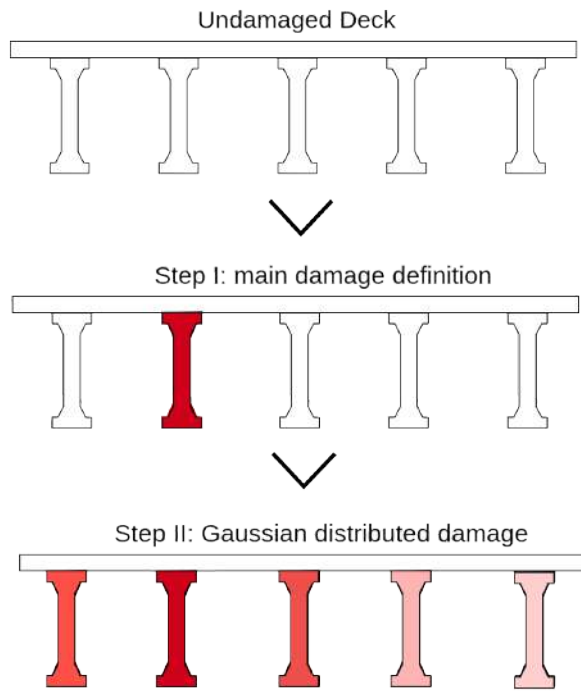


Figure 4.3. Graphical depiction of the damage generation process.

Let A_0 and N_0 be, respectively, cross-section area and the axial force characterizing an undamaged tendon. In the simulations, the cross-section and axial force of a beam whose prestressing system is affected by a main damage, respectively A_d and N_d , are obtained introducing a damage re-

duction coefficient, D_i (< 1), such that:

$$A_d = D_i \cdot A_0 \quad (4.2)$$

$$N_d = D_i \cdot N_0. \quad (4.3)$$

As a direct consequence of Equation (4.3) the damage index D_i is strictly related to the loss of prestress load of each one of the longitudinal beams (for $i = 1, \dots, n$).

In the numerical simulations considered in the present chapter, D_i accounts for thirty different levels of damage, $D_i \in [0, 0.97]$, with a step of 0.03.

Once the main damage is simulated, stochastic diffused damages are generated on the remaining beams. Letting η be the number of remaining beams, the diffused damage reduction coefficients D_{i_j} , $j = 1, \dots, \eta$, – to be used as in Equations (4.2) and (4.3) – are determined as samples of a normal distribution with mean $\alpha \cdot D_i$ and $\sigma = 0.15$, i.e. $D_{i_j} \sim \mathcal{N}(\alpha D_i, 0.15)$. In the present work α is set according three different standard deviation values, namely $\alpha \in \{0, 0.33, 0.67\}$.

4.2.3 Data extraction

To carry out the training and testing phases, data in vectorial form are extracted from the numerical analyses on the three reference bridge decks. As stated in the description of the general framework, the proposed approach uses stress data as input features of the regression model, yet, at this stage, to allow for the comparison of different inputs in the numerical experiments, both stress and vibration data are extracted from the numerical analyses on the three reference bridge decks.

In particular, a modal analysis collects the first 3 frequencies of the structure, and the modal displacements are estimated on each longitudinal beam – for each mode –, in 2 reference points, placed at $L/4$ and $3/4L$. These same information, in a more operational scenario, could be extracted using Operational Modal Analysis (OMA) of accelerometric signals collected on the physical structure [160].

Differently, the stress data consist in the normal stress along the middle section of each beam, evaluated in two points located as shown in Figure 4.4.

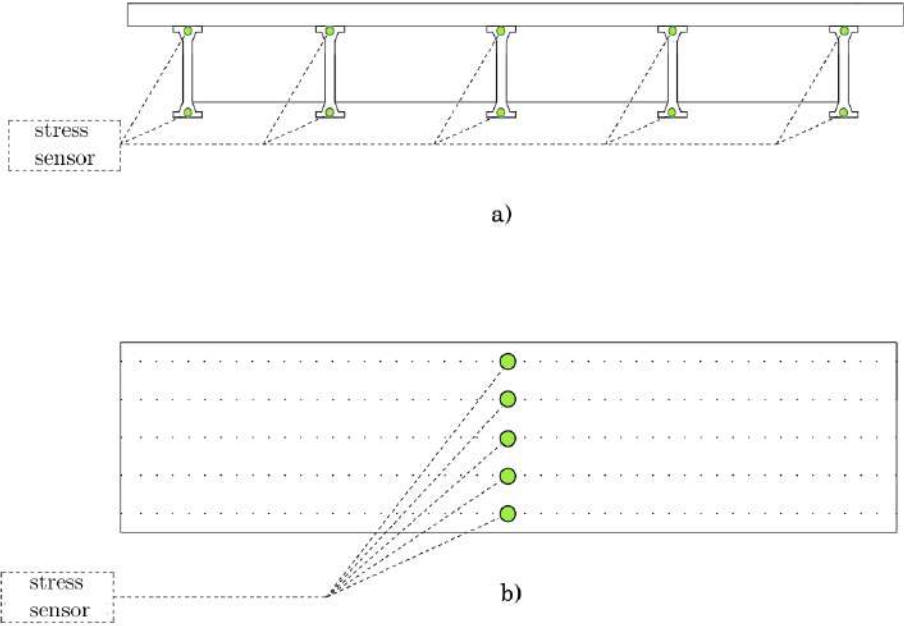


Figure 4.4. Graphical depiction of the positioning of stress sensors. (a) cross-section view at mid-span; (b) deck as seen from above.

The result of this operation consists in a vector of input features, \mathcal{F} , made up by either vibration or stress data, to be used as training information in the damage detection system. The data extracted from the numerical models of the PSC bridges are used to assess the performance of the proposed ELM in damage detection, localization and evaluation.

In order to simulate the presence of the uncertainty characterizing measurements in a real-world scenario, random white noise is added to \mathcal{F} . In particular, this noise addition procedure defines three different noise levels, and each component $\mathcal{F}_i \in \mathcal{F}$ is modified as

$$\mathcal{F}_i = \mathcal{F}_i + \mathcal{F}_i \cdot \xi, \quad \text{with } \xi \sim N(0, \sigma). \quad (4.4)$$

The values of $\sigma \in \{0.003, 0.01, 0.016\}$ define three noise levels, namely

low, medium and high. Using Chebyshev inequality, these σ values relate noise levels to variations that are likely to be within 1%, 3%, and 5%, respectively, of the original \mathcal{F}_i . In the following, these three noise levels will be denoted via such percentage variations.

4.2.4 Extreme Learning Machine

The Extreme Learning Machine (ELM) has been proposed as an extremely efficient paradigm of single hidden layer feedforward neural network (SLFN). According to this model, the only parameters that are learned are the weights β of the edges connecting the hidden layer and the output layer, while the hidden nodes are randomly initialized and then fixed without any iterative tuning.

Besides its efficiency, the ELM is characterized by the same universal approximation capabilities of SLFNs, as shown by several theoretical analyses (e.g. see [88]).

Let \tilde{N} be the number of nodes of the hidden layer, and $g(\cdot)$ an activation function, then the generic output \mathbf{o}_j of a SLFN can be modelled by the following equation:

$$\mathbf{o}_j = \sum_{i=1}^{\tilde{N}} \beta_i g(\mathbf{w}_i \cdot \mathbf{x}_j + b_i), \quad j = 1, \dots, N, \quad (4.5)$$

where \mathbf{w}_i (respectively β_i) are the weights of the connections between the i -th hidden node and the input (output) nodes, and b_i are the biases of the hidden nodes (see Figure 4.5).

Given the vector of target (output) values \mathbf{T} – associated to the input \mathbf{x} –, the exact approximation of the input samples can be expressed through the following vectorial equation:

$$\mathbf{H}\beta = \mathbf{T}, \quad (4.6)$$

where

$$\mathbf{H} = \begin{bmatrix} g(\mathbf{w}_1, b_1, \mathbf{x}_1) & \cdots & g(\mathbf{w}_{\tilde{N}}, b_{\tilde{N}}, \mathbf{x}_1) \\ \vdots & \vdots & \vdots \\ g(\mathbf{w}_1, b_1, \mathbf{x}_d) & \cdots & g(\mathbf{w}_{\tilde{N}}, b_{\tilde{N}}, \mathbf{x}_d) \end{bmatrix}, \text{ and } \mathbf{T} = \begin{bmatrix} t_1 \\ \vdots \\ t_d \end{bmatrix}. \quad (4.7)$$

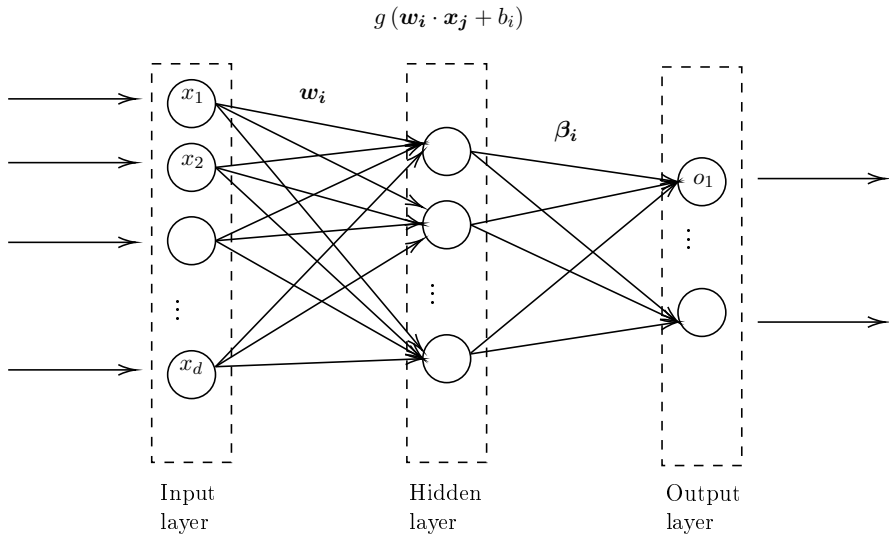


Figure 4.5. Schematic representation of ELM – feedforward neural network.

In traditional SLFN approaches the network is trained to find the optimal set of \mathbf{w} , \mathbf{b} , and $\boldsymbol{\beta}$ such that the minimum of the norm $\|\mathbf{H}(\mathbf{w}, \mathbf{b}, \mathbf{x})\boldsymbol{\beta} - \mathbf{T}\|$ is attained. This step is usually carried out by means of gradient-based algorithms that induce high computational costs.

Contrarily, in the ELM paradigm, the parameters of the hidden nodes \mathbf{w} and \mathbf{b} are randomly generated according to a continuous probability distribution, without being explicitly tuned. The weights of the connections between input layer and the output layer, instead, are yielded by minimizing the squared error in Equation (4.6). One of the optimal least-squares solution of Equation (4.6) is given by:

$$\boldsymbol{\beta} = \mathbf{H}^+ \mathbf{T}, \quad (4.8)$$

where \mathbf{H}^+ indicates the Moore-Penrose pseudoinverse of \mathbf{H} . In contrast to the computationally expensive tuning of classical SLFNs, efficient techniques such as Gaussian elimination and single value decomposition can be used to solve Equation (4.8).

4.2.5 Layout-aware random weight distribution

While the standard implementation of the ELM is based on a completely random generation of \mathbf{w} , recent researches explored the use of problem-specific weight generation procedures to improve the performance and the robustness of ELM in case of either noisy or missing data [124, 125, 86].

As mentioned earlier, the damage-detection methodology described in the present chapter is based on a set of parallel ELM – one for each longitudinal beam of the bridge – each of which takes the full data as input and outputs a health assessment concerning the beam it refers to. In this context, since the input data is related to a network of sensors placed on the structure – either physically or in the numerical simulations – each ELM is embedded with a weight generation procedure that assigns weights according to statistical distributions that depends on the distances between the sensors and the beam to be assessed. The resulting ELM is named layout-aware ELM (LA-ELM)

Let B_h be the beam whose health assessment has to be produced by the ELM. Let \mathbf{w} be the set of input weights connecting the input layer with the hidden layer of the ELM. To scale the input weights in accordance to the positions of sensors with respect to the central axis of B_i , \mathbf{w} can be yielded as the Hadamard product of two matrices, \mathbf{S} and \mathbf{R} :

$$\mathbf{w} = \mathbf{S} \odot \mathbf{R}, \quad (4.9)$$

or equivalently

$$w_{i,j} = S_{i,j} \cdot R_{i,j}, \quad (4.10)$$

where w_{ij} indicates the weight of the edge of the ELM connecting the i -th input node and the j -th hidden node. It is noted how in the context of SHM the i -th input node is related to the measurements of a physical (resp. simulated) sensor, located on the structure. In Equation (4.10) \mathbf{R} is a Gaussian random matrix, i.e. $\mathbf{R}_{i,j} \sim \mathcal{N}(0, 1)$. S_{ij} , instead, is a function of the distance separating the sensor related to the i -th input node and the central axis a of B_h . Let d be the vectorial distance separating a and the sensor related to the i -th input (See Figure 4.6); d can be split into its two projections on the horizontal and vertical axis, namely d_x and d_z . Then,

S_{ij} is obtained as

$$S_{ij} = \frac{\text{sign}(d_z)}{1 + d_x^2}. \quad (4.11)$$

This formulation accounts for two problem-specific behavior that can be

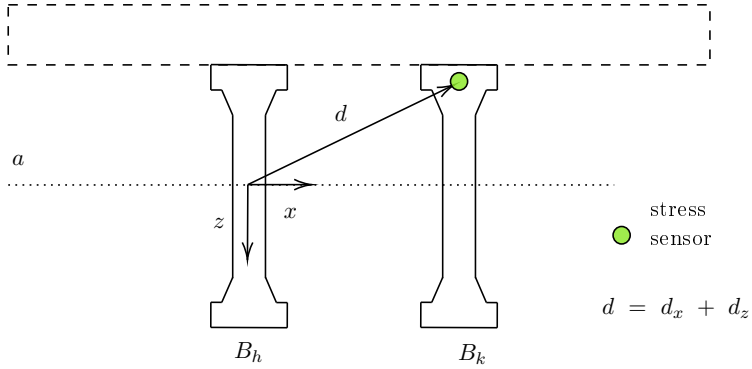


Figure 4.6. Scaling procedure

observed in a PSC deck: (i) the sensors may be located at points where the effects of prestressing are different, in case of damages in the compressed zone there is an increase in compression, while in the traction zone there is a reduction in traction; (ii) losses of tension in a tendon of a beam generate a redistribution of stresses that is mainly noticed in the closer beams. The ratio of Equation (4.11), then, is to adopt weights whose average value is proportional to the distance of the analyzed beam. In this way, the attempt is to amplify the sensitivity of stress redistribution to damage locations, while the the sign at the numerator distinguishes between sensors located in the traction and compressed zone, respectively.

The training process of the LA-ELM is summarized in the pseudocode of Algorithm 2.

4.2.6 Evaluation Metrics

Once the ELM is trained, its regression performance are evaluated on the testing set using three different metrics: Root Mean Square Error (RMSE), coefficient of determination (R^2), and the maximum error recorded (*MaxError*).

Algorithm: LA-ELM(\tilde{N} , \mathbf{x} , \mathbf{T} , B_h)

Initialize \tilde{N} nodes;

Compute distances d of each sensor s_i from beam B_h ;

for each sensor s **do**

 compute d ;

 project d to yield d_z and d_x ;

$$S_{ij} = \frac{\text{sign}(d_z)}{1 + d_x^2};$$

end

$\mathbf{W} = \mathbf{S} \odot \mathbf{R}$;

$H = g(\mathbf{W} \cdot \mathbf{x} + \mathbf{b})$;

$\beta = \mathbf{H}^+ \mathbf{T}$;

return trained LA-ELM(\mathbf{W} , b , β);

Algorithm 2: Pseudo-code for the LA-ELM for the health assessment of a generic beam B_h .

Given a total of N_{test} test samples, and letting y_i and \hat{y}_i ($i = 1, \dots, N$), be the actual and predicted values, respectively, then RMSE measures the square root of the mean squared error:

$$\text{RMSE}(y, \hat{y}) = \sqrt{\frac{1}{N_{test}} \sum_{i=1}^{N_{test}} (y_i - \hat{y}_i)^2}. \quad (4.12)$$

Differently, R^2 provides indications regarding the goodness of adaptation of the regression model to the data, i.e. evaluates how well unseen samples are likely to be predicted correctly. Its mathematical formulation is:

$$R^2(y, \hat{y}) = 1 - \frac{\sum_{i=1}^{N_{test}} (y_i - \hat{y}_i)^2}{\sum_{i=1}^{N_{test}} (y_i - \bar{y})^2}, \quad \text{where } \bar{y} = \frac{1}{N_{test}} \sum_{i=1}^{N_{test}} y_i \quad (4.13)$$

The last metric measured in the numerical experiments is *MaxError*. This value provides the maximum error recorded in the testing phase, i.e.

$$\text{MaxError}(y, \hat{y}) = \max_{i=1, \dots, N_{test}} |y_i - \hat{y}_i|. \quad (4.14)$$

The knowledge of the maximum error committed, especially on large samples, can be used to estimate the maximum possible inaccuracy of the regression method, thus providing useful information when accounting for the safety of an automatic health assessment.

4.3 Computational Results

The validation of the ELM framework herein adopted is organized through four different numerical analyses, reported in Sections 4.3.1 - 4.3.4. The numerical experiments investigated are:

1. ***Input Comparison***: to study the possible advantages of using stress as inputs rather than dynamic measurements.
2. ***Layout-aware random weight testing***: to assess the improvements achieved using the proposed LA-ELM in comparison to the classical ELM implementation.
3. ***Learning models comparison***: to explore the trade-off between accuracy and computational efficiency of the proposed LA-ELM in comparison to other standard Machine Learning algorithms.
4. ***Parametric Analysis***: to evaluate the influence of several independent variables – deck length, beam to be assessed, noise level – on the performance of the proposed methodology.

The subject of the analyses discussed in the present section are the three bridge structures (20 m, 30 m, 40 m) – as reported in Table 4.1 – each of which is analyzed in presence of three different Gaussian noise levels, namely 1%, 3%, and 5%.

In the numerical experiments the Training-Testing split is carried out using a random hold-out approach with a 70:30 ratio. All the errors reported in the following sections are relative to the testing dataset.

All the Machine Learning algorithms featured in the experiments are implemented in Python 3.9 using the Scikit-learn library. All the numerical experiments are conducted on a Virtual private server with a 2.2 GHz Intel Xeon CPU E5-2630 v4 processor with 8 GB of RAM, and a three level cache with levels of 32KB, 4096KB, and 6144KB.

4.3.1 Input comparison: stress and vibration

The first set of numerical experiments is devoted to the study of the regression performance achieved using stress data as input.

The objective of these analyses is to hold a preliminary evaluation of the sensitivity of dynamic characteristics and the global stress distribution to decreases in prestressing force. The parallel of these two sensitivities lies within the scope of the assumptions and simplifications underlying the FE modelling of Section 4.2.1. Accordingly, the standard ELM implementation is trained using either stress (ELM - stress) or vibration (ELM - vibration) data as input. Table 4.2 reports the results gathered in this first comparative analysis.

Table 4.2. Summary of results obtained comparing ELM-vibration and ELM-stress.

L [m]	Noise	ELM - vibration			ELM - stress		
		RMSE	R ²	MaxError	RMSE	R ²	MaxError
20	1%	0,356	0,12	0,67	0,033	1,00	0,06
	3%	0,411	-0,26	0,85	0,046	0,99	0,08
	5%	0,437	-0,46	0,79	0,064	0,96	0,14
30	1%	0,400	-0,18	0,79	0,043	0,99	0,08
	3%	0,432	-0,32	0,84	0,077	0,94	0,17
	5%	0,452	-0,62	0,85	0,101	0,90	0,21
40	1%	0,407	-0,15	0,76	0,052	0,98	0,11
	3%	0,435	-0,39	0,84	0,100	0,90	0,23
	5%	0,435	-0,68	0,91	0,100	0,82	0,33
Avg		0,418	-0,33	0,81	0,068	0,94	0,16
std. dev.		0,029	0,23	0,06	0,027	0,05	0,08

Analyzing the RMSE values, it is possible to observe how consistently the regression achieved by ELM-stress exhibits lower errors with respect to ELM-vibration. In fact, on average, with stress as input values, the ELM scores a RMSE of 0.068, with a standard deviation of 0.027. In contrast, the use of vibration data yields an average RMSE of 0.418 with a standard deviation of 0.029. Analogous observations stem from the analysis of the maximum errors recorded in the regression of the test dataset.

Averaging over all structures and noise levels, the maximum error committed by ELM-vibration (0.81) is approximately five times higher than the maximum error recorded using stress values as input (0.16). Therefore, considering a deployment scenario in which the ELM algorithm is implemented to automatically monitor the tendons of a PSC bridge of interest, these preliminary numerical analyses suggest that the use of stress values as input would lead to a less error-prone monitoring system. To highlight

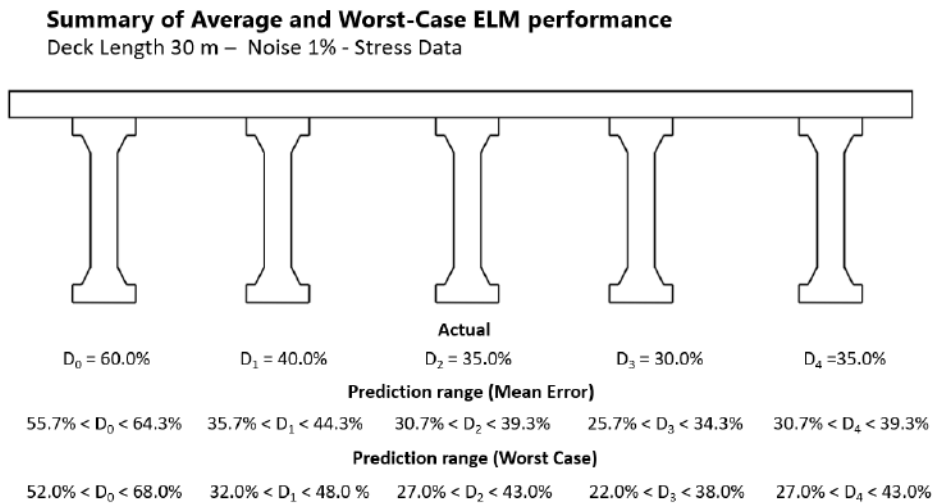


Figure 4.7. Visualization of average and worst case performances recorded for the ELM, in the cases of: $L = 30$ m, Noise = 1% and using stress data.

physical meaning of RMSE values, Figure 4.7 shows examples of average and worst case prediction for the 30 m deck with 1% noise using stress data. In detail, for each beam, the figure shows the actual damage indexes (first row), and the prediction ranges in case of mean error (second row) and maximum error (third row).

Similar conclusions can be drawn analyzing R^2 values. Such metric analyzes the proportion of explained variance in the regression model and provides an indication of goodness of fit, i.a. a proxy measure to evaluate how well unseen samples are likely to be predicted by the model. Values closer to 1 indicate a better fit, while a constant model that always outputs the expected value of the independent variable would score a R^2 value 0.

Analyzing Table 4.2, it is possible to note how ELM-stress is characterized by high R^2 values, on average always greater than 0.82. This observation indicates that in the datasets analyzed the stress-damage relationship accounts for more than 82% of the total variation. Conversely, the R^2 scores of ELM-vibration are either close to zero or negative. This behavior evidences that the use of vibration data leads to a regressor which generally fits worse than the mean value of the independent variable. These observations concerning the goodness of fit of the two models are reflected in the two regression plots, reported in Figure 4.8. For the sake of brevity only the median value of the noise (3%) is presented.

Therefore, the first set of numerical experiments evidenced how the performance achieved using vibrational features as inputs lead to worse results in the analysis of the dataset presented in Section 4.2.1. This finding agrees with the conclusions of Hamed and Frostig [80] and Limongelli et al. [115], that discussed how changes in the magnitude of prestressed force do not appear to affect the natural frequencies of prestressed beams.

For the sake of fairness, as a consequence of this first numerical analysis, all the following numerical tests – whether it be involving the ELM or other learning algorithms – will use stress as input features.

4.3.2 Testing layout-aware random weights

To justify the use of a case-specific weight assignment procedure, the present section reports a comparison between Layout-aware ELM (LA-ELM) and ELM with completely random weights. As stated previously, both networks use stress data as input values. Table 4.3 reports a compact summary of the RMSE value recorded in this comparative experiment. In addition to RMSE averages and standard deviations, the results are reported in terms of relative difference (%gap) with respect to the best value, i.e. for each method and each analysis, such gap is computed as

$$\%gap = \frac{\text{RMSE} - \text{best RMSE}}{\text{best RMSE}} \cdot 100. \quad (4.15)$$

Analyzing the findings reported in Table 4.3 it is possible to note that LA-ELM consistently scores the lower RMSE values between the two approaches. This behavior is correctly underlined by the %gap column, according to which LA-ELM is the approach that yields the best result

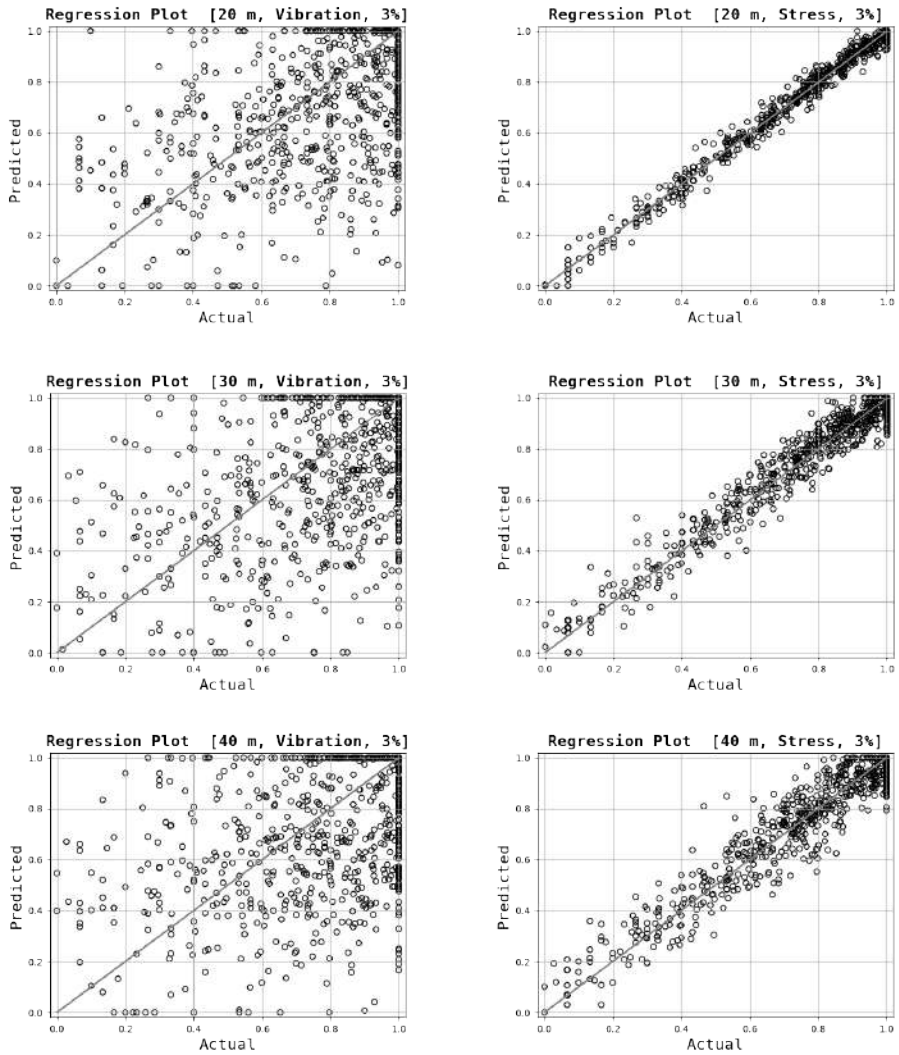


Figure 4.8. Comparison between regression quality achieved using Vibration data (left) and Stress data (right) as inputs, noise level 3%.

L [m]	Noise	LA-ELM		ELM	
		RMSE	%gap	RMSE	%gap
20	1%	0,018	0%	0,033	81,0%
	3%	0,036	0%	0,046	28,9%
	5%	0,056	0%	0,064	13,4%
30	1%	0,030	0%	0,043	43,2%
	3%	0,070	0%	0,077	10,9%
	5%	0,099	0%	0,101	2,7%
40	1%	0,041	0%	0,052	26,5%
	3%	0,098	0%	0,100	1,5%
	5%	0,098	0%	0,100	1,4%
Avg		0.061	0%	0.068	23,29%
std. dev.		0.032	0	0.027	0.260

Table 4.3. Summary of the comparison between Layout-aware ELM (LA-ELM) and ELM with completely random weights.

– always scoring 0% relative difference with respect to the best RMSE. Moreover, to quantify the benefits of a layout-aware weight assignment, it is possible to note how the standard ELM exhibits errors that are on average $\approx 23.3\%$ worse of the best values (i.e. those of LA-ELM). While still present, the benefits of using LA-ELM with respect to the standard approach appear to be less convenient when the length of the beam deck increases. This behavior can be related to the observation that the layout-aware approach is strictly related to the distances separating the sensors, and the number of sensors that yields excellent performance for a 20 m bridge deck could be less decisive in the case of a 40 m bridge deck.

Finally, the statistical significance of the improvements of LA-ELM over the standard ELM is assessed via a two-sided Wilcoxon signed-rank test. In particular, the 12 average RMSE values achieved by each method in the analyses are compared as samples of two distributions, related to LA-ELM and the standard ELM, respectively. A two-sided Wilcoxon signed-rank test – with critical value $\alpha = 0.01$ – suggested that these averages are

significantly different (p-value equal to $4.88 \cdot 10^{-4}$).

As a result of this analysis, the following tests will feature the Extreme Learning Machine in its layout-aware implementation (LA-ELM).

4.3.3 Comparing learning models

Many different Machine Learning algorithmic approaches have been described in the context of Structural Health Monitoring to the aim of detecting damages. Without any claim of providing an exhaustive list, the wide variety of learning algorithms considered ranges from classical methods, such as K-Nearest Neighbors (KNN) [187, 170, 60] and Support Vector Machines (SVM) [26, 98, 77], includes ensemble methods such as the Random Forests (RF) [141, 128], and often features the accurate and computationally demanding neural networks (NN) [121, 34, 134, 1].

The aim of the present computational experiment is to explore the trade-off between performance and computational times when comparing LA-ELM with other learning models. The present analysis is not intended as a direct comparison with other methodologies presented in the same field for different structural specimens. In fact, different structure of interest are characterized by different geometric features and problem-specific challenges. The aim of these tests is to highlight the possible benefits of using a LA-ELM as a base learner to build a continuous SHM framework.

To assess the compromise between the regression capabilities of the learners and their computational expenses, this numerical experiment considered 5 different learning models: LA-ELM, KNN, NN, RF, and SVM, measuring both the RMSE errors achieved and the time spent in the training phase. Since each one of such methods is characterized by its own set of parameters, the training phase included a grid search to find the best set-up for each one of the tested algorithms. Moreover, since the results are reported in terms of best RMSE values, the total times for tuning and training are reported for each method.

Figure 4.9 shows the box-plots of the RMSE distributions characterizing each learning model considered in this study. Observing the distributions it is possible to distinguish two groups. The first group is composed by relatively simple learning models, that exhibit the worse performance on the dataset: KNN, SVM and RF. This behavior suggests that learners of this group do not perform particularly well on the reference dataset,

and present worse capabilities of generalizing the information collected in the training. On the other hand, the second group is made up by the two deep learning algorithms considered in this study, LA-ELM and NN. The two deep learning algorithms are apparently equivalent in terms of scored RMSE – both with median values < 0.05 and maximum RMSE ≈ 0.12 – and outperform the learners of the first group. This observation is expected and can be related to their inherent complexity, that can yield better generalization capabilities.

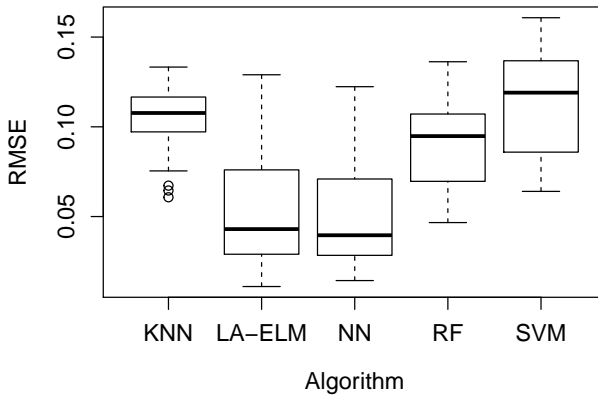


Figure 4.9. Comparison of the RMSE of LA-ELM with respect to other well established supervised learning algorithms.

While the distribution of RMSE evidenced how the two deep-learning models (LA-ELM and NN) perform better than the other three algorithms featured in the numerical analyses, a study of the time spent in the tuning and training phases can give useful information when accounting for the benefit/costs trade-off of employing these learners in operational scenarios. For each learning model other than the LA-ELM, Figure 4.10 reports the computational times recorded, normalized with respect to the average time of LA-ELM, that Figure 4.10 indicated by the solid horizontal line $y = 1$. Additionally, for reference, a dotted and a dashed line report, respectively, the maximum and minimum normalized times of LA-ELM.

As expected, observing the positioning of the time distributions in Figure 4.10 it is possible to note that the shallow learners always require less training time with respect to NN and LA-ELM, given their simpler structure. This phenomenon suggests that a decrease in terms of time of computation needed comes at the price of less accurate regression performance. On the other hand, the LA-ELM is faster than NN by almost one order of magnitude. Additionally, the standard deviations σ are 4.8 and 33.7, respectively, for LA-ELM and NN. These σ values imply that the the training times for the LA-ELM are consistently distributed in a small neighborhood around the mean value, while NN times are more scattered and tend to fluctuate more away from the mean.

The findings in the analysis of the training times is in line with previous studies [89] and suggest that the ELM appears to be characterized by good generalization performance while not implying a heavy computational burden. These characteristics potentially make ELM a well suited framework to tackle many Structural Health Monitoring problems in which efficiency and effectiveness are both key aspect of the operational scenario.

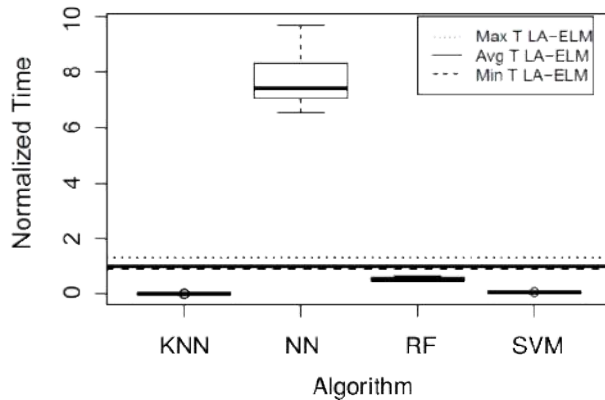


Figure 4.10. Comparison of the computational times required by the compared methodologies, normalized with respect to the average time required by LA-ELM.

4.3.4 Parametric Analysis

The last set of analyses studies how the performance of LA-ELM is affected by the variation of different parameters. In particular, as described in Figure 4.2, the numerical dataset considered includes variations of three different independent variables: the length of the bridge (L), the beam affected by the main damage (Beam n°), and the noise level considered. Each of such independent parameter has its own range of possible values, as reported in Table 4.4.

Table 4.4. Domains of the independent parameters characterizing the dataset.

L [m]	Beam n°	Noise
20, 30, 40	B0 - B4	1%, 3%, 5%

Figure 4.11 shows three scatter-plots relating the effectiveness of LA-ELM – in terms of RMSE scores – with respect to the variations of the three independent parameters of Table 4.4.

The distribution of RMSE values of Figure 4.11 a) evidences a positive correlation of the magnitude of errors and deck length. This behavior is possibly related with the fact that the numerical models of the bridge decks considered are provided with the same amount of measurement points, as shown in Figure 4.4.

The effects of Gaussian noise – Figure 4.11 b) –, as widely expected, are closely correlated with the performance of the method. Higher noise values imply a higher scattering rate in the space of input features, and thus worse regression performance. Nevertheless, the average RMSE values evidenced by the LA-ELM are always lower than 0.15.

Studying the performance of LA-ELM with respect to the beam to be assessed – Figure 4.11 c) – it is possible to observe how the method is consistent across the whole set of longitudinal beams. Only a slight correlation favouring the outermost beams (B0 and B4) can be appreciated, yet by these numerical experiments is not possible to determine whether such slight improvement in performance is due to random noise or to the fact that the outermost beams are generally the most stressed, and thus most sensitive to stress variations.

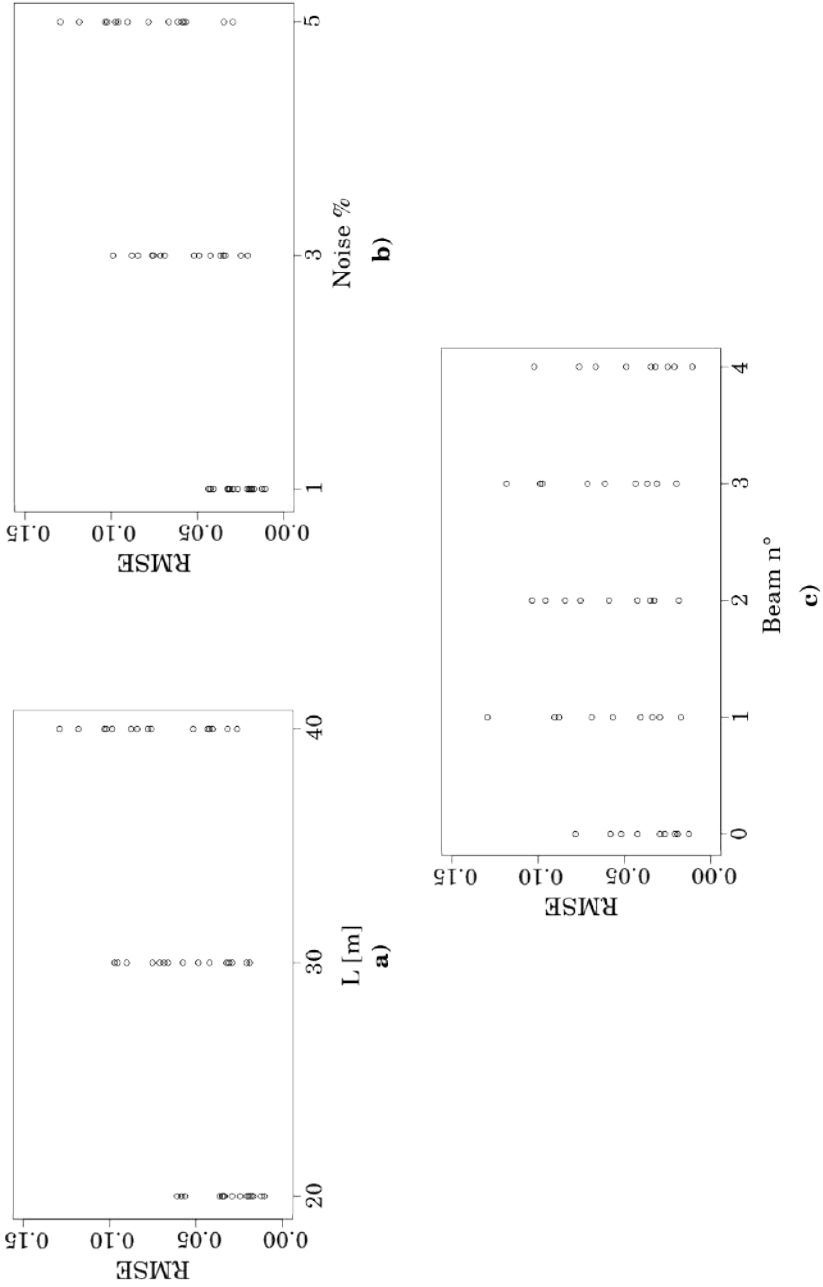


Figure 4.11. Analysis of RMSE scores with respect to different values for: length a), Gaussian noise b), and Beam number c).

4.4 Limitations

The numerical experiments of Section 4.3 suggest that the proposed LA-ELM can analyze stress data to yield favorable results in the detection and localization of damages affecting the prestressing systems of PSC bridges. At the same time, this exploratory study presents some limitations that need to be considered in the evaluation of the results and addressed in future works.

The main point requiring consideration is the simplification implied by a purely numerical analysis. While drawing preliminary conclusions, computational simulations are a capital resource, yet these allow to bypass the inherent complexity that characterizes applications in operating field conditions. For this reason, future investigations need to include real-world data, accounting for the influence of different environmental conditions on the behavior of the structure. Indeed, different air humidity levels and daily temperature variations can induce additional internal forces that cause increased deflections and affect global stress distributions. The use of real-world data will also increase the knowledge of the physical phenomena in action, driving the scientific community towards more accurate models and thus reducing epistemic uncertainties as much as possible. Consequently, further evaluations of the effectiveness of the proposed methodology require the use of both laboratory and field experiments.

The study of in-operation monitoring will also pose additional questions to consider from both technical and management standpoints, including the possibility of correctly estimate moving loads or the operational costs of service interruptions.

Moreover, the proposed analyses on the detection of prestress losses, rather than a direct comparison between the use of stress data and the classical dynamic monitoring, should be intended as a feasibility study investigating the practicability of the novel LA-ELM methodology, whose performance – as other ELM counterparts in different application fields – continues to show high accuracy with limited computational expenses.

Further evaluations on physical structures can effectively appraise the benefits of employing the proposed algorithm, directly comparing its detection capabilities with state-of-the-art statistical pattern recognition meth-

ods based on the study of modal properties variation.

AI in Inspections: Fast Post-seismic assessment of masonry buildings

5.1 Introduction

Since 1997, in Italy, the assessment report used is the Aedes form, whose acronym in English can be translated as "Practicability and damage in the seismic emergency" [49]. It is a form for the fast detection of damages, the definition of prompt intervention measures, and the evaluation of post-seismic practicability of buildings with ordinary structural typology (in masonry, reinforced concrete, steel, or wood) of the building for housing and services [51]. Similar forms have been approved by North American and New Zealand authorities.

Machine Learning and Deep Learning techniques are highly used in the context of structural engineering, especially for Structural Health Monitoring and damage detection applications [59, 73, 127]. These applications are based on the analysis of the different types of data; the most common are vibration data [126, 2, 90], highly sensitive to mass and stiffness, and static data [74, 19], correlated to change of stress state. These more advanced techniques are challenging to use in the post-earthquake fast assessment phase because they require an ad-hoc sensors system during all operational phases of the structure or an accurate study to estimate the pre-seismic

structural condition. Therefore, for ordinary structures, there is a need for a system that can provide results quickly, albeit with a lower level of accuracy. The diffusion and development of Deep Learning (DL) algorithms for image analysis are enabling the development of several solutions based on the use of camera Images or surveys for assessing the state of structures [55, 150]. Such methodologies can directly detect damages from a photo or video frames or process video and derive its dynamic properties.

Several approaches have been defined for the support of engineers during a visual inspection, using a Deep Learning-based system [99, 196]. Most of them are focused on bridges since codes require periodic inspections for this kind of structure. On the other hand, for masonry buildings that are very susceptible to earthquakes, there are no approaches in the literature to support or replace the on-site inspection in order to detect, localize and quantify the structural damage. This study is the first attempt to give a synthetic report of the structural damage for a masonry building through a DL-based approach to the authors' best knowledge.

In this context, we propose the use of a vision-based system to support post-disaster Building Safety Evaluations for masonry buildings. An automatic approach can speed up a process mainly based on manual inspections. In addition, the introduction of a support system based on machine learning in error-prone activities, such as the safety report filling, permits more precise correspondence between the actual state and the detected state.

The main contributions of this work can be summarised as follows:

1. A DL-based approach for crack detection, localization, and quantification on masonry buildings utilizing photos of buildings facades;
2. The preparation from scratch of a dataset of concrete cracks for model training;
3. A baseline methodology to produce a synthetic assessment of the structural damage to support the compilation of inspection forms or highlight compilation errors by technicians.

The rest of the Chapter is structured as follows: Section 5.2 describes the proposed approach for crack detection, localization, and quantification in masonry buildings; Section 5.3 reports and analyses obtained results.

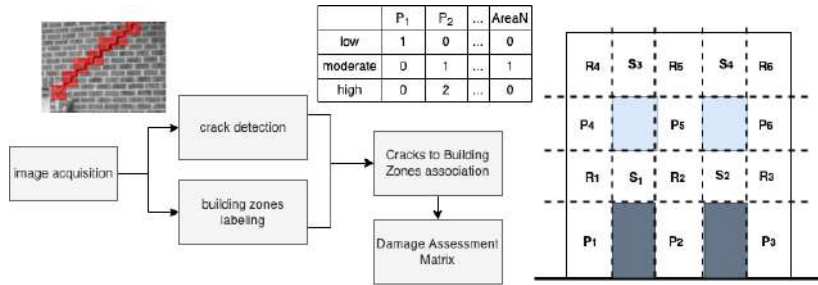


Figure 5.1. The workflow of the proposed approach. On the right there is an example of the building zones subdivision: P_i represents a pier, S_i represents a spandrel, R_i a rigid zone. On the right there is an example of the matrix of damages.

5.2 Materials and Methods

This section, starting from the overall description of the methodology, illustrates the components that contributed to the whole approach.

5.2.1 The Proposed Approach

We propose an image analysis approach, using a set of pictures of the building to be assessed, that provides a synthetic tool to support the compilation and validation of the safety assessment forms filled on site. Figure 5.1 shows a diagram for the overall approach we proposed.

This approach is based on the interaction of two different vision-based predictive models that have the objective to detect, localize and quantify the damage. The Images are acquired during the inspections of the technicians, using high-resolution cameras or by UAVs that detect the different facades of the building following a predetermined path. Both two methodologies can achieve good performance. However, the first allows us to emphasize the details and then highlight the minor damage in the most accessible areas by the technician; vice versa, the drone allows a constant degree of accuracy regardless of the presence of damages. The acquired Images are then processed by the two components of the Damage Assessment system. The first component deals with the identification of the cracks and their intensity. In contrast, the second deals with the localization of the

cracks concerning the schematization adopted in the macro-modeling approach [23]. Starting from detecting the openings, piers, spandrels, and rigid zones will be identified. In particular, as depicted in Figure 5.1, we adopted the following labeling scheme: wall piers are areas on left and right of openings, wall spandrels are areas on top and bottom of openings, rigid zones are areas of intersection between piers and spandrels.

The result of the two components is synthesized in the matrix of damages (matrix in Figure 5.1). This matrix provides information on the amount, intensity, and location of the damage. The generic element of this matrix has the number of cracks detected belonging to the i -th class of damage intensity and located in the j -th macro area. This matrix allows a rapid correlation with the state of the structure. Knowing the extent and quantity of damage, it is possible to estimate the reduction of stiffness of the different macro-areas and, through simplified approaches, evaluate the overall extent of loss of strength of the structure.

5.2.2 Data preparation

Deep Learning (DL) algorithms are data-driven techniques; thus, they profoundly rely on data quality and the amount of data. Primarily, it needs to pay attention to the model's ability to adapt appropriately to new, previously unseen data, i.e., avoid overfitting training data. This aspect is of particular importance in this work. The Images to be analyzed will be taken by instrumentation on drones rather than by technicians during the inspection. So, photos will be highly heterogeneous in brightness, shot angles, and backgrounds. These features make the task analyzed in this work more challenging because, in past works, special consideration was frequently paid when collecting data so that photos are taken in a homogeneous way keeping stable conditions, such as distance, angle, etc. [113, 52, 147]. These rules cannot apply strictly to photos taken by UAVs rather than by technical personnel. In addition, already existing datasets do not provide data about the severity of the cracks.

Therefore, a generic dataset, able to include several scenarios, is critical for increasing the chance of developing a tool that can generalize well and perform adequately in real cases. Considering all these requirements, a new dataset was prepared for this study. The training dataset was populated by labeling photos of post-earthquake surveys in central Italy. Additional

photos were obtained from the Internet. In order to emulate the scenario where different users and instrumentations will work to the data collection, various people photographed cracks with their phones or DSLR cameras. We provided them with simple guidelines, e.g., photographing a whole single facade of a building at a time, being in the front of the facade when possible. The dataset also contained various photos collected by camera drones. In total 115 photos containing cracks, positive patches, and 222 without any crack, negative patches, were gathered. They include several strong light, distortion, and darkness types and have different resolutions. These photos were divided into 224×224 pixels patches, which led to 1652 patches containing cracks. Moreover, 11490 non-crack patches were randomly selected from the gathered photos. For the negative patches, two patches could not overlap. In order to increase the number of crack samples, because crack patches only consist of a small proportion of the collected Images, we generated new patches with the following steps: (i) for a patch containing crack, we got all adjacent patches with an overlapping both horizontal and vertical of 50%; (ii) filtering out all generated patches which not contain cracks; (iii) rotation of each candidate patch by a random angle $\alpha \in [0^\circ, 360^\circ]$. Out of the generated samples from the above steps, the final dataset contained 5423 positive patches.

Multiple annotators labeled the dataset, and they were asked to annotate several pieces of information beyond the crack segmentation. In particular, they annotated the severity of the crack, i.e., low, moderate, high. Low severity was assigned to surface damage visible in close-up photos. Medium severity was assigned to small cracks ($< 5mm$) for which the space is not such that shadows are evident between the crack edges. High severity was associated with all damage effects with significant crack opening with shadows or other major disruption. Of the 5423 positive patches, 813 had a low severity, 1861 moderate, and 2749 high.

In addition, all building openings, i.e., doors and windows, were labeled too. From the 337 photos taken, 2250 building openings were labeled. Windows and doors were considered with their frames. We had to take care of occlusion during the labeling phase, an inevitable feature in the captured data. An occlusion occurs when objects appear in front of objects we label. In that case, we employed a simple strategy: if an object is occluded, the area was still labeled with its corresponding category. This choice arises

from the fact that, in this work, we are mainly interested in identifying the whole area occupied by the object.

5.2.3 Crack detection with Convolutional Neural Networks

In this research, different state-of-the-art CNNs pre-trained on ImageNet [48] were examined for their effectiveness in classifying Images from building surfaces on patch level. The addressed problem was a multi-class classification where the model must discriminate between (i) non-crack, (ii) low severity crack, (iii) moderate severity crack (iv) high severity crack. As the reference dataset described in Section 5.2.2 is relatively small to enable a robust training of a complete deep learning model, transfer-learning via fine-tuning was applied. Fine-tuning was implemented by training only the fully connected (FC) layers at the top of a pre-trained network, using the new data with a low learning rate. In details, an FC layer with 512 features and rectified linear unit (ReLU) activation was added, followed by batch normalization and a dropout layer with a probability of 0.5. Batch normalization is an approach that improves the speed, performance, and stability of artificial neural networks and it is used to normalize the input layer by adjusting and scaling the activations. At the same time, dropout temporarily disconnects the neural connections between connected layers during training. Finally, an FC layer with softmax activation was placed to classify the Images into one of the four classes. CNNs taken into account were: VGG16 [118], DenseNet121 [87], ResNet34 [81], ResNet50 [81]. We trained all our models using Adam optimizer with $\beta_1 = 0.9$, $\beta_2 = 0.99$, $\epsilon = 1^{-5}$, a weight decay of 1^{-2} and a batch size of 64. The considered loss function was the cross entropy (CE) loss function (L_{ce}) and is given as:

$$L_{ce} = -(y \log(p) + (1 - y) \log(1 - p))$$

where y is the ground-truth and p is the probability for that class.

In order to find an optimal learning rate (LR) value, we made use of the *learning rate range test* [176]. LR range test is a technique to estimate the reasonable minimum and maximum boundary values for LR. It runs the model for several epochs while letting the LR increase linearly between low and high LR values after each mini-batch, until the loss value explodes. Plotting the accuracy versus the LR allows choosing the LR one order lower than the point where the loss is minimum.

The performance of the networks was evaluated based on the values of accuracy and F1-score, which are defined as:

$$Accuracy = \frac{TP + TN}{TP + TN + FP + FN}$$

$$F1 = 2 \times \frac{precision \times recall}{precision + recall} = \frac{TP}{TP + \frac{1}{2}(FP + FN)}$$

where TP, TN, FP and FN correspond to true positive, true negative, false positive and false negative, respectively.

Since the problem is a multi-class classification task, the single per-class scores were combined, averaging them. The dataset was split into training, validation, and test sets with ratios 70%, 20%, and 10%, respectively.

5.2.4 Building zones labeling

Section 5.2.1 described how, knowing building openings position, a building facade was subdivided into piers, spandrels, and rigid zones. In this work, building facade openings detection is implemented by means of image segmentation via Convolutional Neural Networks. We categorized the facade image data into two classes: windows and doors. A pseudo-class representing the background categorizes all features that do not belong to other classes. The first deep-learning approach for the semantic segmentation task was based on a fully convolutional neural network (FCN) [120]. In an FCN, the fully connected layers are replaced by convolution layers that act as deconvolution operators. The deconvolution operations restore the output feature maps to the original input resolution, resulting in a class label corresponding to each pixel, i.e., a pixel-wise mask. The spatial resolution of the feature maps, i.e., the outputs of each convolution layer, decreases throughout the feature extraction process, allowing the learned feature maps to be more invariant to small translations of the inputs. However, this downsampling process becomes a considerable concern because the process can potentially erase much information. Herein, we used a U-Net-based architecture, an improvement of FCN. U-Net [203] introduced operations called skip connections, outperforming the FCN approach. The architecture has an efficient symmetric encoder-decoder structure, with a downsampling part, i.e., the encoder, and an upsampling part, i.e., the

decoder. Skip connections concatenate feature maps from the contracting path to the symmetric feature maps in the expansive path. The design allows for features representing small object information to be transmitted to higher levels of the network, better preserving small object information. Because windows and doors are small objects to detect in a building facade dataset, the benefits of the symmetric U-Net architecture are highly relevant to our problem.

Instead of using the encoder as published in the original paper, U-Net was employed as a backbone architecture, but several models replaced the encoder part. We experimented with the same models adopted in the classification task: VGG16, DenseNet121, ResNet34, ResNet50. As the reference dataset is relatively small to enable a robust training of a complete deep learning model, transfer learning via fine-tuning was applied in this task too. In particular, weights computed with the crack classification task described before were adopted as a starting point.

Models were trained with image patches of 512×512 and using Adam optimizer with $\beta_1 = 0.9$, $\beta_2 = 0.99$, $\epsilon = 1^{-5}$, a weight decay of 1^{-2} and a batch size of 10. The considered loss function was the dice loss function which is given as:

$$Dice = \frac{2|A \cap B|}{|A| + |B|} \quad L_{dice} = 1 - Dice$$

where A is the predicted segmentation mask, B the ground-truth one and $|\cdot|$ represents the number of elements in the set.

The learning rate was found with the LR range test technique discussed before. One cycle policy [177] varied the LR during the training. The technique requires an initial interval of values: we choose the maximum value using the range test and the lower as 1/5th or 1/10th of the maximum LR. Starting from this interval, the algorithm went from the lower to the higher value in step one and from the higher back to the lower in step two. We used this approach for each epoch, considering a lower value of 1/10th or 1/100th w.r.t. the maximum one in the few last epochs. An early stopping criterion was used to stop training once the model performance stopped improving on the validation dataset. The dataset was split into training, validation, and test sets with ratios 70%, 20%, and 10%, respectively.

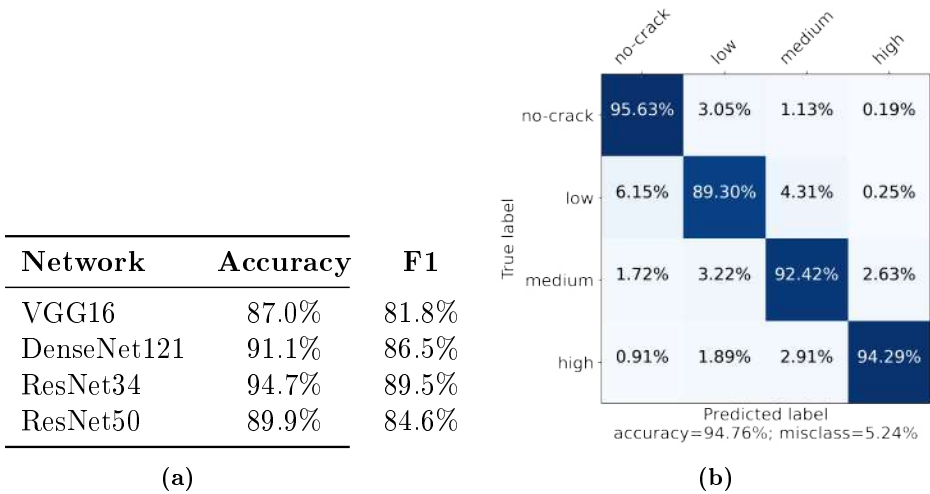


Figure 5.2. Results for the patch classification task. (a) Metrics of the networks;(b) Confusion Matrix for ResNet34 model

A series of post-processing operations were applied to the segmentation masks in order to reduce imperfections by accounting for the standard structure of doors and windows, i.e., rectangular shape. Primarily, noisy data were filtered out using *remove_small_holes* and *remove_small_objects* operations from the Scikit-Image library. Later, using the OpenCV library, all contours in the binary mask were located, and for each one, the bounding rectangle was found.

5.3 Experimental Results

This section presents the results obtained by the trained networks for crack detection and building opening segmentation.

Figure 5.2a enlists the obtained metrics from the trained models on the test set for the crack detection task of Section 5.2.2. While all the considered networks got high accuracy, 87% or more, ResNet34 surpassed the rest by scoring 94.7%, with an F1 score of 89.5%. In order to examine the benefit of transfer learning, ResNet34 was also evaluated without pre-

training with randomly initialized weights. The accuracy and F1 dropped to 86.2% and 81.8%, revealing that transfer learning helped boost performance. Based on the collected metrics, it can be concluded that the network learns rich features that allow for correct classifications on the produced dataset.

Different cases of FP and FN predicted with ResNet34 from the validation set are displayed in Figure 5.3. In Fig. 5.3a, part of an electrical wire is wrongly classified as crack. Evidently, a further expansion of the masonry dataset should better represent these cases. On the contrary, the situation shown in Figure 5.3b needs attention: the model detects a crack, which is not correctly reported in the dataset. In this case, the model shows a superior generalization capacity detecting cracks not annotated during the dataset’s creation. The confusion matrix in Figure 5.2b highlights the performance of the best model. It is deduced that the model excels in predicting the non-crack case correctly. Instead, some difficulty emerges classifying patches with low severity cracks. These issues may be partially explained by the lower number of low-class examples and possibly by some mislabeling introduced by the annotators.

Table 5.1. Metrics of the networks used for building openings segmentation

Network	Pretrained	Parameters	Dice
U-Net-VGG16	Yes	46.1M	70.6%
U-Net-DenseNet121	Yes	41.6M	70.2%
U-Net-Resnet34	Yes	48.0M	71.8%
U-Net-Resnet50	Yes	73.7M	67.9%

Table 5.1 shows the segmentation results from the trained networks. Dice values were very similar among the models, but U-Net-ResNet34 obtained the best, with a value of 71.8%. Although dice value is not very high and other solutions could be investigated, e.g., different segmentation models trained with different loss functions, it is important to note that in this work, the building openings segmentation was of interest only for identifying the areas of the building. This work’s goal was not to find the best segmentation approach for a building facade.

Figure 5.4 shows how the interaction between the zone labeling and



(a)



(b)



(c)



(d)

Figure 5.3. (a) FP example; (b) Wrong FP: patch labeled in the dataset as "no-crack", but it contains a crack that the model detects; (c)(d) FN examples

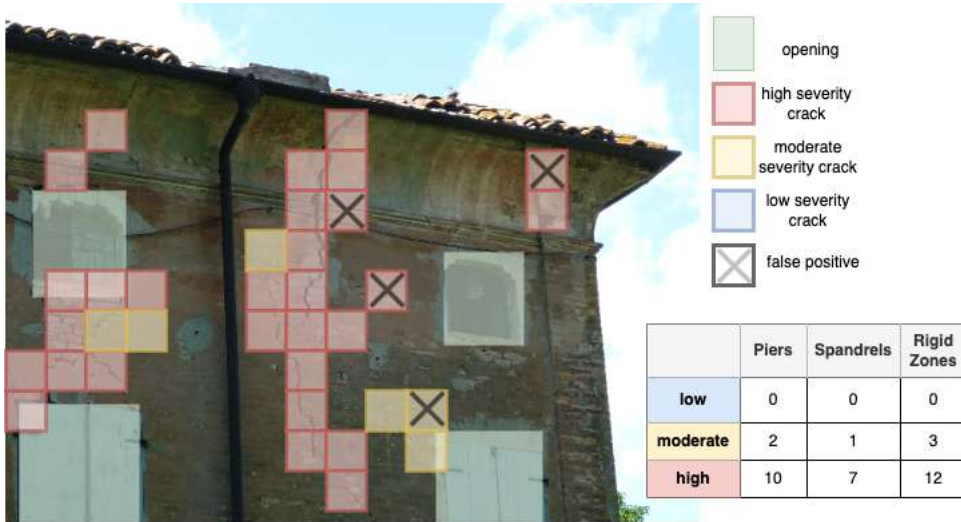


Figure 5.4. Final result example of the overall proposed approach.

the crack detection provides the final output of the proposed approach. The damage assessment matrix summarizes the presence of cracks in the building structure, highlighting their localization in the piers, spandrels, or rigid zone of the whole structure. Technicians can easily use this information to compile the safety form or assess the correctness of an already compiled form.

AI in Maintenance: Minimizing the Carbon Footprint of Bridges

6.1 Introduction

Ensuring an adequate level of safety of existing bridges is one of the main challenges of structural engineering. However, scheduling maintenance activities according to the budget, workforce, and structural performance requirements is a complex task. Therefore, there are several contributions from the scientific literature on the topic proposing different approaches. Most of the related study the planning of cost-effective maintenance while preserving the reliability of the structures [100, 172]. These approaches aim to reduce the expected life-cycle costs while ensuring that the reliability index of the structure is always above a certain target. The specific planning strategies include a broad variety of studies. For example, Ghodoosi et al. [71] described an optimization framework that used a financial model to precisely assess life-cycle costs, and a Genetic Algorithm that served as optimization core of their methodology. The proposed approach was evaluated on a simply supported bridge superstructure, where achieved significant cost reductions. A similar optimization method was considered in combination with Markov-chain models by Morcouis and Lounis [139]. In their formulation the authors considered several groups of

homogeneous facilities, to effectively reduce the computational complexity of the problem. Without any claim of presenting an exhaustive literature review on this vast subject, other notable uses of the same baseline optimization principles can be found, for example, in Liu and Frangopol [117], Miyamoto et al. [136], and Hegazy et al. [83].

Differently, less research was devoted to the emission minimization of maintenance operations. As examples of this stream of research, Peng et al. [152] recently introduced an optimization methodology to optimise the maintenance operations considering sustainability criteria. In their multi-objective formulation, the authors included the failure probability, life-cycle costs, and environmental impact caused by maintenance activities during bridge service process; nevertheless, emissions caused by service interruptions are not considered. Sustainability is also considered in the works of Sun et al. [180] and Gokasar et al. [76]. The former developed a decision support system for maintenance operations that converts emission into costs and embeds them into the life-cycle cost analyses, while the latter devised a tool to produce a bridge maintenance priority ranking. Notably, Gokasar et al. also include in the computation the emissions due to the detour of the truck flow, yet rather than an explicit maintenance schedule for the bridge dataset, the result of their tool consists in a ranking of the bridges whose maintenance needs priority. Ultimately, the works found in the scientific literature mostly approach the scheduling of maintenance operations as a process whose objective is the minimization of costs. Whenever sustainability criteria are evaluated, often the impacts of traffic detour are disregarded, or the output results is simplified. Moreover, most of the studies focus on case studies pertaining single bridges rather than structural portfolios.

This chapter aims to study a framework that minimizes the carbon footprints of the maintenance operations on a portfolio of aging bridges while ensuring adequate safety levels and considering the availability of economic and workforce resources. In this context, the CO₂ emissions are computed as a combination of direct emissions of the maintenance interventions and the pollution caused by the detours. To this end, the core of our methodology is an optimization process based on the Adaptive Large Neighborhood Search algorithm (ALNS) that extensively explores the solution space and interfaces with a Monte Carlo simulation mod-

ule. The stochastic simulation module allows considering the uncertainty that characterizes the structural deterioration process, effectively evaluating the reliability of the solutions analyzed. Accordingly, this chapter formally describes this new optimization driven methodology and compares the maintenance solutions of a diverse set of bridge infrastructures with classical maintenance paradigms, analyzing the performance of the emission-optimized solution in terms of carbon footprint, cost of operations, reliability levels, and job resources required.

6.2 Formal description of the problem

Let $B = \{b_1, b_2, \dots, b_n\}$ be a portfolio of bridges to be maintained, and let T be a time horizon within which the service needs to be guaranteed. The set of possible maintenance interventions $I = \{i_1, i_2, \dots, i_m\}$ is such that each $i \in I$ is associated to a cost, a workforce demand, an improvement in reliability, and a level of traffic interruption. The aim of the problem studied in the present chapter is to schedule a set of maintenance interventions on the bridges of B such that the total CO₂ emission polluted in T is minimized. In this context, the emission related to an intervention i on bridge b_j is computed as the sum of two distinct terms, E_{dir} and E_{det} . The first one represents the emission directly implied by the machinery usage and energy consumption of the intervention, while the second measures the emissions which would result from the detour caused by the closure of the bridge or a traffic limitation. Therefore, E_{det} is computed as:

$$E_{det} = duration \cdot detour \cdot (traffic \cdot car\% \cdot e_{car} + traffic \cdot truck\% \cdot e_{truck}) \quad (6.1)$$

where $traffic$ is the number of vehicles that every day crosses the bridge, $car\%$, and $truck\%$ are respectively the percentages of traffic represented by cars and trucks, while e_{car} , and e_{truck} are the average emission per km of regular vehicles and trucks, respectively. Moreover, each optimized schedule x should satisfy three distinct requirements:

- At any time $t \in [0, T]$, the reliability index of each bridge $b_i \in B$ should be always larger than a user-defined threshold;

- The total costs of the interventions planned on the portfolio within the time horizon should not exceed a maximum budget, B_{max} ;
- At any time $t \in [0, T]$ the workforce usage implied by the interventions planned in x should not exceed the maximum workforce availability, WF_{max} .

In this chapter, the reliability is modelled as proposed by Frangopol et al. [64] (Fig. 6.1). For each bridge, the reliability index can be specified as a combination of two parameters, an initial reliability β_0 and a decaying rate α . At any time, an intervention improves the reliability of a certain amount γ and for a limited yields an improved decaying factor α' .

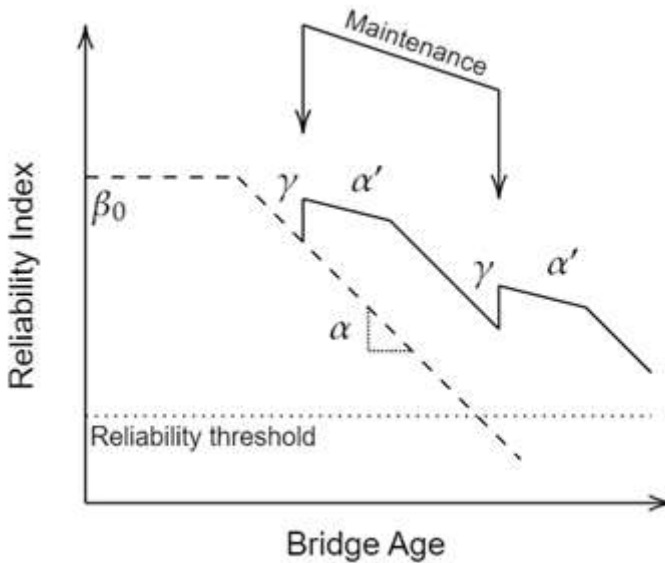


Figure 6.1. Evolution of the reliability index of a bridge.

6.3 Proposed solution methodology

The approach described in the present work relies on two interacting modules: an optimization core to achieve the best possible maintenance

schedule, and a Monte Carlo simulation algorithm to accurately evaluate the reliability indices of the bridges to be maintained. Both components are detailed in the following sections.

6.3.1 Adaptive Large Neighborhood Search

The Adaptive Large Neighborhood Search (ALNS) is a metaheuristic algorithm proposed for solving complex optimization problems. Introduced by Ropke and Pisinger [164], the ALNS generalizes the Large Neighborhood Search (LNS). The LNS is a heuristic algorithm that iteratively modifies an initial solution x with two distinct procedures, one that introduces random perturbations to x , named destroy operator, and a repair operator whose purpose is to optimize the perturbed solution to yield improved performances. Unlike the LNS, the ALNS implements several destroy and repair operators, collected in the sets D and R , to explore more broadly the solution space. According to its optimization strategy, at each iteration, the ALNS randomly selects two operators from D and R to modify the current solution x . Throughout the process, the randomized choice of the heuristics uses selection probabilities related to the past success of each operator.

The pseudocode of Figure 6.2 shows the general structure of the ALNS. The first operations of the algorithm initialize the current solution x , the best solution x_{best} , and the set of probabilities p used in the random selection process. The main loop (lines 4 – 12) explores the solution space and iterates until it verifies the stopping rule. At each iteration, the ALNS selects a destruction and a repair heuristic from the relative sets and modifies x (lines 6 and 7). As a result of these operations, a new solution, \bar{x} , is obtained.

The ALNS accepts \bar{x} as the current solution according to an acceptance rule. In accepting a new current solution, the ALNS balances the drive of improving the objective function with a diversification approach to not stagnate in locally optimal solutions early in the search process. Moreover, if \bar{x} improves the current best objective function, the best solution found is updated. At the end of each iteration, the ALNS updates the selection probabilities of the destruction and repair heuristics. The final output of the algorithm is the best solution found in the search process.

As acceptance criterion the present work uses a Simulated Annealing

```

1 Function ALNS( $x_0$ )
2    $x \leftarrow x_0, x_{best} \leftarrow x_0$ 
3   Initialize probabilities  $p$ 
4   while Stopping rules not met do
5     Select  $r$  and  $d$  according to  $p$ 
6      $\bar{x} \leftarrow d(x)$ 
7      $\bar{x} \leftarrow r(\bar{x})$ 
8     if  $\bar{x}$  is accepted then
9        $x \leftarrow \bar{x}$ 
10      if  $\bar{x}$  improves  $x_{best}$  then
11         $x_{best} \leftarrow \bar{x}$ 
12      Update the probabilities  $p$ 
13  return  $x_{best}$ 

```

Figure 6.2. Pseudocode of a generic ALNS algorithm.

(SA) strategy. CO₂ is a well-known paradigm in the landscape of optimization, as it allows to implement a diversification element in the search process by possibly accepting worsening solutions during the exploration of the solution space. Using a characteristic parameter τ , SA computes the difference ΔE between the objective function value of the new solution \bar{x} and the current solution x . Then, the probability of accepting \bar{x} as the new current solution, $P(\Delta E)$, is:

$$P(\Delta E) = \begin{cases} 1, & \text{if } \Delta E < 0; \\ e^{-\Delta E/T}, & \text{otherwise.} \end{cases} \quad (6.2)$$

During the iterations of the ALNS, τ decreases, so that as the search process progresses, the probability of accepting worsening solutions is reduced.

The pools D and R of destructive and repair heuristics implemented to optimize the carbon footprint of maintenance operations are as follows. Operating on a current maintenance schedule x of the n bridges, D comprises three distinct operators, all of which use an input percentage parameter ρ that regulates the disruption's intensity:

1. Random activity removal (RAR): a random ρ of the maintenance activities scheduled in x are removed from the solution;
2. Random bridge schedule removal (RBR): a random ρ of the bridges

is selected. RBR removes all the maintenance activities scheduled on such bridges;

3. Random activity type removal (RTR): a random ρ of the activity types is selected. RTR removes from x all maintenance interventions of such types.

Respectively, the operators implemented in the set R are:

1. First Possible Improvement (FPI): The set B of bridges is iterated sequentially. On each bridge, FPI schedules the first intervention that improves the objective function value until all the bridges are above the reliability threshold throughout the time horizon.
2. Best Intervention in Bridge Sequence (BBS): The set B of bridges is iterated sequentially. On each bridge, BBS schedules the best intervention in terms of lowest possible emissions until all the bridges are above the reliability threshold throughout the time horizon.

6.3.2 Monte Carlo simulations

Classically, problems of the optimization literature were described using deterministic formulations, yet their applications to real-world scenarios constantly faced the challenges implied by uncertainty. Accordingly, when the optimization algorithms do not account for stochasticity, the solutions achieved may be unstable or not feasible in practical applications [36]. Therefore, a growing stream of research combined the power of metaheuristic algorithms with the assessment provided by Monte Carlo simulations [62]. These hybrid simulation-optimization approaches allow the correct assessment of promising solutions by evaluating the uncertainties that characterize the problem of interest. In the context of bridge maintenance planning, the reliability index of each structure is related to uncertain information. Indeed, either for the epistemic uncertainties of the model assumptions or the noise and incompleteness in data, at each stage of the time-horizon the decaying factor α of the reliability index can be seen as a random variable. To this end, at each time stage t within the time horizon, the reliability index can be obtained as the reliability value corresponding to the previous time instant, $t - 1$, diminished according to

a stochastic α factor. In our framework, this stochasticity is modeled as a Weibull random variable, with shape and scale respectively equal to 0.05 and 2, therefore giving:

$$\beta(t) = \beta(t - 1) - \Delta T \cdot (\alpha - wblrnd(0.05, 2)) \quad (6.3)$$

Conclusively, the proposed approach uses Monte Carlo simulations to accurately evaluate the feasibility of each maintenance schedule under different conditions. To this end, each evaluation of a new solution x features a user-defined number of Monte Carlo sampling of the stochastic variables throughout the time horizon $[0, T]$, and verifies that the maintenance operations planned in x are such that requirement R1 of Section 6.2 is satisfied for each simulated scenario. To balance reliability of the structural assessments and computational performance, the Monte Carlo simulation module follows a two-staged process. In fact, during the execution of the ALNS, the solutions are evaluated using a lower number of simulations, n_{sim} . On the contrary, at the end of the optimization process, the best solution found is assessed with a higher number of simulations, $N_{sim} > n_{sim}$, to appraise the feasibility with higher accuracy.

6.4 Computational Analysis

The numerical experiments that assess the performance of the proposed metaheuristic approach rely on the comparison of the solutions achieved the ALNS with solutions obtained using the time-based and the condition-based maintenance strategies. The analyses use a benchmark containing geographical and logistic information available for existing bridges and consider three different scenarios arranged in decreasing order of mean reliability index. The benchmark set featured in the numerical analyses is thoroughly described in Section 6.4.1, while the computational results are presented in Section 6.4.2. Our proposal is implemented in Matlab 2019 and the experiments were run on a 3.50 GHz Intel Core I9 processor with 64 GB of RAM.

Table 6.1. Summary of the bridges considered in the numerical experiments.

ID	Year Built	L	W	Detour	Avg Daily Traffic	Avg Daily Truck Traffic
#	[y]	[m]	[m]	[Km]	#	%
1	1942	13.7	26.5	0	55700	4
2	1942	17.1	26.5	0	55700	4
3	1942	14.3	26.5	0	55700	4
4	1959	21.9	47.3	2	153700	5
5	1959	12.5	28.0	3	153700	5
6	1963	21.3	8.4	2	12500	5
7	1959	14.9	24.4	2	150600	4
8	1964	17.4	11.9	2	19700	1
9	1964	15.9	14.6	2	24500	1
10	1964	18.6	13.7	2	15800	1
11	1964	22.6	11.4	3	10400	1
12	1962	21.3	41.5	3	10700	1
13	1972	21.6	41.5	2	58000	5
14	2012	23.2	20.1	0	86500	4
15	2012	22.9	18.0	3	86500	4

6.4.1 Benchmark Dataset

The dataset used in the numerical experiments is extracted from the bridge data provided by the Federal Highway Administration (FHWA) of the U.S. Department of Transportation. The full dataset, retrievable online [144], comprises over 600 thousand structures, with the aim of precisely inventorying the bridges of the nation. Each bridge is catalogued using a wide range of information, collected in a maximum of 117 items, including structural and historical data, ownership, geographical location, and so on. The bridges used in the computational experiments of the present section are 15 PSC highway bridges of the District of Columbia. The structures were built between 1942 and 2012, and presented span lengths ranging from 13.7 m to 23.2 m. For each bridge, Table 6.1 reports the main geometric characteristic and a summary of the daily traffic record.

Subsequently, starting from the bridges summarized in Table 6.1, this work considers three scenarios, arranged in decreasing order of mean reli-

Table 6.2. Summary of the possible maintenance operations considered in the analyses.

(Sun, Xiao-Yan, et al.,2015)

ID	Name	Traffic	Average Cost	Average Reliability improvement	Work Force
#	-	-	[Euro/m ²]	[-]	[units/m ²]
1	Surface Repair	Normal	469.00	0.375	0.016
2	Bearing replacement	Closure	7273.00	2.475	0.126
3	Crack injection	Limited	588.00	0.250	0.020
4	Silane treatment	Limited	882.00	0.000	0.031
5	Cathodic protection	Normal	987.00	0.000	0.034
6	Deck-thickening	Closure	699.30	0.000	0.012
7	Steel jacketing	Limited	1440.60	1.800	0.025
8	FRP jacketing	Limited	1254.40	0.975	0.022
9	Section enlarging	Closure	3857.00	1.060	0.067
10	Component replacement	Closure	2667.00	1.605	0.093
11	External prestress	Normal	1484.00	1.390	0.026

ability index at $t = 0$. These scenarios are denoted as “Moderate”, “Low”, and “Critical”, and are characterized by initial mean β values of 3.25, 3.5 and 4.2. Lastly, the maintenance interventions considered in the algorithm are summarized in Table 6.2

6.4.2 Numerical Results

Sec. 6.3 reports the computational results achieved in the numerical experiments. For each scenario, and each maintenance strategies, the solution performance is compared in terms of emissions and costs. Analysing the results, the first behaviour that can be pointed out is that as expected the Time-based maintenance is the strategy characterized by the least competitive performance. This is widely expected, as also pointed out in the scientific literature, since the fixed-time schedule of the time-based maintenance often results into frequent and yet not necessary maintenance operations. Therefore, this property is reflected in both the economic cost and the emissions related to this approach, that are larger than those achieved by the ALNS by one order of magnitude in all three scenarios.

On the contrary, the maintenance schedule achieved by the Condition-based approach is more competitive, both in terms of costs and emissions, as its operations are strictly related to the reliability indexes of the struc-

Table 6.3. Comparison of the optimized solution (ALNS) with the maintenance schedule of the Condition-based and Time-based approaches

Moderate	Maintenance Strategy		
	ALNS	Condition-Based	Time-Based
cost	2.19E+06	2.38E+06	2.10E+07
Emission [CO ₂ ton]	1.04E+04	3.09E+04	1.76E+05

Low	Maintenance Strategy		
	ALNS	Condition-Based	Time-Based
cost [€]	5.41E+06	1.69E+07	3.03E+07
Emission [CO ₂ ton]	4.46E+04	1.17E+05	1.78E+05

Critical	Maintenance Strategy		
	ALNS	Condition-Based	Time-Based
cost [€]	9.57E+06	2.78E+07	1.41E+07
Emission [CO ₂ ton]	7.92E+04	1.29E+05	1.35E+05

tures of interest. The performance achieved by the ALNS in the Moderate scenario are comparable in terms of total costs while improving the emissions of the Condition-based by 66%. Moreover, as the global reliability of the portfolio worsen -i.e., for scenarios Low and Critical the advantages of using the proposed approach are notably increased, as both the costs and the emission values are markedly reduced. These results evidence how the use of an optimization approach is a valuable resource whenever the average number of interventions to be planned within the time horizon is high. To better grasp the evolution in time of the three approaches, using Medium as scenario of reference, Figures 6.3 and 6.4 depict the evolutions of the costs and the emissions of the three maintenance approaches. Analysing the cumulative costs in time, it can be observed how the proactive nature of the Time-based approach implies periodic and significant spikes in the total budget spent, while the Condition-based strategy and the ALNS, being more focused on reliability indices, are able to guarantee the same levels of safety by scheduling targeted maintenance interventions. The cumulative emission values of Figure 6.1 also show that the Time-based strategy implies frequent unnecessary traffic interruptions and thus high

emissions. Moreover, the ALNS can maintain a reduced value for the total emissions by scheduling fewer interventions.

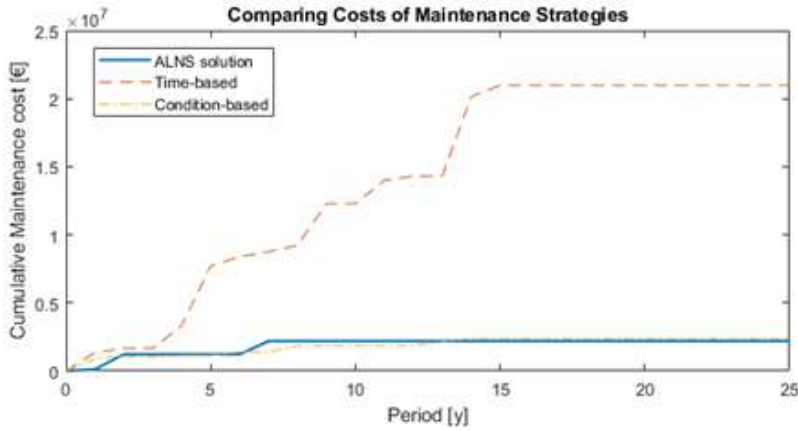


Figure 6.3. Evolution of the costs implied by the three maintenance strategies in time.

This feature is also reflected by Figure 6.1, that reports the evolution of the reliability indices of the three bridges of B characterized by the lowest β at $t = 0$. Analyzing the increases of the reliability, it is possible to note that the ALNS has the tendency to schedule interventions that on average increase β more. While this locally can imply lower costs for the Condition-based maintenance, ultimately means that this strategy is forced to multiple interventions that cause several traffic interruptions and therefore higher emissions.

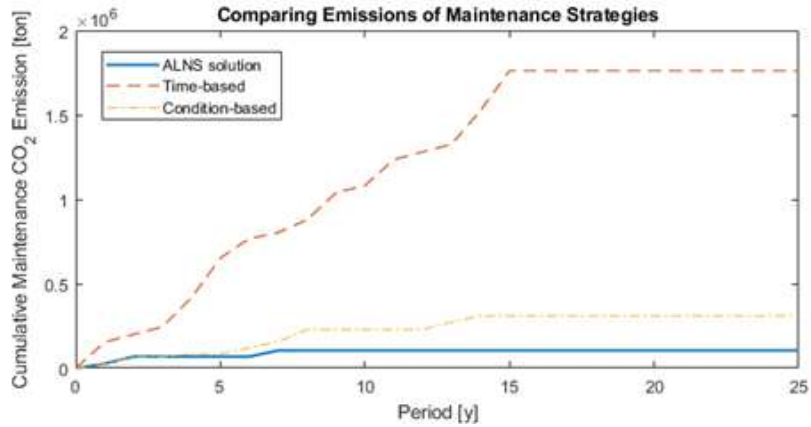


Figure 6.4. Evolution of the emissions caused by the three maintenance strategies in time.

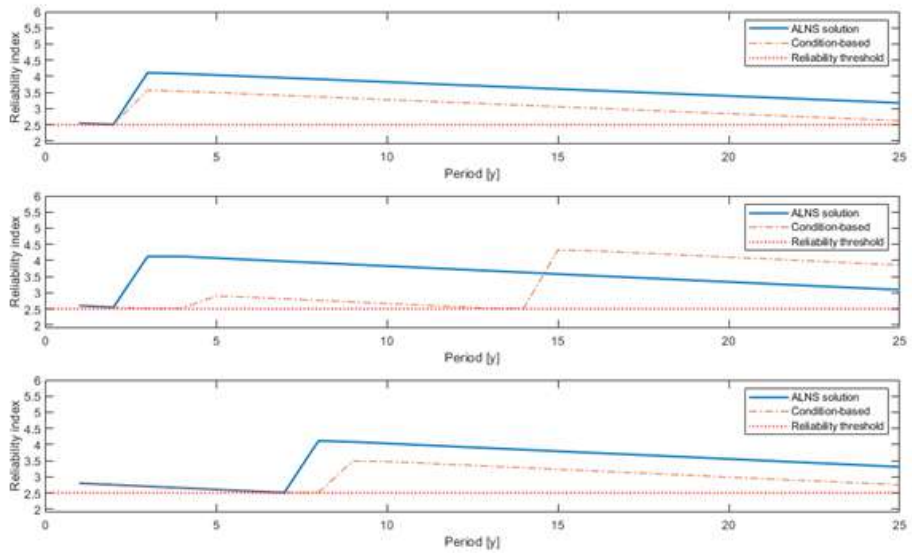


Figure 6.5. Evolution in time of the reliability indices of the three bridges characterized by the lowest values at $t = 0$.

Conclusions

This thesis presents several applications of the AI methodology in structural engineering concerning different phases of the structure's lifecycle. The methodologies presented in this work address traditional structural engineering problems in innovative ways. Implementing smart solutions allows for improving the structural design quality, existing structures' safety, and helping minimize infrastructures' environmental impact.

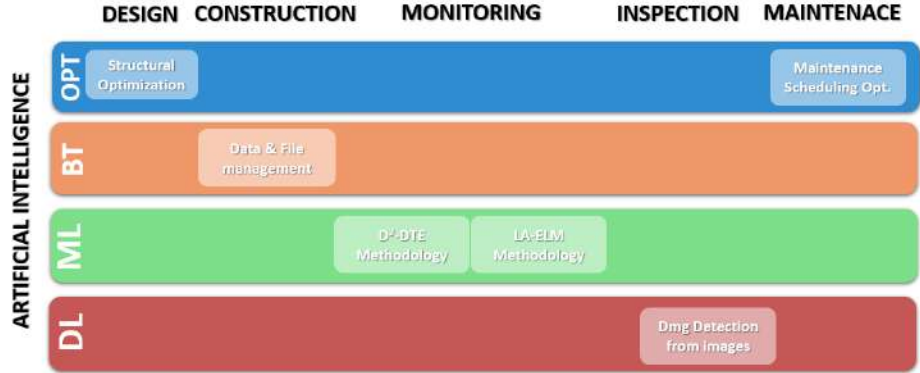


Figure 6.6. Chapters and Technologies.

Figure 6.6 depicts the thesis flow showing for each chapter the implemented technology. OPT consent to improve structural performance in challenging situations, like irregular buildings and reduce carbon emissions by finding the best scheduling solution for maintenance interventions. Then, Machine learning and Image Analysis enable all the possibilities of

artificial intelligence dealing with big data, providing prediction on the health state of structures from sensors data or analyzing the inspection's report. Finally, blockchain and smart contracts consent to certify data integrity to improve trust in material and structure test reports.

For the sake of clarity, in this section, the principal results and limitations of the proposed methodologies are discussed separately.

Chapter 1 proposed a novel formulation of the pre-dimensioning problem of reinforced concrete frame structures, which is aimed to regularize the dynamic behavior of structures in seismic areas. In particular, the mathematical formulation describes the problem in terms of inter-story drifts and modal participating mass ratios, given their pivotal importance in regulatory codes particularly when it comes to reduce non-structural damage in the event of earthquakes with high probability of occurrence. Additionally, since one of the aims of the contribution consists in the description of a solution strategy that could be implemented in the common approaches of structural practitioners, the problem is solved by means of a learn-heuristic algorithm that hybridizes a Genetic Algorithm with a local search and a k-means procedure, to address as well an additional limitation on the different number of cross-sections in the structure.

The mathematical criteria described in Chapter 1 are the core principles guiding the optimization algorithm in exploring the design space. Such evaluation of the structural regularity addresses both the equivalent static load and the dynamic behavior of the structure by evaluating drift ratios and by considering the participating masses of the modes.

As evidenced by the numerical experiments, this mathematical framework, with the addition of specific constraints to limit normal stress levels, achieves good designs. Indeed, the optimization principles strive to achieve the sufficient capacity to prevent collapses for rarer seismic events and simultaneously control damages for more frequent events. Remarkably, the guiding principles put in practice by the optimization algorithm are also pursued in classical design methodologies.

The design of automated optimization strategies allows exploring a wide variety of solutions, therefore enhancing the freedom of design. Accordingly, in their implementation within the well-established processes of the construction sector, specific care needs to be devoted to the feasibility of the optimized solutions from the realization standpoint. To adequately

bridge the gap between innovative solutions and common practices, this work includes an additional constraint that allows the user to limit the maximum number of different cross-sections used.

Chapter 2 proposed a proof-of-concept of the integration of blockchain technology and smart contract into information flows that deploy among different CDEs. The proposal focuses on reducing human errors and increasing the reliability and transparency of decision processes on construction sites concerning the structural system. To this end, the proof-of-concept introduces smart contracts with different levels of complexity: basic -for certifying information flows, intermediate - for also gathering multiparty signatures or consent, and advanced - for comparing automatically exchanged information with data gathered by IoT sensors on site. Preliminary testing of the proof-of-concept consists of a comparison between the latter and the traditional approach in terms of criticalities that arise in the exchange of information and the characteristics of reliability of exchanged information and transparency of decision-making processes. The proposal reduces the risk of human errors in transmitting the information and increases reliability and transparency in construction site information management. To do so, some checking activities are automatically performed by a combination of smart contracts and AI algorithms. It is worth noting that the proposal allows integrating blockchain technology into the construction site activities both today and in the long term. In fact, even when the BIM approach is applied, the construction process of structural systems deploys a huge amount of paper documentation that traces human activities on the construction site. Accordingly, leaving current practices unchanged, the blockchain can have the potential to certify construction site documentation and eliminate dependence on paper, also legally. Additionally, increased reliability and traceability of information flows, that are certified on the blockchain, introduce the possibility of implementing tools to trace back the construction process at any moment. These valuable features will be even more worthy in the next future when other innovative technologies of IoT, 3-D printing, and additive manufacturing will lend to the construction site. Those new construction practices will require suitable checking processes and also suitable storage of sensible data. The proof-of-concept provides an answer to this need using advanced smart contracts and artificial intelligence applications. This last

step would make it possible to close the circle by integrating the use of the BIM approach to manage all the information of the construction site 4.0.

Chapter 3 explored the potential of a SHM framework based on a vibrational approach coupled with a decision trees ensemble learning method, for the damage-detection and localization of r.c and steel structures, denoted as D²-DTE. More specifically, the DTE uses vibration periods and modal shapes of a target structure as inputs, which are simulated through a set of different (possible) damage scenarios, including multiple damages of different type and severity. This allows the learning of the association rules connecting the dynamic properties exhibited by a structure, and the corresponding structural health assessment.

To evaluate the performances of the proposed SHM framework, the numerical validations considered three different test-cases, to properly test the decision tree ensemble on data that is either simulated on numerical models, or recorded on a structure of interest in laboratory conditions.

In the study of damage detection according to different levels of detail, the DTE evidences small distance errors in the localization of single damages, even in the presence of non-negligible random Gaussian noise. This behavior suggests a favorable implementation of this method in the context of continuous monitoring. Indeed, such a paradigm would enable the continuous detection of the dynamic properties of the system, and should produce an alert at the first occurrence of damage in the structure which could be, in principle, localized satisfactorily.

On the other hand, as expected, the classification and localization of two damaged elements led to reduced accuracy due to the more complex interactions taking place in the structural behavior. Nevertheless, as for the single damage configurations, the localization errors detected did not evidence a huge decrease in performance. Indeed, DTE produced minor localization errors across the entire validation set, suggesting that it is possible to identify a limited area – centered around the predicted damage location – that probably encloses the real damaged element.

Additionally, for the sake of comparison, the proposed methodology is used in the analysis of two well-known benchmark datasets: the IASC-ASCE benchmark model, and the QUGS. In particular, the performances achieved in these two test cases compare favorably with respect to a reference solution approach based on Convolution Neural Networks, always

scoring an accuracy higher than 98%.

In conclusion, given the growing interest in the integration of ML algorithms with SHM, future investigations should increase the maturity level of smart monitoring technologies for real-case scenarios. On this line, future works will include further experiments with data collected in operational conditions and low damage levels, to bring added value in the assessment of the sensitivity of our method in a real world scenario. In addition to these analyses, further advancements can be achieved increasing the computational efficiency of the training process of our methodology, reducing the number of training samples needed to correctly build the learning model.

Since the D²-DTE belongs to the family of methods that classify damages learning the properties of a simulated dataset, an accurate modelling of the structural system is a pivotal component of the proposed damage detection system. Therefore, when targeting a structure of interest, enhanced and reliable results could be gathered by preceding the D²-DTE with a pre-processing stage in which an adequate numerical model is achieved via model-updating techniques [14, 183].

Additionally, to enhance the performances achieved in the inclusion of ML in SHM, future research will investigate cutting-edge classification algorithms – as Enhanced Probabilistic Neural Networks [5] and the Neural Dynamic Classification [157] – to improve robustness in case of low signal-to-noise ratio, and to include an optimized exploration of the feature spaces to find the optimal subset of input features to achieve an accurate classification, respectively.

In particular, further studies can involve the relationship between temperature variations and the corresponding dynamic measurements. In fact, an in-depth study of the effects of such variations can improve the quality of the dynamic identification and localization, especially when dealing with limited damages. In addition, to properly evaluate reliability of a damage detection system especially when describing a decision-making framework, a significant effort has to be carried out to estimate and approximate the effects of the epistemic uncertainties related to model assumptions or experiment design.

Finally, a favorable step towards robustness could involve the inclusion of additional sensor types to describe the state of a real structural sys-

tem more extensively, introducing measurements such as temperature and displacements, and a subsequent testing on datasets that properly enclose complex dynamic behaviors of existing structures, such as Z24 [122].

Chapter 4 described a damage-detection approach based on the Extreme Learning Machine algorithm – named LA-ELM – to address the problem of automatically locating and quantifying losses of tensions affecting the prestressing system of a PSC bridge. The proposed methodology uses stress data as input features and embeds a layout-aware weight generating procedure to guide the learning model towards a spatially-consistent network topology.

The computational experiments tested the LA-ELM in the analysis of the numerical models of three different bridge specimens. The tests evidenced that, for the specific type of damage considered, stress appear to be significantly more sensitive than vibration periods and modal shapes. The results achieved in the regression analysis evidence low RMSE errors, whose total average is ≈ 0.07 . The performance quality slightly decreases when the Gaussian noise level increases, as expected, yet the errors remain limited. A similar trend can be observed with respect to the length L of the deck, with the RMSE values that increase when L is increased. This result could be justified observing that the same amount of stress data points is used in the analysis structures of sensibly different lengths. Therefore, future studies could optimize the regression quality controlling the number and positioning of sensors of the structure.

Moreover, a two-sided Wilcoxon signed-rank test ($\alpha = 0.01$) evidenced that the layout-aware weight generating process yields statistically significant improvements (p-value = $4.88 \cdot 10^4$) with respect to a naive implementation of ELM, in which the weights are drawn randomly.

A comparison of LA-ELM with other learning algorithms evidence that the proposed methodology is characterized by a competitive trade-off between accuracy and computational expenses. Conclusively, the fast training process and low errors recorded by the LA-ELM suggest a favorable implementation of this technique as base-learner in a real-time monitoring scenario. However, further testings require the study of real datasets that properly enclose complex dynamic behaviors of existing structures, to accurately assess the challenges to be faced in the monitoring of a real-world structure.

Chapter 5 proposed a methodology to define a support system for the compilation of forms for the safety assessment of masonry buildings after a seismic event. In an emergency context, this tool is fundamental to guarantee the precision and accuracy of the data collected by field engineers, and therefore, the quality of emergency operations and reconstruction plans. The system is founded on an integrated approach based on two DL-based models that work together, evaluating cracks and localizing them in the macro-areas of the facades of a masonry building. For the training of the predictive models, a dataset with photos from masonry structures was assembled containing complex backgrounds and various crack types and sizes. Different Deep Learning (DL) networks were evaluated, and by leveraging the effect of transfer learning, crack detection on masonry surfaces was performed on a patch level. ResNet34 obtained the highest accuracy, which was 94.7%. In addition, a DL model for building openings segmentation was assessed in order to subdivide the building facade into piers, spandrels, and rigid zones. U-Net-ResNet34 obtained the best result with a dice score of 71.8%. Mixing these pieces of information, the damage assessment matrix was proposed as a synthetic perspective of the structural damage of the building.

Currently, the system has some constraints related to the characterization of the cracks discovered on the building surface. The proposed approach was founded on patch-based crack detection. Although it permitted promising results in terms of accuracy with a small dataset, it allowed quantifying the damage just in terms of the number of the detected areas interested by a crack. This number depends on the patch's size and cannot describe proper measurements of crack characteristics, including the area, perimeter, width, length, and orientation. So, the system can be improved both in its current components and by adding new components in the future. In particular, the results of DL methods heavily rely on the dataset's quality. Thus, the expansion of the current masonry dataset is highly recommended. A semantic segmentation approach could be analyzed to detect cracks and characterize them in terms of area, width and length. Finally, new modules could be added to allow the automatic compilation of forms, the digitization of their results in a Building Information Modeling (BIM) environment, and the optimized design of rehabilitation interventions.

The framework presented in Chapter 6 studied the carbon footprint optimization of the maintenance operations on a set of aging bridges. To this end, the problem was formally described in terms of an objective function that cumulates both direct emissions of the interventions and the pollution caused by the detours implied by traffic interruptions. The maintenance schedule pursued in this work is subject to three different constraints, requiring that at any time within the time horizon, the reliability indices of the structures need to be above a certain threshold and that the total costs and periodic workforce implied by the operations need to be below the maximum values allowed. To solve the problem, this chapter presents a hybrid optimization-simulation algorithm that combines the intensification ability of an ALNS metaheuristic with the stochastic simulation of the Monte Carlo approach. Accordingly, the proposed solution approach can broadly explore the solution space in the pursuit of optimized solutions while correctly accounting for the uncertainty that characterizes the optimization scenario. In the numerical experiments, the proposed approach was compared with two well-established maintenance strategies: the Time-based approach and the Condition-based approach. The computational results evidence that the ALNS-based algorithm can achieve improving solutions in terms of emissions with respect to the two competitors and at least comparable values in terms of total costs. In future research, this approach will be combined within a specific structural health monitoring framework so that at any time, the reliability indices can be estimated with higher accuracies and formulate a feedback framework that automatically plans CO₂-efficient maintenance interventions as soon as the monitoring process detect structural criticalities. Moreover, the optimization core of the methodology will be extended so that bridge portfolio of larger sizes can be managed in short computational times.

Bibliography

- [1] O. Abdeljaber, O. Avci, and D. J. Inman. Active vibration control of flexible cantilever plates using piezoelectric materials and artificial neural networks. *Journal of sound and Vibration*, 363:pp. 33–53, 2016. doi: <https://doi.org/10.1016/j.jsv.2015.10.029>.
- [2] O. Abdeljaber, O. Avci, S. Kiranyaz, M. Gabbouj, and D. J. Inman. Real-time vibration-based structural damage detection using one-dimensional convolutional neural networks. *Journal of Sound and Vibration*, 388:154–170, 2017.
- [3] A. Adams, N. Galindez, T. Hopper, T. Murphy, P. Ritchie, V. Storlie, J. Weisman, et al. Manual for refined analysis in bridge design and evaluation. Technical report, United States. Federal Highway Administration. Office of Infrastructure, 2019. URL <https://www.fhwa.dot.gov/bridge/pubs/hif18046.pdf>. (Visited on August 2021).
- [4] F. E. M. Agency. Earthquake-resistant design concepts-an introduction to the nehrp recommended seismic provisions for new buildings and other structures. *FEMA P-749. Federal Emergency Management Agency Report, The National Institute of Building Sciences, Building Seismic Safety Council, Washington*, 2010.
- [5] M. Ahmadlou and H. Adeli. Enhanced probabilistic neural network with local decision circles: A robust classifier. *Integrated Computer-Aided Engineering*, 17(3):197–210, 2010.
- [6] E. Androulaki, A. Barger, V. Bortnikov, C. Cachin, K. Christidis, A. De Caro, D. Enyeart, C. Ferris, G. Laventman, Y. Manevich, et al. Hyperledger fabric: a distributed operating system for permissioned

- blockchains. In *Proceedings of the thirteenth EuroSys conference*, pages 1–15, 2018.
- [7] G. Apostolakis. Optimal evolutionary seismic design of three-dimensional multistory structures with damping devices. *Journal of Structural Engineering*, 146(10):04020205, 2020.
- [8] J. A. Aslam, R. A. Popa, and R. L. Rivest. On estimating the size and confidence of a statistical audit. *EVT*, 7:8, 2007.
- [9] O. Avci, O. Abdeljaber, S. Kiranyaz, M. Hussein, and D. J. Inman. Wireless and real-time structural damage detection: A novel decentralized method for wireless sensor networks. *Journal of Sound and Vibration*, 424:158–172, 2018.
- [10] M. Azimi and G. Pekcan. Structural health monitoring using extremely compressed data through deep learning. *Computer-Aided Civil and Infrastructure Engineering*, 35(6):597–614, 2020.
- [11] A. Azizinamini, B. Keeler, J. Rohde, and A. Mehrabi. Application of a new nondestructive evaluation technique to a 25-year-old prestressed concrete girder. *PCI journal*, 41(3), 1996. doi: <https://doi.org/10.15554/pci.05011996.82.95>.
- [12] N. Bagge, J. Nilimaa, and L. Elfgren. In-situ methods to determine residual prestress forces in concrete bridges. *Engineering Structures*, 135:pp. 41–52, 2017. ISSN 18737323. doi: <https://doi.org/10.1016/j.engstruct.2016.12.059>.
- [13] M. A. K. Bahrin, M. F. Othman, N. H. N. Azli, and M. F. Talib. Industry 4.0: A review on industrial automation and robotic. *Jurnal teknologi*, 78 (6-13), 2016.
- [14] P. G. Bakir, E. Reynders, and G. De Roeck. Sensitivity-based finite element model updating using constrained optimization with a trust region algorithm. *Journal of Sound and Vibration*, 305(1-2):211–225, 2007.
- [15] A. Baliga. Understanding blockchain consensus models. *Persistent*, 4(1): 14, 2017.
- [16] E. Baran, C. Shield, and C. French. A comparison of methods for experimentally determining prestress losses in pretensioned prestressed concrete girders. *Special Publication*, 231:pp. 161–180, 2005. doi: 10.14359/14926.
-

-
- [17] F. Barbosa, J. Woetzel, and J. Mischke. Reinventing construction: A route of higher productivity. Technical report, McKinsey Global Institute, 2017.
- [18] D. P. Billington. Historical perspective on prestressed concrete. *PCI journal*, 49(1):pp. 14–31, 2004. ISSN 0887-9672. doi: <https://doi.org/10.15554/pcij.09011976.48.71>.
- [19] E. Bocherens, S. Bourasseau, V. Dewynter-Marty, S. Py, M. Dupont, P. Ferdinand, and H. Berenger. Damage detection in a radome sandwich material with embedded fiber optic sensors. *Smart materials and structures*, 9(3): 310, 2000.
- [20] M. Bonopera, K. C. Chang, and Z. K. Lee. State-of-the-art review on determining prestress losses in prestressed concrete girders. *Applied Sciences (Switzerland)*, 10(20):pp. 1–14, 2020. ISSN 20763417. doi: <https://doi.org/10.3390/app10207257>.
- [21] L. Breiman. Bagging predictors. *Machine learning*, 24(2):123–140, 1996.
- [22] L. Breiman. *Classification and regression trees*. Routledge, 2017.
- [23] A. Brencich, L. Gambarotta, and S. Lagomarsino. A macroelement approach to the three-dimensional seismic analysis of masonry buildings. In *11th European Conference on Earthquake Engineering*, volume 90, pages 1–10, 1998.
- [24] J. Brimberg, N. Mladenović, R. Todosijević, and D. Urošević. Less is more: solving the max-mean diversity problem with variable neighborhood search. *Information Sciences*, 382:179–200, 2017.
- [25] R. Brincker, L. Zhang, and P. Andersen. Modal identification from ambient responses using frequency domain decomposition. In *Proc. of the 18th International Modal Analysis Conference (IMAC), San Antonio, Texas*, 2000.
- [26] A. Bulut, A. K. Singh, P. Shin, T. Fountain, H. Jasso, L. Yan, and A. Elgamal. Real-time nondestructive structural health monitoring using support vector machines and wavelets. In *Advanced Sensor Technologies for Nondestructive Evaluation and Structural Health Monitoring*, volume 5770, pages 180–189. International Society for Optics and Photonics, 2005. doi: <https://doi.org/10.1117/12.597685>.
- [27] A. Cabboi, C. Gentile, and A. Saisi. From continuous vibration monitoring to fem-based damage assessment: application on a stone-masonry tower. *Construction and Building Materials*, 156:252–265, 2017.
-

-
- [28] J. M. Caicedo, S. J. Dyke, and E. A. Johnson. Natural excitation technique and eigensystem realization algorithm for phase i of the iasc-asce benchmark problem: Simulated data. *Journal of Engineering Mechanics*, 130(1): 49–60, 2004.
- [29] G. M. Calvi, M. Moratti, G. J. O’Reilly, N. Scattarreggia, R. Monteiro, D. Malomo, P. M. Calvi, and R. Pinho. Once upon a Time in Italy: The Tale of the Morandi Bridge. *Structural Engineering International*, 29(2): pp. 198–217, 2019. ISSN 16830350. doi: <https://doi.org/10.1080/10168664.2018.1558033>.
- [30] C. V. Camp and F. Huq. Co2 and cost optimization of reinforced concrete frames using a big bang-big crunch algorithm. *Engineering Structures*, 48: 363–372, 2013.
- [31] A. Cancelli, S. Laflamme, A. Alipour, S. Sritharan, and F. Ubertini. Vibration-based damage localization and quantification in a pretensioned concrete girder using stochastic subspace identification and particle swarm model updating. *Structural Health Monitoring*, 19(2):pp. 587–605, 2020. doi: <https://doi.org/10.1177/1475921718820015>.
- [32] Y.-J. Cha, W. Choi, G. Suh, S. Mahmoudkhani, and O. Büyüköztürk. Autonomous structural visual inspection using region-based deep learning for detecting multiple damage types. *Computer-Aided Civil and Infrastructure Engineering*, 33(9):731–747, 2018.
- [33] T. H. Chan and T. H. Yung. A theoretical study of force identification using prestressed concrete bridges. *Engineering Structures*, 22(11):pp. 1529–1537, 2000. ISSN 01410296. doi: [https://doi.org/10.1016/S0141-0296\(99\)00087-5](https://doi.org/10.1016/S0141-0296(99)00087-5).
- [34] C.-M. Chang, T.-K. Lin, and C.-W. Chang. Applications of neural network models for structural health monitoring based on derived modal properties. *Measurement*, 129:457–470, 2018.
- [35] P. C. Chang, A. Flatau, and S. Liu. Health monitoring of civil infrastructure. *Structural health monitoring*, 2(3):257–267, 2003.
- [36] M. Chica, A. A. Juan Pérez, O. Cordon, and D. Kelton. Why simheuristics? benefits, limitations, and best practices when combining metaheuristics with simulation. *Benefits, Limitations, and Best Practices When Combining Metaheuristics with Simulation (January 1, 2017)*, 2017.
-

-
- [37] J. W. Chong, Y. Kim, and K. H. Chon. Nonlinear multiclass support vector machine–based health monitoring system for buildings employing magnetorheological dampers. *Journal of Intelligent Material Systems and Structures*, 25(12):1456–1468, 2014.
- [38] A. K. Chopra. *Dynamics of Structures: Theory and Applications to Earthquake Engineering*. Pearson College eds., 1995.
- [39] P.-j. Chun, H. Yamashita, and S. Furukawa. Bridge damage severity quantification using multipoint acceleration measurement and artificial neural networks. *Shock and Vibration*, 2015, 2015.
- [40] S. A. Civjan, J. O. Jirsa, R. Carrasquillo, and D. Fowler. Instrument to evaluate remaining prestress in damaged prestressed concrete bridge girders. *PCI journal*, 43(2), 1998. doi: <https://doi.org/10.15554/pci.j.03011998>. 62.71.
- [41] E. Commission. Eurocode 8: Design of structures for earthquake resistance - part 1 : General rules, seismic actions and rules for buildings. *European Committee for Standardization.*, 2004.
- [42] E. Davey and R. Cafe. TfL report warned of hammersmith flyover collapse risk. *BBC News, London*, 2012. URL <https://www.bbc.com/news/uk-england-london-20533457>. (accessed on February 2021).
- [43] R. de Almeida Cardoso, A. Cury, F. Barbosa, and C. Gentile. Unsupervised real-time shm technique based on novelty indexes. *Structural Control and Health Monitoring*, 26(7):e2364, 2019.
- [44] D. De Domenico, G. Ricciardi, and I. Takewaki. Design strategies of viscous dampers for seismic protection of building structures: a review. *Soil Dynamics and Earthquake Engineering*, 118:144–165, 2019.
- [45] A. Deivasigamani, A. Daliri, C. H. Wang, and S. John. A review of passive wireless sensors for structural health monitoring. *Modern Applied Science*, 7(2):pp. 57, 2013. doi: <http://dx.doi.org/10.5539/mas.v7n2p57>.
- [46] M. delle Infrastrutture e dei Trasporti. Norme tecniche per le costruzioni. *Italian Standard (NTC)*. Ministero delle Infrastrutture e dei Trasporti, Decreto Ministeriale, 2008.
- [47] M. delle Infrastrutture e dei Trasporti. Norme tecniche per le costruzioni. *Italian Standard (NTC)*, Decreto Ministeriale, 2018.
-

-
- [48] J. Deng, W. Dong, R. Socher, L.-J. Li, K. Li, and L. Fei-Fei. Imagenet: A large-scale hierarchical image database. In *2009 IEEE conference on computer vision and pattern recognition*, pages 248–255. Ieee, 2009.
- [49] I. C. P. Department. Aedes form. www.protezionecivile.gov.it/en/normativa/dpcm-dell18-luglio-2014, 2014. Accessed: 2022-03-20.
- [50] G. M. Di Giuda, G. Pattini, E. Seghezzi, M. Schievano, and F. Paleari. The construction contract execution through the integration of blockchain technology. In *Digital transformation of the design, construction and management processes of the built environment*, pages 27–36. Springer, Cham, 2020.
- [51] M. Dolce, E. Speranza, R. Dalla Negra, M. Zuppiroli, and F. Bocchi. Constructive features and seismic vulnerability of historic centres through the rapid assessment of historic building stocks. the experience of ferrara, italy. In *Built Heritage: Monitoring Conservation Management*, pages 165–175. Springer, 2015.
- [52] S. Dorafshan, R. J. Thomas, and M. Maguire. Comparison of deep convolutional neural networks and edge detectors for image-based crack detection in concrete. *Construction and Building Materials*, 186:1031–1045, 2018.
- [53] A. Downey, A. D’Alessandro, M. Baquera, E. García-Macías, D. Rolfes, F. Ubertini, S. Laflamme, and R. Castro-Triguero. Damage detection, localization and quantification in conductive smart concrete structures using a resistor mesh model. *Engineering Structures*, 148:924–935, 2017.
- [54] A. Downey, A. D’Alessandro, F. Ubertini, and S. Laflamme. Automated crack detection in conductive smart-concrete structures using a resistor mesh model. *Measurement Science and Technology*, 29(3):035107, 2018.
- [55] Z. Dworakowski, P. Kohut, A. Gallina, K. Holak, and T. Uhl. Vision-based algorithms for damage detection and localization in structural health monitoring. *Structural Control and Health Monitoring*, 23(1):35–50, 2016.
- [56] S. Dyke. Report on the building structural health monitoring problem phase 1 analytical, Jan 2011. URL <https://datacenterhub.org/resources/2806>.
- [57] F. Elghaish, S. Abrishami, and M. R. Hosseini. Integrated project delivery with blockchain: An automated financial system. *Automation in construction*, 114:103182, 2020.
-

-
- [58] C. R. Farrar and K. Worden. An introduction to structural health monitoring. *Philosophical Transactions of the Royal Society A: Mathematical, Physical and Engineering Sciences*, 365(1851):303–315, 2006.
- [59] C. R. Farrar and K. Worden. *Structural Health Monitoring.: A Machine Learning Perspective*. John Wiley & Sons, 2012.
- [60] K. Feng, A. González, and M. Casero. A kNN algorithm for locating and quantifying stiffness loss in a bridge from the forced vibration due to a truck crossing at low speed. *Mechanical Systems and Signal Processing*, 154, 2021. ISSN 10961216. doi: <https://doi.org/10.1016/j.ymssp.2020.107599>.
- [61] P. Ferrari, B. Vigna, and F. Villa. Integrated piezoresistive pressure transducer and manufacturing process, Patent DE69627645T2, Jul. 1996. URL <https://patents.google.com/patent/DE69627645T2/de?q=Patent\+DE69627645T2>. (accessed on August 2021).
- [62] P. Festa, T. Pastore, D. Ferone, A. A. Juan, and C. Bayliss. Integrating biased-randomized grasp with monte carlo simulation for solving the vehicle routing problem with stochastic demands. In *2018 Winter Simulation Conference (WSC)*, pages 2989–3000. IEEE, 2018.
- [63] M. Flah, I. Nunez, W. B. Chaabene, and M. L. Nehdi. Machine learning algorithms in civil structural health monitoring: a systematic review. *Archives of Computational Methods in Engineering*, pages pp. 1–23, 2020. doi: <https://doi.org/10.1007/s11831-020-09471-9>.
- [64] D. M. Frangopol, J. S. Kong, and E. S. Gharaibeh. Reliability-based life-cycle management of highway bridges. *Journal of computing in civil engineering*, 15(1):27–34, 2001.
- [65] L. Gallucci, C. Menna, L. Angrisani, D. Asprone, R. S. L. Moriello, F. Bonavolontà, and F. Fabbrocino. An embedded wireless sensor network with wireless power transmission capability for the structural health monitoring of reinforced concrete structures. *Sensors*, 17(11):2566, 2017.
- [66] Y. Gao and K. M. Mosalam. Deep transfer learning for image-based structural damage recognition. *Computer-Aided Civil and Infrastructure Engineering*, 33(9):748–768, 2018.
- [67] P. Garambois, S. Besset, and L. Jézéquel. Multi-objective structural robust optimization under stress criteria based on mixed plate super-elements and genetic algorithms. *Structural and Multidisciplinary Optimization*, 53(2): 205–213, 2016.
-

-
- [68] E. García-Macías, L. Rodríguez-Tembleque, A. Sáez, and F. Ubertini. Crack detection and localization in rc beams through smart mwcnt/epoxy strip-like strain sensors. *Smart Materials and Structures*, 27(11):115022, 2018.
- [69] M. Gashler, C. Giraud-Carrier, and T. Martinez. Decision tree ensemble: Small heterogeneous is better than large homogeneous. In *2008 Seventh International Conference on Machine Learning and Applications*, pages 900–905. IEEE, 2008.
- [70] C. Gentile and A. Saisi. Oma-based structural health monitoring of historic structures. In *8th International Operational Modal Analysis Conference, IOMAC 2019*, pages 671–688. International Operational Modal Analysis Conference (IOMAC), 2019.
- [71] F. Ghodoosi, S. Abu-Samra, M. Zeynalian, and T. Zayed. Maintenance cost optimization for bridge structures using system reliability analysis and genetic algorithms. *Journal of Construction Engineering and Management*, 144(2):04017116, 2018.
- [72] S. Gholizadeh, N. Razavi, and E. Shojaei. Improved black hole and multi-verse algorithms for discrete sizing optimization of planar structures. *Engineering Optimization*, 51(10):1645–1667, 2019.
- [73] T. Ghosh Mondal, M. R. Jahanshahi, R.-T. Wu, and Z. Y. Wu. Deep learning-based multi-class damage detection for autonomous post-disaster reconnaissance. *Structural Control and Health Monitoring*, 27(4):e2507, 2020.
- [74] B. Glisic, D. L. Hubbell, D. H. Sigurdardottir, and Y. Yao. Damage detection and characterization using long-gauge and distributed fiber optic sensors. *Optical Engineering*, 52(8):087101, 2013.
- [75] B. Glisic, Y. Yao, S.-T. Tung, S. Wagner, J. Sturm, and N. Verma. Strain sensing sheets for structural health monitoring based on large-area electronics and integrated circuits. *Proceedings of the IEEE*, 104(8):pp. 1513–1528, 2016. doi: 10.1109/JPROC.2016.2573238.
- [76] I. Gokasar, M. Deveci, and O. Kalan. Co2 emission based prioritization of bridge maintenance projects using neutrosophic fuzzy sets based decision making approach. *Research in Transportation Economics*, 91:101029, 2022.
- [77] G. Gui, H. Pan, Z. Lin, Y. Li, and Z. Yuan. Data-driven support vector machine with optimization techniques for structural health monitoring and
-

- damage detection. *KSCCE Journal of Civil Engineering*, 21(2):pp. 523–534, 2017. doi: 10.1007/s12205-017-1518-5.
- [78] E. Guidetti, M. A. Gavarti, D. Caltabiano, and G. Bertagnoli. Stress sensor for monitoring the health state of fabricated structures such as constructions, buildings, infrastructures and the like, Patent US10935444B2, Apr. 2018. URL <https://patents.google.com/patent/US10935444B2/en?q=Patent\+US10935444B2>. (accessed on August 2021).
- [79] J. T. Halsey and R. Miller. Destructive testing of two forty-year-old prestressed concrete bridge beams. *PCI journal*, 41(5), 1996. doi: <https://doi.org/10.15554/pcij.09011996.84.93>.
- [80] E. Hamed and Y. Frostig. Natural frequencies of bonded and unbonded prestressed beams-prestress force effects. *Journal of Sound and Vibration*, 295(1-2):pp. 28–39, 2006. ISSN 10958568. doi: <https://doi.org/10.1016/j.jsv.2005.11.032>.
- [81] K. He, X. Zhang, S. Ren, and J. Sun. Deep residual learning for image recognition. In *Proceedings of the IEEE conference on computer vision and pattern recognition*, pages 770–778, 2016.
- [82] L. He, E. Reynders, J. H. García-Palacios, G. Carlo Marano, B. Briseghella, and G. De Roeck. Wireless-based identification and model updating of a skewed highway bridge for structural health monitoring. *Applied Sciences*, 10(7), 2020. doi: <https://doi.org/10.3390/app10072347>.
- [83] T. Hegazy, E. Elbeltagi, and H. El-Behairy. Bridge deck management system with integrated life-cycle cost optimization. *Transportation Research Record*, 1866(1):44–50, 2004.
- [84] F. Hejazi, I. Toloue, M. Jaafar, and J. Noorzai. Optimization of earthquake energy dissipation system by genetic algorithm. *Computer-Aided Civil and Infrastructure Engineering*, 28(10):796–810, 2013.
- [85] T. Hop. The effect of degree of prestressing and age of concrete beams on frequency and damping of their free vibration. *Materials and Structures*, 24(3):pp. 210–220, 1991. ISSN 00255432. doi: <https://doi.org/10.1007/BF02472987>.
- [86] P. Horata, S. Chiewchanwattana, and K. Sunat. Robust extreme learning machine. *Neurocomputing*, 102:pp. 31–44, 2013. doi: <https://doi.org/10.1016/j.neucom.2011.12.045>.
-

-
- [87] G. Huang, Z. Liu, L. Van Der Maaten, and K. Q. Weinberger. Densely connected convolutional networks. In *Proceedings of the IEEE conference on computer vision and pattern recognition*, pages 4700–4708, 2017.
- [88] G.-B. Huang, L. Chen, C. K. Siew, et al. Universal approximation using incremental constructive feedforward networks with random hidden nodes. *IEEE Transactions Neural Networks*, 17(4):pp. 879–892, 2006. doi: <https://doi.org/10.1109/TNN.2006.875977>.
- [89] G.-B. Huang, Q.-Y. Zhu, and C.-K. Siew. Extreme learning machine: theory and applications. *Neurocomputing*, 70(1-3):pp. 489–501, 2006. doi: <https://doi.org/10.1016/j.neucom.2005.12.126>.
- [90] F. Huseynov, C. Kim, E. J. O'Brien, J. Brownjohn, D. Hester, and K. Chang. Bridge damage detection using rotation measurements—experimental validation. *Mechanical Systems and Signal Processing*, 135:106380, 2020.
- [91] D. Inaudi. Long-term static structural health monitoring. In *Structures Congress 2010*, pages 566–577, 2010.
- [92] D. Inaudi and B. Glišić. Overview of 40 bridge monitoring projects using fiber optic sensors. *Bridge Maintenance, Safety, Management, Health Monitoring and Informatics - Proceedings of the 4th International Conference on Bridge Maintenance, Safety and Management*, pages pp. 2514–2521, 2008. doi: 10.1201/9781439828434.ch312.
- [93] T. Jensen, J. Hedman, and S. Henningsson. How tradelens delivers business value with blockchain technology. *MIS Quarterly Executive*, 18(4), 2019.
- [94] X. Jiang and H. Adeli. Pseudospectra, music, and dynamic wavelet neural network for damage detection of highrise buildings. *International Journal for Numerical Methods in Engineering*, 71(5):606–629, 2007.
- [95] E. A. Johnson, H.-F. Lam, L. S. Katafygiotis, and J. L. Beck. Phase i iasc-asce structural health monitoring benchmark problem using simulated data. *Journal of engineering mechanics*, 130(1):3–15, 2004.
- [96] D. Kifokeris and C. Koch. Blockchain in construction logistics: state-of-art, constructability, and the advent of a new digital business model in sweden. In *EC3 Conference 2019*, volume 1, pages 332–340. University College Dublin, 2019.
-

-
- [97] J.-T. Kim, J.-H. Park, D.-S. Hong, and W.-S. Park. Hybrid health monitoring of prestressed concrete girder bridges by sequential vibration-impedance approaches. *Engineering Structures*, 32(1):pp. 115–128, 2010. doi: <https://doi.org/10.1016/j.engstruct.2009.08.021>.
- [98] Y. Kim, J. W. Chong, K. H. Chon, and J. Kim. Wavelet-based ar-svm for health monitoring of smart structures. *Smart Materials and Structures*, 22(1), 2012. doi: <https://doi.org/10.1088/0964-1726/22/1/015003>.
- [99] C. Koch, S. G. Paal, A. Rashidi, Z. Zhu, M. König, and I. Brilakis. Achievements and challenges in machine vision-based inspection of large concrete structures. *Advances in Structural Engineering*, 17(3):303–318, 2014.
- [100] J. S. Kong and D. M. Frangopol. Life-cycle reliability-based maintenance cost optimization of deteriorating structures with emphasis on bridges. *Journal of Structural Engineering*, 129(6):818–828, 2003.
- [101] V. Kumar, L. Aygun, N. Verma, J. Sturm, and B. Glišić. Sensing sheets based on large area electronics for structural health monitoring of bridges. *Proceedings of SPIE - The International Society for Optical Engineering*, 10970, 2019. doi: [10.1117/12.2514223](https://doi.org/10.1117/12.2514223).
- [102] L. La Mendola, M. C. Oddo, M. Papia, F. Pappalardo, A. Pennisi, G. Bertagnoli, F. Di Trapani, A. Monaco, F. Parisi, and S. Barile. Performance of two innovative stress sensors imbedded in mortar joints of new masonry elements. *Construction and Building Materials*, 297, 2021. doi: <https://doi.org/10.1016/j.conbuildmat.2021.123764>.
- [103] S. Laflamme, H. Saleem, B. Vasan, R. Geiger, D. Chen, M. Kessler, and K. Rajan. Soft elastomeric capacitor network for strain sensing over large surfaces. *IEEE/ASME Transactions on Mechatronics*, 18(6):pp. 1647–1654, 2013. doi: [10.1109/TMECH.2013.2283365](https://doi.org/10.1109/TMECH.2013.2283365).
- [104] S. Laflamme, P. Ubertini, F., H. Saleem, A. D’Alessandro, A. Downey, H. Ceylan, and A. Materazzi. Dynamic characterization of a soft elastomeric capacitor for structural health monitoring. *Journal of Structural Engineering (United States)*, 141(8), 2015. doi: [10.1061/\(ASCE\)ST.1943-541X.0001151](https://doi.org/10.1061/(ASCE)ST.1943-541X.0001151).
- [105] H.-F. Lam, K.-V. Yuen, and J. L. Beck. Structural health monitoring via measured ritz vectors utilizing artificial neural networks. *Computer-Aided Civil and Infrastructure Engineering*, 21(4):232–241, 2006.
-

-
- [106] H. Lasi, P. Fettke, H.-G. Kemper, T. Feld, and M. Hoffmann. Industry 4.0. *Business & information systems engineering*, 6(4):239–242, 2014.
- [107] K. Lau and I. Lasa. Corrosion of prestress and post-tension reinforced-concrete bridges. In *Corrosion of Steel in Concrete Structures*, pages pp. 37–57. Elsevier, 2016. doi: <https://doi.org/10.1016/B978-1-78242-381-2.00002-X>.
- [108] S. S. Law and Z. R. Lu. Time domain responses of a prestressed beam and prestress identification. *Journal of Sound and Vibration*, 288(4-5):pp. 1011–1025, 2005. ISSN 10958568. doi: <https://doi.org/10.1016/j.jsv.2005.01.045>.
- [109] J.-H. Lee, S.-K. Yeh, and W. Fang. Vertically integrated double-bridge design for cmos-mems tri-axial piezo-resistive force sensor. In *2020 IEEE 33rd International Conference on Micro Electro Mechanical Systems (MEMS)*, pages 693–696. IEEE, 2020. doi: [10.1109/MEMS46641.2020.9056191](https://doi.org/10.1109/MEMS46641.2020.9056191).
- [110] K. Lee, S. Jeong, S. H. Sim, and D. H. Shin. A novelty detection approach for tendons of prestressed concrete bridges based on a convolutional autoencoder and acceleration data. *Sensors (Switzerland)*, 19(7), 2019. ISSN 14248220. doi: <https://doi.org/10.3390/s19071633>.
- [111] J. Li, D. Greenwood, and M. Kassem. Blockchain in the built environment and construction industry: A systematic review, conceptual models and practical use cases. *Automation in construction*, 102:288–307, 2019.
- [112] R. Li, Y. Yuan, W. Zhang, and Y. Yuan. Unified vision-based methodology for simultaneous concrete defect detection and geolocalization. *Computer-Aided Civil and Infrastructure Engineering*, 33(7):527–544, 2018.
- [113] S. Li, X. Zhao, and G. Zhou. Automatic pixel-level multiple damage detection of concrete structure using fully convolutional network. *Computer-Aided Civil and Infrastructure Engineering*, 34(7):616–634, 2019.
- [114] W. Li, H. Pu, P. Schonfeld, J. Yang, H. Zhang, L. Wang, and J. Xiong. Mountain railway alignment optimization with bidirectional distance transform and genetic algorithm. *Computer-Aided Civil and Infrastructure Engineering*, 32(8):691–709, 2017.
- [115] M. P. Limongelli, D. Siegert, E. Merliot, J. Waeytens, F. Bourquin, R. Vidal, V. Le Corvec, I. Gueguen, and L. M. Cottineau. Damage detection in a post tensioned concrete beam – Experimental investigation. *Engineering Structures*, 128:pp. 15–25, 2016. ISSN 18737323. doi: <https://doi.org/10.1016/j.engstruct.2016.09.017>.
-

-
- [116] Y.-z. Lin, Z.-h. Nie, and H.-w. Ma. Structural damage detection with automatic feature-extraction through deep learning. *Computer-Aided Civil and Infrastructure Engineering*, 32(12):1025–1046, 2017.
- [117] M. Liu and D. M. Frangopol. Optimal bridge maintenance planning based on probabilistic performance prediction. *Engineering Structures*, 26(7):991–1002, 2004.
- [118] S. Liu and W. Deng. Very deep convolutional neural network based image classification using small training sample size. In *2015 3rd IAPR Asian conference on pattern recognition (ACPR)*, pages 730–734. IEEE, 2015.
- [119] C.-H. Loh, C.-H. Chen, and T.-Y. Hsu. Application of advanced statistical methods for extracting long-term trends in static monitoring data from an arch dam. *Structural Health Monitoring*, 10(6):587–601, 2011.
- [120] J. Long, E. Shelhamer, and T. Darrell. Fully convolutional networks for semantic segmentation. In *Proceedings of the IEEE conference on computer vision and pattern recognition*, pages 3431–3440, 2015.
- [121] V. Lopes Jr, G. Park, H. H. Cudney, and D. J. Inman. Impedance-based structural health monitoring with artificial neural networks. *Journal of Intelligent Material Systems and Structures*, 11(3):pp. 206–214, 2000. doi: <https://doi.org/10.1106/H0EV-7PWM-QYHW-E7VF>.
- [122] J. Maeck and G. De Roeck. Description of z24 benchmark. *Mechanical Systems and Signal Processing*, 17(1):127–131, 2003.
- [123] F. Magalhães, Á. Cunha, and E. Caetano. Dynamic monitoring of a long span arch bridge. *Engineering Structures*, 30(11):3034–3044, 2008.
- [124] Z. Man, K. Lee, D. Wang, Z. Cao, and C. Miao. A new robust training algorithm for a class of single-hidden layer feedforward neural networks. *Neurocomputing*, 74(16):pp. 2491–2501, 2011. doi: <https://doi.org/10.1016/j.neucom.2010.11.033>.
- [125] Z. Man, K. Lee, D. Wang, Z. Cao, and S. Khoo. Robust single-hidden layer feedforward network-based pattern classifier. *IEEE Transactions on Neural Networks and Learning Systems*, 23(12):pp. 1974–1986, 2012. doi: [10.1109/TNNLS.2012.2218616](https://doi.org/10.1109/TNNLS.2012.2218616).
- [126] G. Mariniello, T. Pastore, C. Menna, P. Festa, and D. Asprone. Structural damage detection and localization using decision tree ensemble and vibration data. *Computer-Aided Civil and Infrastructure Engineering*, 2020.
-

-
- [127] G. Mariniello, T. Pastore, D. Asprone, and E. Cosenza. Layout-aware extreme learning machine to detect tendon malfunctions in prestressed concrete bridges using stress data. *Automation in Construction*, 132:103976, 2021.
- [128] G. Mariniello, T. Pastore, C. Menna, P. Festa, and D. Asprone. Structural damage detection and localization using decision tree ensemble and vibration data. *Computer-Aided Civil and Infrastructure Engineering*, 36(9):pp. 1129–1149, 2021. doi: <https://doi.org/10.1111/mice.12633>.
- [129] S. Mazzoni, F. McKenna, M. H. Scott, G. L. Fenves, et al. Opensees command language manual. *Pacific Earthquake Engineering Research (PEER) Center*, 264, 2006.
- [130] F. McKenna. Opensees: a framework for earthquake engineering simulation. *Computing in Science & Engineering*, 13(4):58–66, 2011.
- [131] P. E. Mergos. Efficient optimum seismic design of reinforced concrete frames with nonlinear structural analysis procedures. *Structural and Multidisciplinary Optimization*, 58(6):2565–2581, 2018.
- [132] N. Metawa, M. K. Hassan, and M. Elhoseny. Genetic algorithm based model for optimizing bank lending decisions. *Expert Systems with Applications*, 80:75–82, 2017.
- [133] J. C. Miles, G. Sisk, and C. J. Moore. The conceptual design of commercial buildings using a genetic algorithm. *Computers & Structures*, 79(17):1583–1592, 2001.
- [134] J. Min, S. Park, C.-B. Yun, C.-G. Lee, and C. Lee. Impedance-based structural health monitoring incorporating neural network technique for identification of damage type and severity. *Engineering Structures*, 39:pp. 210–220, 2012. doi: <https://doi.org/10.1016/j.engstruct.2012.01.012>.
- [135] H. Mirzaei and K. Nasseradi. Fast seismic life cycle cost optimization of steel moment frames to improve seismic performance. *KSCE Journal of Civil Engineering*, 23(3):1180–1189, 2019.
- [136] A. Miyamoto, K. Kawamura, and H. Nakamura. Bridge management system and maintenance optimization for existing bridges. *Computer-Aided Civil and Infrastructure Engineering*, 15(1):45–55, 2000.
- [137] N. Mladenović, R. Todosijević, and D. Urošević. Less is more: basic variable neighborhood search for minimum differential dispersion problem. *Information Sciences*, 326:160–171, 2016.
-

-
- [138] N. Mladenović, A. Alkandari, J. Pei, R. Todosijević, and P. M. Pardalos. Less is more approach: basic variable neighborhood search for the obnoxious p-median problem. *International Transactions in Operational Research*, 27(1):480–493, 2020.
- [139] G. Morcous and Z. Lounis. Maintenance optimization of infrastructure networks using genetic algorithms. *Automation in construction*, 14(1):129–142, 2005.
- [140] G.-T. Nguyen and K. Kim. A survey about consensus algorithms used in blockchain. *Journal of Information processing systems*, 14(1):101–128, 2018.
- [141] W. Nick, J. Shelton, K. Asamene, and A. C. Esterline. A study of supervised machine learning techniques for structural health monitoring. *MAICS*, 1353:pp. 36, 2015. doi: 10.7763/IJMLC.2015.V5.526.
- [142] A. Nimitawat and P. Nanakorn. Automated layout design of beam-slab floors using a genetic algorithm. *Computers & structures*, 87(21-22):1308–1330, 2009.
- [143] A. Nimitawat and P. Nanakorn. A genetic algorithm for beam-slab layout design of rectilinear floors. *Engineering Structures*, 32(11):3488–3500, 2010.
- [144] F. H. A. F. of the U.S. Department of Transportation. Nbi database. *Automation in Construction*, 132:103976, 2021.
- [145] C. K. Oh, C. Joh, J. W. Lee, and K.-Y. Park. Corrosion detection in psc bridge tendons using kernel pca denoising of measured mfl signals. *Sensors*, 20(21), 2020. doi: <https://doi.org/10.3390/s20215984>.
- [146] G. Oliveira, F. Magalhães, Á. Cunha, and E. Caetano. Continuous dynamic monitoring of an onshore wind turbine. *Engineering Structures*, 164:22–39, 2018.
- [147] Ç. F. Özgenel and A. G. Sorguç. Performance comparison of pretrained convolutional neural networks on crack detection in buildings. In *ISARC. Proceedings of the International Symposium on Automation and Robotics in Construction*, volume 35, pages 1–8. IAARC Publications, 2018.
- [148] A. Oztekin, L. Al-Ebbini, Z. Sevkli, and D. Delen. A decision analytic approach to predicting quality of life for lung transplant recipients: A hybrid genetic algorithms-based methodology. *European Journal of Operational Research*, 266(2):639–651, 2018.
-

-
- [149] T. Pastore, A. Martínez-Gavara, A. Napoletano, P. Festa, and R. Martí. Tabu search for min-max edge crossing in graphs. *Computers & Operations Research*, 114:104830, 2020.
- [150] B. Patterson, G. Leone, M. Pantoja, and A. A. Behrouzi. Deep learning for automated image classification of seismic damage to built infrastructure. In *Eleventh US National Conference on Earthquake Engineering*, 2018.
- [151] T. Paulay and M. N. Priestley. *Seismic design of reinforced concrete and masonry buildings*, volume 768. Wiley New York, 1992.
- [152] J. Peng, Y. Yang, H. Bian, J. Zhang, and L. Wang. Optimisation of maintenance strategy of deteriorating bridges considering sustainability criteria. *Structure and Infrastructure Engineering*, 18(3):395–411, 2022.
- [153] M. Pilkington. Blockchain technology: principles and applications. In *Research handbook on digital transformations*. Edward Elgar Publishing, 2016.
- [154] R. Poli and W. B. Langdon. Schema theory for genetic programming with one-point crossover and point mutation. *Evolutionary Computation*, 6(3): 231–252, 1998.
- [155] N. Pollini. Fail-safe optimization of viscous dampers for seismic retrofitting. *Earthquake Engineering & Structural Dynamics*, 49(15):1599–1618, 2020.
- [156] M. J. N. Priestley. Performance based seismic design. *Bulletin of the New Zealand society for earthquake engineering*, 33(3):325–346, 2000.
- [157] M. H. Rafei and H. Adeli. A new neural dynamic classification algorithm. *IEEE transactions on neural networks and learning systems*, 28(12):3074–3083, 2017.
- [158] M. H. Rafei and H. Adeli. A novel machine learning-based algorithm to detect damage in high-rise building structures. *The Structural Design of Tall and Special Buildings*, 26(18):e1400, 2017.
- [159] M. H. Rafei and H. Adeli. A novel unsupervised deep learning model for global and local health condition assessment of structures. *Engineering Structures*, 156:598–607, 2018.
- [160] C. Rainieri and G. Fabbrocino. *Operational modal analysis of civil engineering structures*, volume 142. Springer, 2014. ISBN 978-1-4939-0767-0.
-

-
- [161] M. Regona, T. Yigitcanlar, B. Xia, and R. Y. M. Li. Opportunities and adoption challenges of ai in the construction industry: a prisma review. *Journal of Open Innovation: Technology, Market, and Complexity*, 8(1):45, 2022.
- [162] S. Rezaeian and A. Der Kiureghian. A stochastic ground motion model with separable temporal and spectral nonstationarities. *Earthquake Engineering & Structural Dynamics*, 37(13):1565–1584, 2008.
- [163] L. Rokach. Ensemble-based classifiers. *Artificial Intelligence Review*, 33(1-2):1–39, 2010.
- [164] S. Ropke and D. Pisinger. An adaptive large neighborhood search heuristic for the pickup and delivery problem with time windows. *Transportation science*, 40(4):455–472, 2006.
- [165] A. Rytter. *Vibrational based inspection of civil engineering structures*. PhD thesis, Dept. of Building Technology and Structural Engineering, Aalborg University, 1993.
- [166] M. Saiidi, B. Douglas, and S. Feng. Prestress force effect on vibration frequency of concrete bridges. *Journal of Structural Engineering*, 120(7):pp. 2233–2241, 1994. doi: [https://doi.org/10.1061/\(ASCE\)0733-9445\(1994\)120:7\(2233\)](https://doi.org/10.1061/(ASCE)0733-9445(1994)120:7(2233)).
- [167] S. O. Sajedi and X. Liang. Vibration-based semantic damage segmentation for large-scale structural health monitoring. *Computer-Aided Civil and Infrastructure Engineering*, 2019.
- [168] S. Salamone, I. Bartoli, R. Phillips, C. Nucera, and F. L. Di Scalea. Health monitoring of prestressing tendons in posttensioned concrete bridges. *Transportation Research Record*, 2220(1):pp. 21–27, 2011. doi: <https://doi.org/10.3141/2220-03>.
- [169] A. Santos, E. Figueiredo, M. Silva, R. Santos, C. Sales, and J. C. Costa. Genetic-based em algorithm to improve the robustness of gaussian mixture models for damage detection in bridges. *Structural Control and Health Monitoring*, 24(3), 2017. doi: <https://doi.org/10.1002/stc.1886>.
- [170] H. Sarmadi and A. Karamodin. A novel anomaly detection method based on adaptive mahalanobis-squared distance and one-class knn rule for structural health monitoring under environmental effects. *Mechanical Systems and Signal Processing*, 140, 2020. doi: <https://doi.org/10.1016/j.ymssp.2019.106495>.
-

-
- [171] H. Sarmadi, A. Entezami, B. Saeedi Razavi, and K.-V. Yuen. Ensemble learning-based structural health monitoring by mahalanobis distance metrics. *Structural Control and Health Monitoring*, 28(2), 2021. doi: <https://doi.org/10.1002/stc.2663>.
- [172] D. Saydam and D. M. Frangopol. Risk-based maintenance optimization of deteriorating bridges. *Journal of Structural Engineering*, 141(4):04014120, 2015.
- [173] P. Sharafi, L. H. Teh, and M. N. Hadi. Conceptual design optimization of rectilinear building frames: A knapsack problem approach. *Engineering Optimization*, 47(10):1303–1323, 2015.
- [174] D. Shaw, J. Miles, and A. Gray. Determining the structural layout of orthogonal framed buildings. *Computers & structures*, 86(19-20):1856–1864, 2008.
- [175] D. Sheng, L. Ding, B. Zhong, P. E. Love, H. Luo, and J. Chen. Construction quality information management with blockchains. *Automation in construction*, 120:103373, 2020.
- [176] L. N. Smith. Cyclical learning rates for training neural networks. In *2017 IEEE Winter Conference on Applications of Computer Vision (WACV)*, pages 464–472. IEEE, 2017.
- [177] L. N. Smith. A disciplined approach to neural network hyper-parameters: Part 1—learning rate, batch size, momentum, and weight decay. *arXiv preprint arXiv:1803.09820*, 2018.
- [178] G. Song, H. Gu, and Y.-L. Mo. Piezoceramic-based smart aggregate for unified performance monitoring of concrete structures, Patent US7987728B2, Jul. 2007. URL <https://patents.google.com/patent/US7987728B2/en?q=Patent\+US7987728B2>. (accessed on August 2021).
- [179] A. S. s.p.a. "ACCA Software SPA: Edilus CA", website - accessed April 9, 2020. <https://www.acca.it/software-calcolo-strutturale-cemento-armato>.
- [180] X.-Y. Sun, J.-G. Dai, H.-L. Wang, W.-W. Dong, and J. Wang. Decision support system for optimizing the maintenance of rc girder bridge superstructures in consideration of the carbon footprint. *Journal of Bridge Engineering*, 20(12):04015022, 2015.
- [181] M. Swan. *Blockchain: Blueprint for a new economy*. " O'Reilly Media, Inc.", 2015.
-

- [182] P. Toth and S. Martello. *Knapsack problems: Algorithms and computer implementations*. Wiley, 1990.
- [183] H. Tran-Ngoc, L. He, E. Reynders, S. Khatir, T. Le-Xuan, G. De Roeck, T. Bui-Tien, and M. A. Wahab. An efficient approach to model updating for a multispan railway bridge using orthogonal diagonalization combined with improved particle swarm optimization. *Journal of Sound and Vibration*, page 115315, 2020.
- [184] Ž. Turk and R. Klinc. Potentials of blockchain technology for construction management. *Procedia engineering*, 196:638–645, 2017.
- [185] P. Tuttipongsawat, E. Sasaki, K. Suzuki, M. Fukuda, N. Kawada, and K. Hamaoka. PC tendon damage detection based on phase space topology changes in different frequency ranges. *Journal of Advanced Concrete Technology*, 17(8):pp. 474–488, 2019. ISSN 13468014. doi: <https://doi.org/10.3151/jact.17.474>.
- [186] O. S. L. Vera, Y. Oshima, and C.-W. Kim. Flexural performance correlation with natural bending frequency of post-tensioned concrete beam: Experimental investigation. *Journal of Civil Structural Health Monitoring*, 10(1): pp. 135–151, 2020. doi: <https://doi.org/10.1007/s13349-019-00374-3>.
- [187] J. Vitola, F. Pozo, D. A. Tibaduiza, and M. Anaya. A sensor data fusion system based on k-nearest neighbor pattern classification for structural health monitoring applications. *Sensors*, 17(2):pp. 417, 2017. doi: <https://doi.org/10.3390/s17020417>.
- [188] J. Wang, P. Wu, X. Wang, and W. Shou. The outlook of blockchain technology for construction engineering management. *Frontiers of engineering management*, pages 67–75, 2017.
- [189] L. Wang, A. Kolios, T. Nishino, P.-L. Delafin, and T. Bird. Structural optimisation of vertical-axis wind turbine composite blades based on finite element analysis and genetic algorithm. *Composite Structures*, 153:123–138, 2016.
- [190] N. Wang, Q. Zhao, S. Li, X. Zhao, and P. Zhao. Damage classification for masonry historic structures using convolutional neural networks based on still images. *Computer-Aided Civil and Infrastructure Engineering*, 33(12): 1073–1089, 2018.
- [191] Y. Wang and Y. Ni. Bayesian dynamic forecasting of structural strain response using structural health monitoring data. *Structural Control and Health Monitoring*, 27(8), 2020. doi: <https://doi.org/10.1002/stc.2575>.
-

-
- [192] Z. Wang, T. Wang, H. Hu, J. Gong, X. Ren, and Q. Xiao. Blockchain-based framework for improving supply chain traceability and information sharing in precast construction. *Automation in construction*, 111:103063, 2020.
- [193] J. Yan, A. Downey, A. Cancelli, S. Laflamme, A. Chen, J. Li, and F. Ubertini. Concrete crack detection and monitoring using a capacitive dense sensor array. *Sensors*, 19(8):1843, 2019.
- [194] R. Yang, R. Wakefield, S. Lyu, S. Jayasuriya, F. Han, X. Yi, X. Yang, G. Amarasinghe, and S. Chen. Public and private blockchain in construction business process and information integration. *Automation in construction*, 118:103276, 2020.
- [195] X.-W. Ye, Y.-H. Su, and P.-S. Xi. Statistical analysis of stress signals from bridge monitoring by fbg system. *Sensors (Switzerland)*, 18(2), 2018. doi: 10.3390/s18020491.
- [196] C. Yuan, B. Xiong, X. Li, X. Sang, and Q. Kong. A novel intelligent inspection robot with deep stereo vision for three-dimensional concrete damage detection and quantification. *Structural Health Monitoring*, page 14759217211010238, 2021.
- [197] S. Yuyama, K. Yokoyama, K. Niitani, M. Ohtsu, and T. Uomoto. Detection and evaluation of failures in high-strength tendon of prestressed concrete bridges by acoustic emission. *Construction and Building Materials*, 21(3): pp. 491–500, 2007. doi: <https://doi.org/10.1016/j.conbuildmat.2006.04.010>.
- [198] N. Zealand. Nzs 1170.5: 2004, structural design actions part 5: Earthquake actions-new zealand. *Wellington, New Zealand: Standards New Zealand*, 2004.
- [199] J. Zhang, G. De Roeck, E. Reynders, and G. Lombaert. Optimal sensor placement for modal identification of repetitive structures. In *Proceedings of ISMA*, volume 27, pages 2355–2364, 2016.
- [200] J. Zhang, K. Maes, G. De Roeck, E. Reynders, C. Papadimitriou, and G. Lombaert. Optimal sensor placement for multi-setup modal analysis of structures. *Journal of Sound and Vibration*, 401:214–232, 2017.
- [201] L. Zhang and R. Brincker. An overview of operational modal analysis: major development and issues. In *1st international operational modal analysis conference*, pages 179–190. Aalborg Universitet, 2005.
-

-
- [202] X. Zhou, Y. Ni, and F. Zhang. Damage localization of cable-supported bridges using modal frequency data and probabilistic neural network. *Mathematical Problems in Engineering*, 2014, 2014.
- [203] Z. Zhou, M. M. R. Siddiquee, N. Tajbakhsh, and J. Liang. Unet++: A nested u-net architecture for medical image segmentation. In *Deep learning in medical image analysis and multimodal learning for clinical decision support*, pages 3–11. Springer, 2018.
- [204] X. Zhu, J. Shi, F. Xie, and R. Song. Pricing strategy and system performance in a cloud-based manufacturing system built on blockchain technology. *Journal of Intelligent Manufacturing*, 31(8):1985–2002, 2020.
-

Author's publications

1. Ciotta, V., Mariniello, G., Asprone, D., Botta, A., & Manfredi, G. (2021). Integration of blockchains and smart contracts into construction information flows: Proof-of-concept. *Automation in Construction*, 132. doi:10.1016/j.autcon.2021.103925
2. Giacco, G., Mariniello, G., Marrone, S., Asprone, D., & Sansone, C. (2022). Toward a System for Post-earthquake safety evaluation of Masonry buildings doi:10.1007/978-3-031-06430-2_26
3. Mariniello, G., Pastore, T., Asprone, D., & Cosenza, E. (2021). Layout-aware extreme learning machine to detect tendon malfunctions in pre-stressed concrete bridges using stress data. *Automation in Construction*, 132 doi:10.1016/j.autcon.2021.103976
4. Mariniello, G., Pastore, T., Bilotta, A., Asprone, D., & Cosenza, E. (2022). Seismic pre-dimensioning of irregular concrete frame structures: Mathematical formulation and implementation of a learn-heuristic algorithm. *Journal of Building Engineering*, 46. doi:10.1016/j.jobbe.2021.103733
5. Mariniello, G., Pastore, T., Menna, C., & Asprone, D. (2019). Vibration-based learning algorithm for damage localization in structural health monitoring. Paper presented at the Proceedings of the 1st Fib Italy YMG Symposium on Concrete and Concrete Structures, FIBPRO 2019, 90-97.
6. Mariniello, G., Pastore, T., Menna, C., Festa, P., & Asprone, D. (2021). Structural damage detection and localization using decision tree ensemble and vibration data. *Computer-Aided Civil and Infrastructure Engineering*, 36(9), 1129-1149. doi:10.1111/mice.12633
7. Mariniello, G., Pastore, T. & Asprone, D. (2022). A metaheuristic framework to minimize carbon footprint in the maintenance of aging infrastruc-

- tures. Concrete Innovation for Sustainability, Proceedings for the 6th fib International Congress 2022, 2296-2305, Oslo, Norway, June 12 – 16, 2022.
8. Mariniello, G., Scalvenzi, M., Pastore, T., Losanno, D., Parisi, F., & Asprone, D. (2023). A Data-driven Methodology for Damage Detection of Roadway Bridges Using Stress Data Distributions. ICASP2023 (submitted)
 9. Pastore, T., Mariniello, G., Menna, C, Capozzi, V., Papa, G., Micchia, A.& Asprone, D. Designing Lightweight Solar Plants: a Hybrid Max-Min Ant System for the Structural Optimization of Solar Trackers, submitted to Expert systems with applications (submitted)
-